The Hashemite Kingdom of Jordan
Scientific Research Support Fund
The Hashemite University

JJEES

Jordan Journal of Earth and Environmental Sciences

Volume (11) Number (3)

Cover photo © Khaled Moumani

JJEES is an International Peer-Reviewed Research Journal

ISSN 1995-6681 jjees.hu.edu.jo September 2020

Jordan Journal of Earth and Environmental Sciences (JJEES)

JJEES is an International Peer-Reviewed Research Journal, Issued by Deanship of Scientific Research, The Hashemite University, in corporation with, the Jordanian Scientific Research Support Fund, the Ministry of Higher Education and Scientific Research.

Editorial Board:

Associate Editorial Board: (Arranged Alphabetically)

International Advisory Board: (Arranged Alphabetically)

Editorial Board Support Team:

Submission address:

Manuscripts should be submitted electronically to the following e-mail:

jjees@hu.edu.jo

For more information and previous issues:

www.jjees.hu.edu.jo

Hashemite Kingdom of Jordan

Scientific Research Support Fund

Hashemite University

Jordan Journal of Earth and Environmental Sciences

JJEES

An International Peer-Reviewed Scientific Journal

Financed by the Scientific Research Support Fund

Volume 11 Number (3)

http:// jjees.hu.edu.jo/

ISSN 1995-6681

Cover page photo: "Small scale faults within the Cambrian Sandstones of Umm Ishrin Formation in Wadi As Siq / Gharandal, Wadi Araba (Exposure 40 cm2)."

Photo courtesy of Khaled Moumani

JJEES
Jordan Journal of Earth and Environmental Sciences

JJEES

JJEES (2020) 11 (3): 157-163
ISSN 1995-6681

Jordan Journal of Earth and Environmental Sciences

Assessment of Horizontal and Vertical Wind Erosion and their Interrelationship in a Bare Land in Gozalhalag Area, River Nile State, Sudan

Motasim Abdelwahab

Omdurman Islamic University, Faculty of Agriculture, Department of Arid Land and Desert Agriculture, Sudan

Received 28 September, 2019; Accepted 1 March, 2020

Abstract

A field experiment in a bare land was conducted over two-successive seasons (August 2008- March 2009, August 2009-March 2010) to assess wind erosion. The intensity of wind erosion (IWE) was measured monthly in four directions, namely West (W), North West (NW), North (N), and North East (NE), using vertical (IWEv) and horizontal (IWEh) soil traps. In the two seasons, the IWE and IWEv/IWEh ratio varied according to month and direction. In the first season, IWEh ranged from 99.9 (W) to 109.8 (NE) with a mean of 104.4 tons/ha/day, a standard deviation (STD) of 4.1 tons/ha/day and a coefficient of variation (CV) of 4%. Furthermore, IWEh ranged from 2.1 (Nov.) to 260 (Sept.) with a mean of 104.4 tons/ha/day, a STD of 97.5 tons/ha/day and a CV of 93.4%. The IWEv values obtained for each month or direction were lower than the corresponding IWEh values. The overall mean IWEh value was 2.4 and 2.0 fold the overall mean IWEv value in the first and second seasons, respectively. The variation according to direction was much lower than the monthly variation. Regression between IWEv and IWEh gave a highly significant polynomial relationship, ($P< 0.001$, $r^2=0.98$) and ($P< 0.001$, $r^2=0.94$) for the first and second seasons, respectively.

Keywords: Wind erosion, Wind erosivity, Soil traps, River Nile.

1. Introduction

Wind erosion occurs, naturally, in all lands wherever the surface soil is loose and dry and blown by erosive winds. However, it is predominant and has serious adverse impacts on agricultural lands in the arid and semi-arid lands characterized by low, variable, erratic, and unpredictable rainfall, and high temperature, high wind velocity, and consequent high rates of evapotranspiration. In developing countries it is accelerated by environmentally non-sustainable land use and management systems. Wind erosion is governed by two main factors, namely soil or wind erodibility as an indicator of the vulnerability of the soil mass to detachment by wind, and wind erosivity as an indicator of the ability of the wind energy to transport the detached soil particles.

Abdelwahab et al. (2014) assessed the status and rate of wind erosion in part of the River Nile State. Remote sensing data during the period 1987-2005, showed that the total area of loose and shifting sand dunes in some areas in south east Atbara, north Atbara and south Atbara, increased by 1.3%, 110.1% and 34.4%, respectively. Moreover, the total area of irrigated tree crops decreased by about 11.6% and 8.2% in south east Atbara and north Atbara respectively. In south Atbara there is a meager increase in the area of irrigated tree crops. According to these indications, wind erosion may be described as very severe, moderate, and slight in north Atbara, south east Atbara, and south Atbara, respectively.

Abdelwahab and Mustafa (2015) assessed the monthly and diurnal variation of wind speed and direction and wind erosivity in the River Nile State. They found that winds and erosive winds (velocity>5.4 m/s) varied widely in direction and speed during each month and day even within the same climatic season. The high percentages of erosive wind contribution in the summer season blowing from SW and S directions were 75.6%, and 10.5 respectively, whereas the high percentages of erosive wind contribution in the winter season blowing from NNW and N directions were 59.4%, and 19.9. Erosive wind ranged from 0 (Nov., 2008) to 369.8 (Feb., 2009) with a mean of 255.1 $(m/s)^3$, and a CV of 43.6%. The wind pressure of the erosive winds ranged from 0 (Nov., 2008) to 27.1 (Jan., 2009) with a mean of 21.1 (Nm^{-2}) and a CV of 42.1%. The trend of the monthly variation of wind pressure was qualitatively similar to that of wind erosivity (Wr).

Dawelbait et al. (2013) identified changes in the ground cover of the endangered range plant species in north Kordofan state. They found changes in range attributes which were

* Corresponding author e-mail: abdo.momti76sag@gmail.com

clearly noticed and that some important plants are being endangered. Their study recommended a strategy for range land rehabilitation to be adopted in relation to composition of important, palatable endangered plant species. These studies are very important as they contribute to the determination of the trends of range land for the sake of controlling degradation in plant and natural vegetation composition; furthermore, carrying capacity should be calculated to avoid the negative impact of overgrazing.

Biro et al. (2013) analyzed and monitored the land use land cover (LULC) changes using multi-temporal Landsat data for the years 1979, 1989 and 1999 and ASTER data for the year 2009. In addition, efforts were made to discuss the impact of LULC changes on the selected soil properties. Three main LULC types were selected to investigate the properties of soil, namely, cultivated land, fallow land and woodland. Moreover, soil samples were also collected at two depths of surface soil from ten sample plots for each of the LULC type. For these soil samples, various soil properties such as texture, bulk density, organic matter, soil pH, electrical conductivity, sodium adsorption ratio, phosphorous and potassium were analyzed. The results showed that a significant and extensive change of LULC patterns has occurred over the last three decades in the study area. Further, laboratory tests revealed that soil properties were significantly affected by these LULC changes. The change of the physical and chemical properties of the soil may have attributed to the changes in the LULC resulting in land degradation, which in turn has led to a decline in soil productivity. Adam et al. (2014) assessed land degradation in Rawashda, area Gedaref state by using remote sensing, GIS, and soil techniques.

Ali et al. (2012) assessed and mapped soil degradation at Gadambalyia schemes in Gedaref state, in relation to sorghum productivity. Satellite images and GIS were integrated with soil quality to detect and map the type and degree of severity of soil degradation. Soil quality indicators were determined and compared with the same indicators that were determined previously at the same locations in 1976. The System Integration Risk model was used to classify the area of schemes according to soil chemical and physical degradation. The results revealed that the soil qualities in 2005 were significantly affected ($P< 0.001$) both negatively and positively, compared with the 1976 data. Soil chemical degradation ranged from low to severe, while the soil physical properties were not significantly degraded.

A national research project on the assessment and mapping of wind erodibility in various states was undertaken in the Desertification and Desert Cultivation Studies Institute (Medani and Mustafa, 2004; Mustafa and Medani, 2003; Mohammed and Mustafa, 2005; Rehan and Mustafa, 2005; Abdelwahab et al., 2009; Mohammed and Mustafa, 2011; Hassan and Mustafa, 2011; Abdelgadir et al., 2013). Soil indicators were recommended for the prediction of non-erodible soil particles (NEP) and wind erodibbility of the soils (WE). For example, Mustafa and Medani (2003) recommended the use of (Silt + Sand) / (Clay + $CaCO_3$) ratio for the prediction of NEP and WE of the soils of Khartoum State. WE showed a quadratic increase with the increase of this ratio. It was concluded that this is a better indicator than the clay ratio alone, which was previously recommended by other authors. Previous wind erosion studies included an assessment of the intensity of wind erosion (IWE) in El-Obeid (Kheirelseid, 1998), north east Al-Butana (Haikal, 2005) and the central part of the Northern State (Abuzied et al., 2015). Managing soils under intensive use and restoring eroded lands are top priorities to a sustained agronomic and forestry production besides conserving soil and water resources. Assessing and Monitoring eroded lands in the affected areas in Sudan are essential for designing control measures for enhancing agricultural development particularly in arid lands. The present study was undertaken to achieve the following objectives:

I. To generate comprehensive comparative quantitative data on the intensity of wind erosion (IWE) in bare lands in the Gozalhalag area, River Nile State, using both horizontal and vertical traps.
II. To investigate the direction and monthly variation of the intensity of wind erosion.
III. To generate the interrelationship between the intensity of wind erosion measured by horizontal traps (IWEh) and the intensity of wind erosion measured by vertical traps (IWEv).

2. Materials and Methods

2.1. The Study Area

The River Nile State lies between latitudes 16° and 22° N and longitudes 31° 88¢ and 35° 70¢ E. It is dominated by hyper–arid and arid climatic zones with mainly two seasons, a hot summer from April to September and a cold winter from October to March. The mean annual rainfall is less than 100 mm, and temperatures as high as 49° C are not uncommon during the period extending from April to June (Izzeldin and Ahmed, 2004). Winds prevail from the N and NNE with a mean maximum speed of 17.6 km/hr; these winds cause the greatest sand movement blowing from October to May, and become worse from February to May. The wind direction is stable throughout the year except for the months of July, August, and September when the wind blows from S, SW, and SSW directions (table 1). The wind speed is measured at 15.2 m height every three hours. In the River Nile State, the erosive winds (velocity>5.4 m/s) varied

widely in direction and speed during each month and day even within the same climatic season. The high percentages of erosive wind contribution in the summer season blowing from SW and S directions were 75.6%, and 10.5 respectively, whereas the high percentages of erosive wind contribution in the winter season blowing from NNW and N directions were 59.4%, and 19.9. Erosive wind ranged from 0 (Nov., 2008) to 369.8 (Feb., 2009) with a mean of 255.1 $(m/s)^3$, and a CV of 43.6%.

Under such climatic conditions, wind erosion is the predominant desertification process. The current study was conducted in a bare land in Gozalhalag village, about 50 km south east Atbara, River Nile State, to produce broad–base data on wind erosion in two-seasons (August 2008-March 2009, August 2009-March 2010).

Table 1. Monthly dominant wind direction and mean wind speed (1980-2000) in the study area.

Month	Atbara station	
	Direction	Wind speed (m/s)
January	N	2.7
February	N	3.2
March	N	2.7
April	N	3.6
May	N	1.8
June	N	2.3
July	SW	2.3
August	SSW	2.3
September	SSW	1.8
October	N	1.8
November	N	2.3
December	N	2.7

Source: Sudan Meteorological Department.

2.2. Methods

Oil cans [25 cm (l) × 23 cm (w) x 27 cm (h)] were used as horizontal sand traps for the measurement of wind erosion. They were buried in the soil leaving the open end level with the soil surface. A vertical sand trap was constructed locally as described by Leatherman (1978). It consisted of two PVC tubes. The first one was 60 cm long with an inside diameter (i.d.) equal to 5.1 cm, permanently closed at the bottom end, and inserted completely in the soil with its open end leveled with the soil surface. This tube is stationary. The second tube, was 90 cm long and 4 cm i.d. and was closed at the top and bottom with a moveable metallic cap in the bottom, and had two similar slits, which were 2 cm wide and 30 cm long, cut in the two opposite sides of the tube. One slit serviced as a collection orifice aligned toward the wind direction, while the other was covered with a fine metallic screen to restrict soil particle movement and allow for a free wind flow. In each field, IWE (ton/ ha/day) was assessed using three replicates for both vertical and horizontal traps in the following directions: West (W), North West (NW), North (N) and North east (NE), these directions were selected due to the predominance of northerly winds in the State. Vertical traps were installed at a spacing of 60 cm between the same direction and 1 m from another direction. The replicate traps were installed so that they do not obstruct free wind flow to the other traps. The horizontal traps were placed at a spacing of one meter from the vertical. Each month the horizontal traps were removed and soil particles were collected and weighed. Furthermore, the particles collected in the metallic moveable tube of the vertical traps were also weighed. To convert trapped soil particles into (ton/ ha/day) the following equations were used:

$$IWEv = \frac{\text{Mass (g) x 100}}{\text{Area (2x30cm) x days (30)}}$$

$$IWEh = \frac{\text{Mass (g) x 100}}{\text{Area (23x25cm) x days (30)}}$$

where:

IWEv= intensity of wind erosion measured by vertical traps.

IWEh= intensity of wind erosion measured by horizontal traps.

Mass (g) = the weight of soil particles collected in the traps in grams.

Area (2x30cm)= the dimension slit of the vertical trap 2 cm wide and 30 cm long.

Area (23x25cm)= the dimension of oil cans 23 cm wide and 25 cm long serving as horizontal traps; and 30 refers to the numbers of days in month.

2.3. Statistical Analysis

The statistical design for this factorial experiment was randomized complete block design. Analysis of variance and separation of means were undertaken according to Gomez and Gomez (1984).

3. Results and Discussion

3.1. First Season (August 2008-March 2009)

Table 2 shows the effects of wind direction and month on IWEh. For the main direction effect, the mean IWEh ranged from 99.9 (W) to 109.8 (NE) with a mean of 104.4 tons/ha/day, a standard deviation (STD) of 4.13 tons/ha/day and a coefficient of variation (CV) of 4%.The mean IWEh by the NE wind was significantly greater than that produced by the W direction. However, it was not significantly different from that given by N or NW winds, which were not significantly different from that produced by W winds. The mean IWEh values for the main month effect ranged from 260 (Sept.) to 2.1 (Nov.) with a mean of 104.4 tons/ha/day, a STD of 97.49 tons/ha/day and a CV of 93.4%. Statistically, IWEh was in the following significant order: Sept. > Aug. > Oct. > Mar. > Jan = Feb > Dec. = Nov.; the equal sign indicates that there was no significant effect.

Table 2. Effect of direction and month on the IWEh (tons ha^{-1} day^{-1}) measured in the bare field surface during the first season*

Direction	Months								
	Aug.	Sept.	Oct.	Nov.	Dec.	Jan.	Feb.	Mar.	Mean
W	216.2	258	128.0	1.4	5.4	60	58	72.5	99.9 b
NW	224.1	260	130.0	2.3	9.0	66	58	75.4	103.1ab
N	229.0	260	129.3	2.2	2.1	67	64	84.1	104.7ab
NE	270.1	262	133.3	2.4	1.3	67	61	81.2	109.8 a
Mean	235 b	260 a	130.2c	2.1f	4.5f	65 e	60.3e	78.3d	

**Means followed by the same letter in the same row or column are not significantly different from each other at the 0.01 level by Duncan Multiple Range Test.*

Table 3 shows the effects of wind direction and month on IWEv. The mean IWEv values ranged from 30.7 (W) to 57.9 (NE) with a mean of 43.3 tons/ha/day, a STD of 11.52 tons/ ha/day and a CV of 26.6%. The mean IWEv value produced by the NE wind was significantly greater than that produced by the wind blowing from the three other directions. The IWEv produced by N winds was significantly greater than that produced by W winds, but it was not significantly different from that produced by NW winds. The IWEv values produced by W and NW winds were not significantly different. The mean monthly data ranged from 80.7 (Sept.) to 0.65 (Dec.) with a mean of 43.3 tons/ ha/ day, a STD of 29.52 tons/ ha/ day and a CV of 68.1%. The monthly IWEv values were in the following statistically significant order: Sept. = Aug. > Oct. = Mar. = Feb = Jan. >. Nov. = Dec. This order is nearly similar to that for IWEh. The seasonal overall mean data obtained by the vertical traps was 41.5% compared to that obtained by the horizontal traps. The IWEv values obtained for each month or direction were lower than the corresponding IWEh values.

Table 3. Effect of direction and month on the IWEv (tons ha^{-1} day^{-1}) measured in the bare field surface during the first season*

Direction	Months								
	Aug.	Sept.	Oct.	Nov.	Dec.	Jan.	Feb.	Mar.	Mean
W	36.0	57.0	65.0	1.3	0.93	28.3	28.3	29.0	30.7 c
NW	42.0	90.0	24.0	2.0	0.37	51.0	51.0	50.0	38.8 bc
N	115.0	50.0	63.3	3.0	0.58	40.0	45.3	49.4	45.8 b
NE	101.7	125.6	83.3	1.1	0.71	51.0	50.0	50.0	57.9 a
Mean	73.7 ab	80.7 a	58.9 c	1.9 d	0.65d	42.6c	43.7c	44.6c	

**Letters as explained in Table1.*

Table 4 shows that the ratio of (IWEv/IWEh) according to month and direction. With respect to direction, the ratio ranged from 47.3 (NE) to 69.3 (W) with a mean of 58.5% and a CV of 15.9%. As for the monthly variation, the ratio ranged from 9.5 (Nov.) to 85.6% (Dec.) with a mean of 49.1% and a CV of 51.2%: 38.2 (W) to 67.2 (NW) with a mean of 56.2%. Figure 1 depicts a highly significant ($P < 0.001$) polynomial relationship between IWEv and IWEh.

Table 4. The ratio of IWE measured by vertical (IWEv) to that measured by horizontal (IWEh) traps as affected by month and direction of measurement in the bare field surface during the first season.

Month	IWEv	IWEh	Ratio, %	Direction	IWEv	IWEh	Ratio, %
January	42.6	65	65.5	W	30.7	99.9	30.7
February	43.7	60.3	72.5	NW	38.8	103.1	37.6
March	44.6	78.3	57	N	45.8	104.7	43.7
August	73.7	235	31.4	NE	57.9	109.8	52.7
September	80.7	260	31	Mean			41.2
October	58.9	130.2	45.2	STD			9.3
November	1.9	2.1	90.5	CV			22.7
December	0.65	4.5	14.4				
Mean			50.9				
STD			25.1				
CV			49.4				

Ratio=(IWEv/IWEh)x100

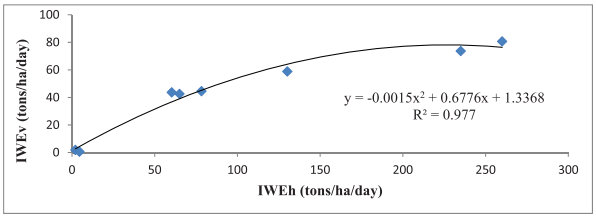

Figure 1. Regression relationship between intensity of wind erosion obtained by horizontal (IWEh) and vertical (IWEv) traps installed at the bare field surface in the first season.

3.2. Second Season (August 2009-Mrach 2010)

Table 5 shows the mean IWEh values for the main direction effect. The mean IWEh values ranged from 47.1 (W) to 49.2 (N) with a mean of 46.3 tons/ ha/ day, a STD of 3.51 tons/ ha/ day and a CV of 7.6%. The mean IWEh produced by wind blowing from the four directions were not significantly different. The mean IWEh values for the main month effect ranged from 2.3 (Sept.) to 97.3 (Aug.) with a mean of 46.3 tons/ ha/ day, a STD of 38.56 tons/ ha day and a CV of 83.2%. The monthly main effect was in the following significant order: Aug. = Mar. > Jan = Feb. > Oct. = Dec.> Nov. = Sept. The IWEh in the second season was much lower than that in the first season. The overall mean IWEh value in the second season was 44.3% of that in the first season. There was also variation in the order of magnitude of mean values in the corresponding months or directions.

Table 5. Effect of direction and month on the IWEh (tons ha^{-1} day^{-1}) measured in the bare field surface during the second season*

Direction	Months								
	Aug.	Sept.	Oct.	Nov.	Dec.	Jan.	Feb.	Mar.	Mean
W	116.9	1.7	18.4	4.3	30.0	55.8	59.7	91.2	47.1 a
NW	70.5	2.5	29.0	6.0	4.5	63.0	63.1	91.1	41.2 a
N	90.8	2.4	42.6	8.5	1.9	70.1	64.0	100.9	47.7 a
NE	111.1	2.4	18.4	1.2	33.4	64.2	64.6	97.9	49.2 a
Mean	97.3 a	2.3 d	27.1 c	5.0 d	17.5 cd	63.3 b	63.9 b	95.3 a	

**Letters as explained in Table1.*

Table 6 shows that the mean IWEv values for the main direction effect ranged from 16.8 (W) to 29.8 (NE) with a mean of 22.7 tons/ ha/ day, a STD of 5.39 tons/ ha/ day and a CV of 23.8%. The mean IWEV produced by NE winds was significantly different from that produced by W winds, but not different from that blown by N wind. North wind gave higher IWEv from W winds but not different from NW winds, which gave significantly higher IWEv than W winds. The monthly IWEv data ranged from 0.4 (Nov.) to 49.9 (Mar.) with a mean of 22.7 tons/ ha/day, a STD of 22.39 tons/ ha/ day and a CV of 98.4%. The main effect of the month showed that IWEv was in the following significant order: Mar. = Aug. = Jan = Feb. > Oct. = Sept. = Dec. = Nov. The seasonal overall mean data obtained by vertical traps was 49% compared to that obtained by the horizontal traps. The IWEv values obtained for each month or direction were lower than the corresponding IWEh values.

Table 7 shows that the ratio of (IWEv/IWEh) varied with month and direction. The ratio ranged from 35.7(W) to 60.6 (NE) with a mean of 50.8 and a CV of 21.1% and from 7.6 (Nov.) to 82.6% (Sept.) with a mean of 43% and a CV of 67 %. Figure 2 depicts a highly significant ($P<0.001$) polynomial relationship between IWEv and IWEh.

Table 6. Effect of direction and month on the IWEv (tons ha^{-1} day^{-1}) measured in the bare field surface during the second season*

Direction	Months								
	Aug.	Sept.	Oct.	Nov.	Dec.	Jan.	Feb.	Mar.	Mean
W	35.2	1.4	1.7	0.17	1.9	27.1	27.4	39.2	16.8 c
NW	25.0	2.0	2.0	0.31	1.7	46.6	39.2	53.8	21.3bc
N	36.0	2.8	4.8	0.68	1.3	39.5	46.6	51.0	26.2ab
NE	74.1	1.3	8.5	0.37	1.1	50.2	47.6	55.6	29.8a
Mean	49.3a	1.9b	4.3b	0.38b	1.5b	40.9a	40.2a	49.9a	

**Letters as explained in Table1.*

Table 7. The ratio of the intensity of wind erosion measured by vertical (IWEv) compared to that measured by horizontal (IWEh) traps as affected by month and direction of measurement in the bare field surface during the second season.

Month	IWEv	IWEh	Ratio, %	Direction	IWEv	IWEh	Ratio, %
January	40.9	63.3	64.6	W	16.8	47.1	35.7
February	40.2	63.9	62.9	NW	21.3	41.2	51.7
March	49.9	95.3	52.4	N	26.2	47.7	45.9
August	49.3	97.3	50.7	NE	29.8	49.2	60.6
September	1.9	2.3	82.6	Mean			48.5
October	4.3	27.1	15.9	STD			10.4
November	0.38	5.0	7.6	CV			21.5
December	1.5	17.5	8.6				
Mean			43.2				
STD			28.7				
CV			66.4				

Ratio=(IWEv/IWEh)x100

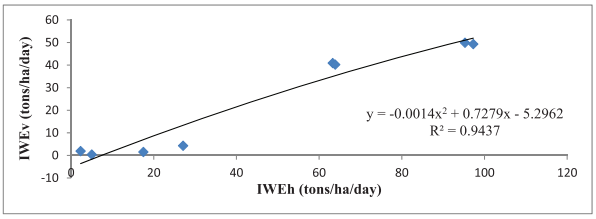

Figure 2. Regression relationship between intensity of wind erosion obtained by horizontal (IWEh) and vertical (IWEv) traps installed at the bare field surface in the second season.

3.3. Discussion

The intensity of wind erosion measured by horizontal traps (IWEh) in all directions and months was found significantly much higher than the intensity of wind erosion measured by vertical traps (IWEv). The overall mean IWEh value was 2.4 and 2.0 fold the overall mean IWEv value in the first and second seasons, respectively. This was attributed to the fact that horizontal traps collected soil particles transported by the three mechanisms of wind erosion, namely saltation, surface creep, and suspension; whereas vertical traps collected particles transported by saltation only (Abdelwahab and Mustafa, 2013). The seasonal overall mean data obtained by vertical traps were 41.5% and 49% compared to those obtained by the horizontal traps in the first and second season respectively. The IWE measured by both traps in the first season were much higher than those measured in the second season. The overall mean IWEh and IWEv in the first season were 2.3 and 1.9 fold compared to those in the second season, respectively. This effect was attributed to the higher wind erosivity in the first season. The wind erosivity was 2483 and 2309.3m^3/sec^3 for the first and second seasons, respectively (Abdelwahab and Mustafa, 2013). There is a variation in the order of magnitude of the monthly IWE. The variation according to direction was much lower than the monthly variation due to the higher monthly variability of wind erosivity. The IWE values obtained in Aug. and Sept. were caused mainly by S and SW winds, which were stronger but shorter in duration; these winds are slowdown the desert progress towards the south. However the prevailing N. winds caused high IWE values in Jan. (NNW), Feb. (NW), and Mar. (NW), and days of dust storms. Finally, the effects of high temperature on pressure and wind velocity in summer caused the transportation of heavier and denser particles compared to the opposite effect of low temperature in (Oct., Nov., and Dec.). This finding agrees with the previous findings of Abuzied (2009) and Farah (2003), which emphasized the minimum sand transport recorded in November and December.

In the two seasons, the ratio of (IWEv/IWEh) varied with month and direction; this may be attributed to the high impact of wind erosivity in the targeted area. Furthermore in the two seasons the regression between IWEv and IWEh gave a highly significant polynomial relationship ($P< 0.001$, $r^2=0.98$) and ($P< 0.001$, $r^2=0.94$), respectively. This result can be only attributed to the overlaps and interdependence in the movement of soil particles for each of the two types of traps.

4. Conclusions and Recommendations

The prevailing wind directions are north, north east, and North West in Jan., Feb., and Mar. The southerly winds were caused mainly by S and SW winds, which were stronger but shorter in duration. Regression between IWEv and IWEh gave a highly polynomial relationship; significant ($P< 0.001$, $r^2=0.98$) and ($P< 0.001$, $r^2=0.94$) for the first and second seasons respectively. The River Nile State occupies a large area with varying metrological conditions. Accordingly, there is a pressing need for establishing new meteorological stations in some appropriate locations. Comprehensive studies on wind velocity and direction should be undertaken in the early stages of establishing a scheme to help in making the design of the shelterbelt. Very little attention is given to studies on wind data analysis; unfortunately, most research on 1WE assessment is conducted in part of the affected states due to the limited financial resources given to research on anti-desertification in this area.

References

Abdelgadir, I.A., Mustafa, M.A., Ganawa, E.S. (2013). Assessment and mapping of wind erodibility of soils of south western Kassala State in Sudan. Sudan Journal Desertification Research 5: 19-33.

Abdelwahab, M.H., Mustafa, M.A., Ganawa, E.S. (2009). Spatial variation of wind erodibility of soils from the Northern State, Sudan. Sudan Journal of Desertification Research 1: 56-70.

Abdelwahab, M.H. and Mustafa, M.A. (2013). Assessment of wind erosion in bare and Lucerne-cultivated lands in south east Atbara, River Nile State, Sudan. Sudan Journal of Desertification Research 5(1): 88-100.

Abdelwahab, M.H. and Mustafa, M.A. (2015). Monthly and diurnal variation of wind speed and direction and wind erosivity in River Nile State, Sudan. The International Journal of the Environmental and Water 4 (4): 1-10.

Abdelwahab, M.H., Doka, A.M., Mustafa, M.A. (2014). Assessment of wind erosion using remote sensing techniques in Atbara Area, River Nile State, Sudan. Sudan Journal of Desertification Research 6 (1): 1-14.

Abuzied, H.M. (2009). Mapping and Assessment of Wind Erosion in Central Northern State, Sudan, Ph.D. Thesis, Desertification and Desert Cultivation Studies Institute, University of Khartoum, Sudan.

Abuzied, H.M., Mustafa, M.A., Hamid, A.A. (2015). Rate of sand movement by saltation and surface creep in the Central Part of the Northern State, Sudan. Sudan Journal of Desertification Research 7 (1): 40-51.

Adam, A.H., Elhag, A.M., Salih, A., Adam, S.M. (2014). Land degradation assessment in Rawashda Area, Gedaref State, Sudan using remote sensing, GIS and soil techniques. International Journal of Scientific and Research Publications 4(2): 1-9.

Ali, H.O., Almalik, E.M., Augusseau, X., Eljack, E.A. (2012). Assessment and mapping of soil degradation at Gadambalyia Schemes, El Gedarif State, Sudan. Sudan Journal of Desertification Research 4(1): 95-110.

Biro, K., Pradhan, B., Buchroithner, M., Makeschin, F. (2013). Land use/ Land cover Change Analysis and it is Impact on Soil Properties in the Northern Part of Gedarif Region, Sudan Land Degradation and Development 24: 90-120.

Dawelbait, E.M., Khatir, A.A., Morakaah, A.M. (2013). Change in ground cover and identification of endangered range plant species in North Kordofan State, Sudan. Sudan Journal Desertification Research 5(1): 101-112.

Farah, A.M. (2003). Wind erosion in Khartoum State, Ph.D. Thesis, Faculty of Agriculture, University of Khartoum, Sudan.

Gomez, K.A. and Gomez, A.A. (1984) Statistical Procedures for Agricultural Research. 2nd Edition, an International Rice Research Institute Book, Wiley-Interscience Publication, John Wiley and Sons, New York.

Haikal, S.M.S. (2005). Assessment and Mapping of Wind Erosion in North East Butana Area, Ph.D. Thesis, (Desertification and Desert Cultivation studies) University of Khartoum, Sudan.

Hassan, A.A. and Mustafa, M.A. (2011). Assessment and mapping of wind erodibility of Aridisols and Entisols in the Nile State, Sudan. Sudan Journal of Desertification Research 3(1): 49-61.

Izzeldin, S.I. and Ahmed, S.H. (2004). A proposed Plan of Action for Research on Desertification in the Sudan: Northern and Nile States. The National Forum of Scientific Research on Desertification in the Sudan Al Sharga Hall, University of Khartoum, Khartoum, Sudan 16-18 March, 2004: 325pp.

Kheirelseid, A.M.R. (1998). Wind Erosion Study in North Khordufan, El-Obeid. Ph. D. (Agric.) thesis, University of Khartoum, Khartoum, Sudan.

Leatherman, S.P. (1978). New Aeolian sand traps design. Sedimentology 25: 303-306.

Medani, G.H. and Mustafa, M.A. (2004). Wind erodibility of soils from North Darfur State. University of Khartoum. Journal of Agricultural Science 11(3): 369-384.

Mohammed, A.Y. and Mustafa, M.A. (2005). Wind Erodibility of Soils from the White Nile State, Sudan. In the proceeding of the Regional Workshop "Scientific Research and National Research Plans of Action for Combating Desertification.", Tuesday 22-Thursday 24 November 2005, Al Sharga Hall, University of Khartoum.

Mohammed, M.A.E. and Mustafa, M.A. (2011). Assessment and mapping of wind erodibility of Aridisols and Entisols in the Red Sea State, Sudan, University of Khartoum. Journal of Agricultural Sciences 19(2): 128-144.

Mustafa, M.A. and Medani, G.H. (2003). Wind erodibility of soils from Khartoum State. University of Khartoum. Journal of Agricultural Science 11(2): 149-164.

Rehan, S.A. and Mustafa, M.A. (2005). Wind erodibility of soils from the Gezira State, Sudan in the proceeding of the Regional Workshop "Scientific Research and National Research Plans of Action for Combating Desertification." Tuesday 22-Thursday 24 November 2005, Al Sharga Hall, University of Khartoum.

JJEES

JJEES (2020) 11 (3): 164-173
ISSN 1995-6681

Jordan Journal of Earth and Environmental Sciences

Analysis of Mesostructures along Jarash- Irbid Highway, Northern Jordan

Abdullah Diabat*[1], Tahreer Assaqir[2], Najmeddin Yusuf[3], Muhammad Atallah[4]

[1]Al al-Bayt University, Institute of Earth and Environmental Sciences, Department of Applied Earth and Environmental Sciences, Al al-Bayt University, Jordan

[2, 3, 4]Yarmouk University, Faculty of Sciences, Department of earth and environmental sciences, Jordan

Received 26 January 2020; Accepted 29 March 2020

Abstract

Geologic structural surveys were conducted in many road cuts and quarries along the Irbid-Jarash highway, north of Thughart Asfour village. Meso-scale tectonic structures which were found in these stations including: folds, faults (Strike-slip, normal and reverse), joints, flower structures, boudinage structures and shear fractures, revealed that the area has undergone a local tensional as well as compressional stresses related to the regional one. More than 1385 fracture measurements were done using scanline, circle, and common methods in order to investigate the orientation and density of the fractures in different parts of the study area. Two dominant trends of joint sets (N-S and NNW to NW) and other minor trends (E-W, ENE-WSW and WNW-ESE) were found in the Cretaceous carbonate rocks (Wadi Es Sir Limestone Formation). The dominant trend sets represent the range of conjugated, hybrid, and extensional fractures in which the acute bisector of these represents the main trend of extensional fracture set, which in turn is consistence with the SHmax (maximum horizontal compressive stress axis) oriented NNW-SSE. Geometries of fractures in the carbonate rocks represent a continuum of structures at various stages of development that can be classified into two main geometric categories corresponding to increasing levels of brittle strain; bed- confined fractures and throughgoing fractures. Many throughgoing fractures develop subsequent to bed-confined joints by the coalescence of pre-existing joints. The spatial distribution of throughgoing fractures varies as a function of structural position. The highest frequency and estimated strain intensity have been located at the fold crests and fault zones.

Keywords: Mesostructures, Throughgoing fractures, Bed-confined joints, Wadi Es Sir Limestone Formation, Northern Jordan.

1. Introduction

Mesostructures or mesoscopic structures range in size from one centimeter to a few meters and include small faults, small folds, stylolites, cleavages, shear zones, veins, and joints (Hancock, 1985). In many studies of deformed rocks, the presence of mesostructures has provided a useful tool for analyzing the stress and strain patterns in host or regional structures (Hancock and Atiyya, 1979; Eyal and Reches, 1983; Eyal et al., 2001).

The study of mesoscopic structures helps in strain analysis, provides information that can help in the interpretation of regional structural relations, and can provide clues about deformation conditions and sense of movement during deformation. The development of mesofracture sets and systems, that are symmetrically-oriented about sedimentary layers and hinge lines, leads to a shortening or an elongation parallel to or normal for those directions (Hancock, 1985). Fracture density can be measured and described in a number of ways, namely total cumulative length of fracture within a given volume of rock divided by area of the circle. The measurement of fracture density used in conjunction with the circle inventory method is the summed length of all fractures within an inventory circles, divided by the area of the circle (Davis et al., 2011).

Eyal and Reches (1983) analyzed the mesostructures in Northern Palestine and found evidence from the mesostructures to support the hypothesis of strike- slip movement along the Dead Sea Transform. In Jordan, few detailed studies were carried out concerning mesostructures (e.g., Atallah, 1996; Al-Taj et al., 2003; Diabat et al., 2004; Diabat, 2009; Diabat, 2013; Radaideh and Melichar, 2015; Al-Awabdeh et al., 2016). Other areas in Jordan except for the DST fault have received little attention of tectonic and/ or structural studies. The area upon which this study is focused is one of these poorly-investigated areas in Jordan. The study area is located few kilometers to the north of Jarash city and is bounded by the coordinates: 32º 19′ & 32º 23′N and 35º 54′ & 35º 56′E (Figure 1). The field covered in this study extends along the Jerash- Irbid Highway, north of Thughrat Asfour village, where numerous mesostructures can be observed in

* Corresponding author e-mail: adiabat@aabu.edu.jo

road-cut exposures and quarries of Wadi Es Sir Limestone Formation providing an excellent opportunity to investigate the kinematics related to their development.

The aim of this study is to increase knowledge about the various structures, and get better resolution of the bed-confined fractures and throughgoing fractures of the study area.

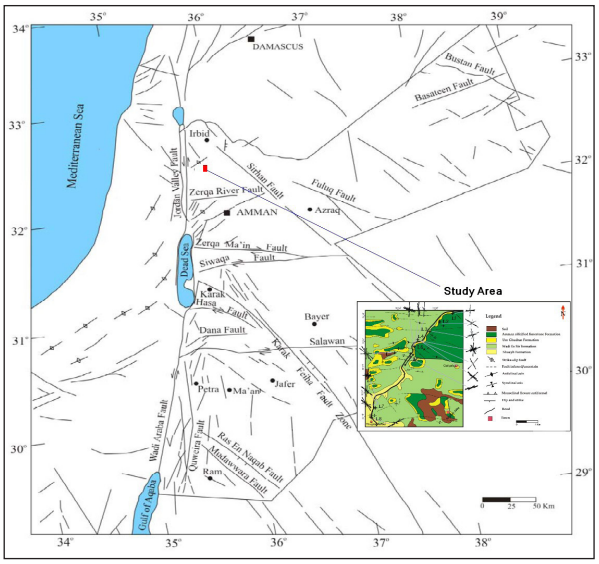

Figure 1. Structural pattern of Jordan and location of the study area (modified after Diabat and Masri, 2005).

2. Geological Setting

2.1. Stratigraphy

2.1.1. Ajloun Group

2.1.1.1. Shuayb Formation

The formation which conformably overlies the Hummar Formation consists mainly of yellow to yellow gray, thin- to medium-bedded marly limestone, nodular limestone, and dolometic limestone. The base of the formation is marked by the change from the hard dolometic limestone of the Hummar Formation which forms together with lower part of Shuayb a prominent cliff. The top is defined by a sudden change from gentle slopes to hard, thick-bedded and then to the massive dolomite and dolometic limestone of Wadi Es Sir Limestone Formation which form prominent cliffs and steep slopes. The Shuayb Formation was deposited in the Early Turonian in a moderate to shallow subtidal marine environment (Powell, 1989).

2.1.1.2. Wadi Es Sir Limestone Formation

The formation consists of three distinctive units. The lower part is comprised of dolomite, dolometic limestone, the middle part consists of soft marly limestone and limestone, and the upper unit consists almost totally of thick-bedded to massive limestone. The thick-bedded to massive limestone of the formation forms distinctive rocky steep slopes. The formation was deposited on a wide shallow marine carbonate platform within tidal to lagoon regimes. The formation marks the maximum extent of the marine transgress pulses during the Cenomanian to the late Turonian- middle Coniacian time (Abed, 2000).

2.1.2. Belqa Group

2.1.2.1. Wadi Umm Ghudran Formation

The best section of this formation is provided by the road-cut on the Irbid-Jarash road 0.5 km south east of Balila. The lower half consists of 15~m of yellow to white gray; locally pink gray, and buff, reworked, fragmental and fossiliferous chalky limestone which marks the unconformity with the underlying Ajlun Group. The upper half consists of about 15m of limestone and chalky limestone typically pink to yellow grey, hard, medium, to thin-bedded, fossiliferous to coquinal, and with chert concretions and bands toward the top, alternating with yellow to white grey, medium-bedded and soft chalk marl. The formation was deposited in a moderate to a deep- water pelagic environment during the late Coniacian to the Santonian time (Abdelhamid, 1995).

2.1.2.2. Amman Silicified Limestone Formation

The formation consists of dark brown to grey thick-bedded chert, phosphatic chert, silcified limestone, marl, siliceous coquina and brecciated chert which were formed in a shallow-marine environment during Santonian to Campanian (Abed, 2000).

2.1. Tectonic Setting

The study area is located to the east of the Dead Sea Transform (DST) (Figure 1). The DST separates the Arabian and Sinai-Palestine sub- plates, and connects the Red Sea in the south with the collision belt of southern Turkey. The Dead Sea Transform is left lateral, and is comprised of a zone of en-echelon strike-slip faults. Motion on the (DST) initiated in the Miocene and has a cumulated lateral displacement of about 105 km (e.g. Quennell, 1951; Quennell, 1983; Freund et al., 1970; Garfunkel, 1981). Geological observations indicate that two distinct paleostress regimes operated adjacent to the Dead Sea rift: 1) WNW- shortening and NNE-extension, beginning in the Turonian and associated with the development of the Syrian Arc fold belt and is attributed to the Syrian Arc Stress field (SAS). 2) Middle Miocene to recent NNW shortening and ENE extension, associated with the 105- km sinistral displacement along the Dead Sea Transform and the opening of the Red Sea, and is attributed to the Dead Sea stress field (DSS) (Eyal, 1996; Diabat et al., 2004). The concurrent development of the DST system has resulted in a complex tectonic history that has led to several phases of deformation in the relatively young Upper Cretaceous rocks (Eyal, 1996).

3. Methodology

This research depends essentially on field investigations. The methods of investigation include the following integrated components:

- The scanline method involves laying a tape along the length of an outcrop determining its orientation. Then, the position along it where each fracture intersects the tape, the orientation, length of the fracture, and the type of fracture are recorded.

- The Circle-Window method involves drawing a circle on the outcrop that encompasses at least thirty different fractures to make sure that the results are unbiased and statistically significant. Once the circle is on the outcrop, one counts the number of fractures that intersect the circle and the number of fractures that terminate within the circle. These two measurements provide an accurate density and intensity of the fractures.

- The Common method involves measuring a random-fracture orientation.

The specific locations were chosen to allow the determination of the change in density and intensity of the fractures nearing different structural features, such as faults and shear zones, and on differently-oriented surfaces, for instance horizontal and vertical surfaces, that were near each other.

Nine stations were selected which represented different parts of the study area. In the circle method, a circle of a known as well as a predetermined radius is traced on the surface hosting fracture; in this case, it was a bedding plane all the time and it requires measuring all the fractures occupied by the circle. The orientation, length, and width of each fracture within the circle were measured. Circles, having a radius of 3.5 m at least were traced out on the bedding plane by the help of chalk and a measuring tape; orientation of fractures were measured in terms of strike; length and width were measured by the help of a simple ruler and a measuring tape. To avoid repetition, each fracture was traced with chalk after the measurement. As for measuring orientation, only traces of the straight lines of the fractures were evident at the bedding plane and because of that only strikes of the fractures were measured.

4. Results

The study area has been sub-divided into nine main stations, namely along the Irbid- Jerash Highway; in abandoned quarries, and road-cuts. Table (1) and figure (2) show the location and type of structures that have been investigated in each station.

Table 1. Location, measurements and fractures density (f/m) of the stations in the study area.

Station No.	Coordinates	No. of data	Type of structures	Measuring method	Scanline method (f/m)	Circle method (f/m)
1	32º 22.633′ N 35º 56.268′ E	100	Fractures (joints, and faults)	Common	-	-
2	32º 22.425′ N 35º 55.890′ E	90	Joints, faults, and bedding planes	Scanline /common	7.8	-
3	32º 22.016’ N 35 º 55.592’ E	118	joints/bedding planes	scanline /common	14.8	-
4	32º 21.780′ N 35º 55.319′ E	231	Fractures (joints, strike-slip faults)	common/ circle / scanline	5.1	5.8
5	32º 21.701′ N 35º 55.223′ E	312	Fractures (joints, strike-slip faults)	Common/ circle /scanline	6.3	1.7
6	32º 21.701′ N 35º 55.223′ E	79	Fractures, normal faults, thrust faults, strike slip faults	common /scanline	7.9	-
7	32º 19.674′ N 35º 56.085′ E	387	Fractures (joints, strike-slip faults), bedding planes	common /circle /scanline	6.2	8.1
8	32º 19.305’ N 35º 55.147’ E	37	Fractures (joints, normal faults, strike-slip faults)	common/ scanline	5.75	-
9	32º 21.229’ N 35º 54.348’ E	31	joints, strike-slip faults	common / scanline	4.7	-

Orientation data were collected from the Wadi Es Sir Limestone Formation (Turonian) (Figure 2). The sections consist of limestone beds, interlayer with marlstone and chalky limestone, and vary in thickness at different places. The majority of rocks are highly-fractured. The fractures encountered in the study area are either extensional spanning numerous beds, or are constructed in a defined layer. Joint orientations continued from one to three joint sets in each station. The majority of joints have surface structures such as the plumose structure or mineralization. More than 70 throughgoing fractures were measured in the study area; they exhibit a wide range of geometries and dimensions.

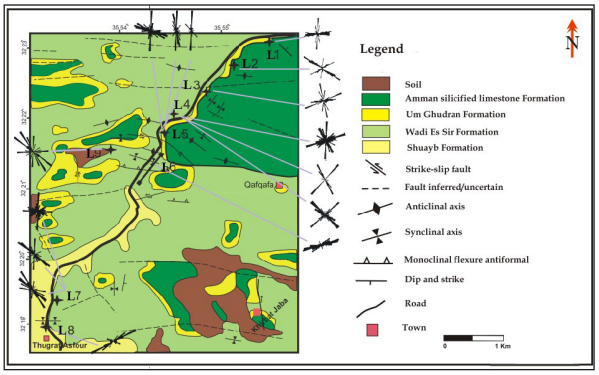

Figure 2. Geological map with displayed trends of measured structures in each station.

All throughgoing fractures are steeply dipping to vertical, and despite the considerable scattering in orientation, they reveal dominant ENE- WSW, NW-SE and N-S trends. Many extensional fractures have been filled with calcite.

Bedding plane orientations that have been measured along road–cuts and other places show a gentle dip (<15º). Faults encountered in the study area include the three main types (normal, reverse and strike-slip). The most abundant is the strike- slip with a ratio of 70%. At less amounts, the normal faults are distributed in many stations especially road cuts, forming small horsts and grabens, and listric structures.

The data for each station were plotted using stereographic projection and rose diagrams. The geological map of the study area is shown in figure (2) with the detailed structural features and rose diagrams.

Station 1

One-hundred measurements were taken from an abandoned quarry located at the eastern side of the Irbid-Jerash road (Figure 2 and Table 1). The measurements included joints and strike-slip faults. Two main set trends were observed; N-S and E-W.

Some of these fractures are confined to specific beds and others are throughgoing. Slickenlines appear clearly on the fault planes that indicate the movement direction.

Station 2

Ninety measurements were taken from road cuts at the eastern side of the Irbid– Jarash road (Table 1 and Figure 2). Measurements include bedding planes, joints, and small faults. Bedding plane orientations have been measured forming an anticline slightly plunging toward NNW (Figure 3). Fracture planes are vertical to sub-vertical and have a main trend oriented NW-SE and two minor trends oriented NNE-SSW and NE-SW. The majority of fractures are confined to the bedding and show a high density forming swarms of closely-spaced joints (5cm). Fractures were measured using the scanline method and other common methods (Table 1) (Figures 4 - 5):

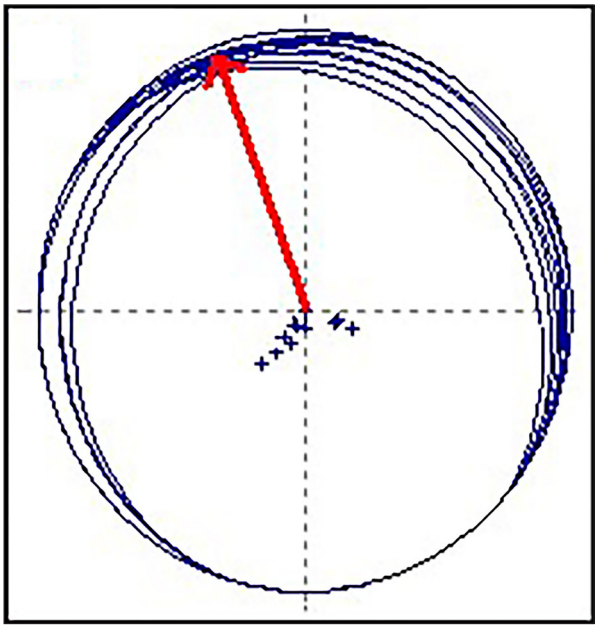

Figure 3. Stereoplot of local slightly plunging anticline towards NNW.

The red arrow is the plunge direction; the great circles are the bedding planes; while crosses are the poles to bedding planes.

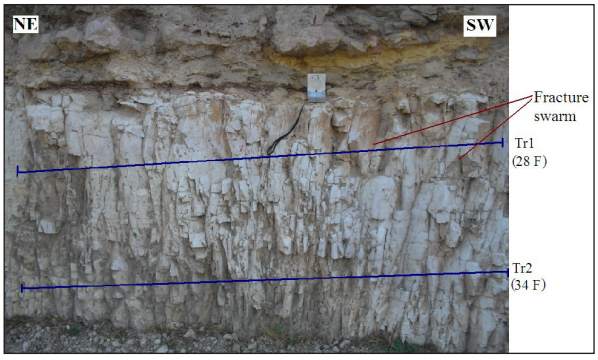

Figure 4. Fracture swarms of closely-spaced extensional to hybrid fractures. Tr.1 and Tr. 2 represent the number of measured fractures.

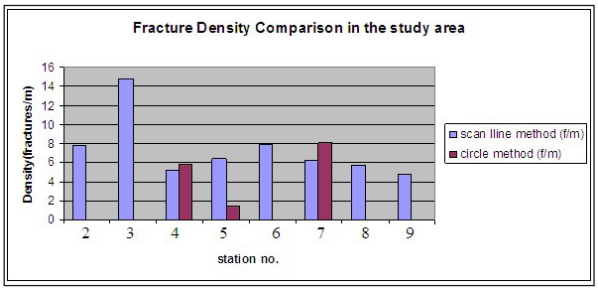

Figure 5. Histogram represents fractures density in each station.

Many structures can be traced along the road cut; a positive flower structure occurred as a consequence of the compressive stresses affecting the stratigraphic layering.

A fault zone spanning the entire exposure was observed at the road cut. The zone of deformation is characterized by the presence of gouge, crushed rocks, and a dragging of strata.

Station 3

One-hundred and eighteen measurements were taken from a quarry at the eastern side of the Irbid- Jerash road using scanline and common methods (Table 1 and Figure 3). Rocks are highly deformed forming a gentle anticline plunging to NNE (Figure 6). Joints show two main set trends ENE-WSW and NNW-SSE. Fractures in most cases are aligned in a vertical sequence. A major multilayer dextral fault was encountered in this station striking E-W and dipping 60º toward the south (Figure 7). The fault plane is highly polished and the rocks adjacent to the fault zone are highly deformed, tilted, and brecciated.

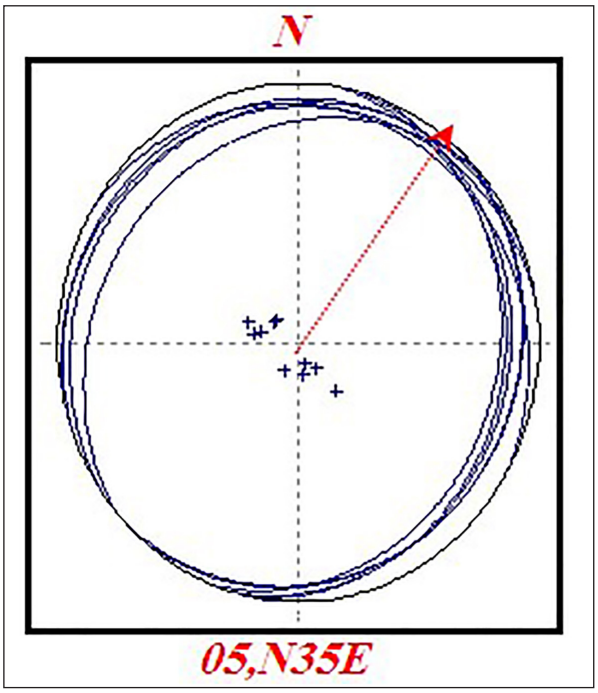

Figure 6. Stereoplot of a gently plunging anticline. The number and arrow in red color is the plunge and plunge direction (05/ N35E) of the anticline; crosses are poles to bedding planes.

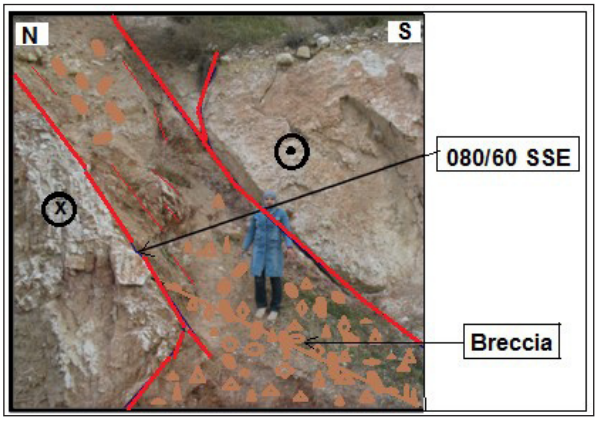

Figure 7. A dextral fault zone cut across the dipping strata.

Station 4

Two-hundred and thirty-one fracture measurements were taken from a quarry at the western side of the Irbid-Jerash road (Table 1 and Figure 2). Fractures density has been calculated using scanline, circle, and common methods (Table 1). Two main fracture sets oriented ENE-WSW, N-S and two minor sets oriented NNW-SSE, NW-SE were observed. Joints are steeply dipping, aligned in a vertical to a sub-vertical sequence. The investigated fractures are grouped into two main types due to their development (according to Gross and Eyal, 2007):

Bed-confined joints: which are confined to individual beds (unmineralized joints) and are closely-spaced.

Multilayer joints that cut across numerous beds (throughgoing fractures) that developed subsequent to the bed-confined joints. They commonly form by coalescence (linkage and preferential widening) of preexisting joints. They are grouped into three main categories based on their geometries;

a. Incipient: steeply dipping, sub-parallel fracture segments consisting of slightly widened and bed-confined cross joints.

b. Linked throughgoing fracture: continuously connected from their lower to upper tips, and in some cases are composed of numerous, vertically-aligned cross joints linked together across stratigraphic intervals by short segments consisting of bed-parallel and shallow-dipping fractures resulting in a zigzag geometry.

c. Throughgoing fractures with aperture: they are linked structures that have developed significant mechanical aperture (>0.5cm) across the majority of opposing segment walls. The apertures reflect dominantly an opening mode of displacement.

Slickenlines are preserved on fault surfaces serving as excellent kinematic indicators of a strike-slip motion (Figure 8). Plumose structures are formed on joint surfaces to represent the point at which the joint started to grow representing the inhomogeneous behavior in rocks when subjected to stress.

Figure 8. Slickenlines with calcite steps as a sense of movement indicator of sinistral strike-slip fault, in which the missing plane moved in the direction of the blue arrow.

Station 5

Three-hundred and twelve fracture measurements were taken from a quarry at the eastern side of the Irbid- Jerash road (Table 1 and Figure 2). Circle and scanline methods were also applied in this station to compare the fractures' density with the other stations (Table 1). Joints' orientation is grouped into two trends; N-S and WNW-ESE. Many joints aligned in vertical to sub-vertical planes. Other throughgoing joint sets have a parallel trend and are oriented NNW. Joints were enlarged by water solutions forming small cavities (Figure 9). Many throughgoing fractures are linked along the sequence and others are filled with calcite.

Figure 9. Systematic throughgoing fractures enlarged by solutions.

Station 6

Seventy-nine fracture planes were taken at the eastern side of the Irbid-Jerash road cut using scanline method (Table 1 and Figure 3). The main fracture set trend is oriented ENE- WSW and a minor set is oriented NNW-SSE. The characteristic feature along the road cut is the presence of many types of mesostructures e.g. local folds, the high density of normal faults forming horsts and grabens.

Most of normal faults were observed in this station along the road cut. Their geometries vary from short to multilayers that span the entire exposure. These faults cluster into two populations based on orientation, forming a conjugated system with a mean dip of (60º- 75º), and the majority of these faults strike NW-SE.

Special structural features were observed in the rock layers in this station including the boudinage structure (Figure 10). Dipping strata are highly-faulted by reverse faults and thrust faults forming wedge–thrust faults (Figure 11). They are curved and accompanied by folding and uplift depending on the direction of curvature with respect to the sense of displacement.

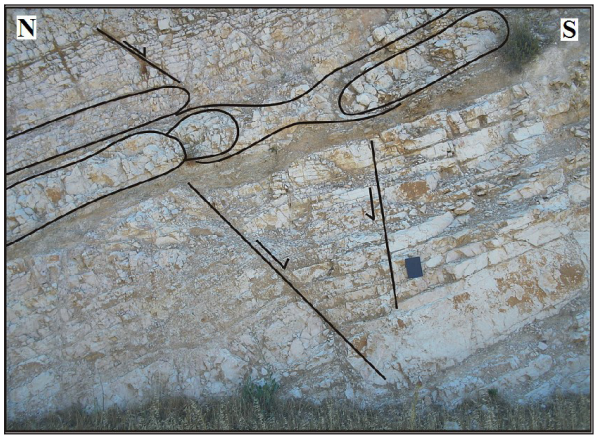

Figure 10. Boudinage structure formed due to the competent and incompetent contrast layers.

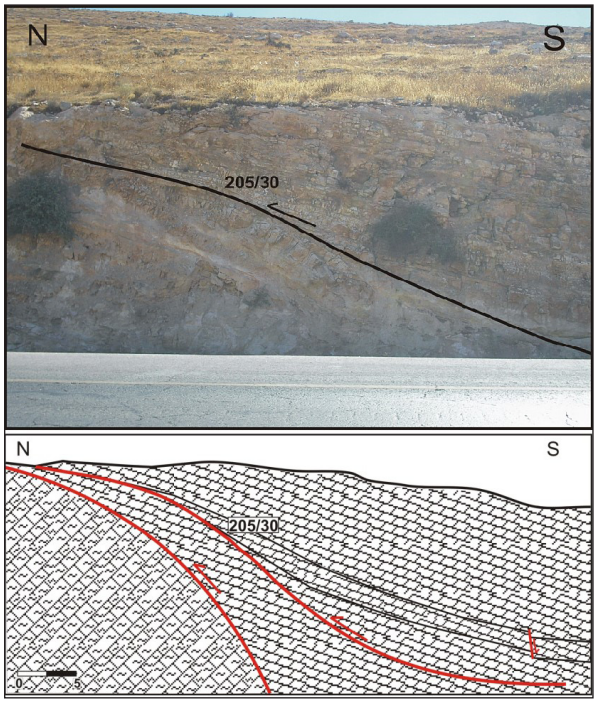

Figure 11. Photo and sketch cross- section showing a wedge thrust fault which resulted from local north-south compression.

Station 7

Three-hundred and eighty-seven measurements were recorded for joints in this quarry in the southern part of the study area at the eastern side of the Irbid-Jerash road (Figure 2). Three methods of data collection were applied in this station (Table 1). A comparison with the other quarries was made using the circle method and scanline to conclude the intensity of fractures in each quarry (Table 1). Joints oriented into two main trends; N-S and E-W. Many joints terminate at bed boundaries (bed-confined) displaying regular spacing and are vertically aligned. Other fractures cut across the whole exposure forming linked throughgoing fractures, throughgoing fractures with aperture and in the late phase of development and those of the opening mode that are filled with calcite (Figs. 12 - 13). Many slickenlines served on the fault surface to indicate the strike-slip or oblique motion. Fault surfaces in general have a vertical alignment trending

E-W and some of them have been karstified. Layers slightly dip (20º) toward the south east.

Figure 12. Karstified throughgoing fracture filled with calcite.

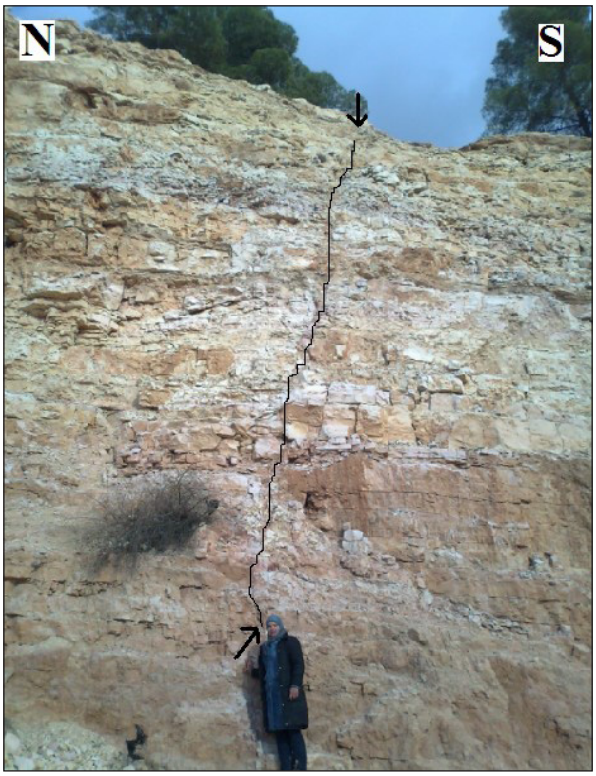

Figure 13. Single linked throughgoing fracture.

Station 8

Thirty-seven joint measurements were taken from this station in the southern part of the study area at the western side of the Irbid- Jerash road (Table 1 and Figure 3). The fractures show a main set trend ENE-WSW and minor set trends in ESE-WNW extending vertically along the bed sequence. Fractures density increase within and near fault zones. The scanline method was applied on fractures (Figure 14) and fracture density has been calculated.

Rock layers that are highly deformed resulting in many structures were observed on the road cut. Negative flower structures developed on which the slip on subsidiary faults had a normal sense component in transtensional zones within strike-slip systems. Listric faults which occurred when fault surfaces in some cases are not planar (Figure 15) were observed. Slickenlines on fault planes that indicate the strike-slip and oblique movements were also observed.

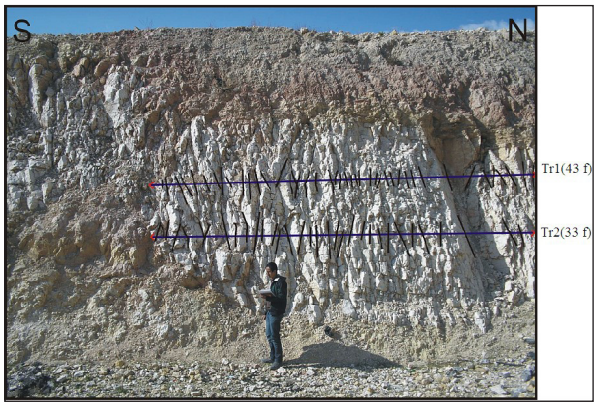

Figure 14. Fracture swarm's density using scanline method. Tr1 (43 f) and Tr2 (33 f) represent the number of measured fractures along traverses.

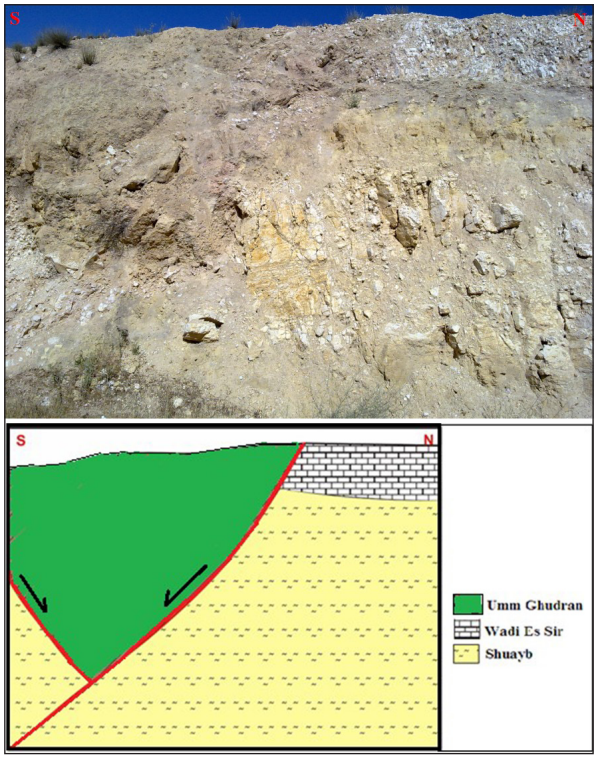

Figure 15. A photograph and sketch cross section showing a negative flower structure.

Station 9

This station includes three neighboring quarries located at the western side of the Irbid-Jerash highway (Figure 2). Measurements were taken for both fractures and bedding planes (Table 1). The orientations of bedding planes were measured; the dip is 20º toward 170º. Fractures of both types were encountered including throughgoing and bed-confined fractures. Fractures are aligned sub-vertically to vertically along the stratigraphic layering, some of them are dipping 60º. In addition, many slickensides and slickolites were encountered serving on fault planes which indicate the strike-slip motion. The orientation of slickensides on the fault planes was measured; the movement was very clear and the rocks were highly deformed within the fault zones which formed the fault breccia consisting of limestone and chert fragments. A small normal fault was observed in the stratigraphic layering but in limited extension, the apparent down throw does not exceed 30-40 cm (Figure 16).

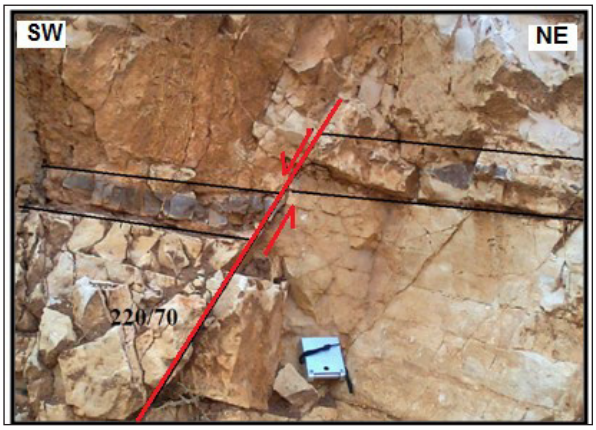

Figure 16. A small normal fault with down throw (20 cm).

5. Discussion

The present study reveals meso-scale structural features throughout the Upper Cretaceous rocks. These features mostly affected the hard limestone units of Wadi Es Sir Limestone Formation and can be classified as compressional or extensional structures.

The compressional structures are folds, thrust\ reverse faults, positive flower structure and stylolites. The extensional structures are normal faults and their associated structures include horsts and grabens, listric faults, negative flower structure, boudinage structure, joints and veins. Axes of boudinage are arranged in a nearly E-W direction. Boudinage and pull-apart structures are an expression of local layer-parallel extension, and are often laterally replaced by small-scale thrusts and asymmetric small-scale folds in the same layer in the area of the local layer-parallel contraction (station 6). Rock layers are highly-deformed resulting in many structures that were observed on the road cut including negative flower structures which developed where the slip on subsidiary faults had a normal sense component in transtensional zones within strike-slip systems, and listric faults.

In general, fractures were traced intensively all through the study area, and more than 1385 fracture measurements were collected a long road cuts and quarries. The field work reveals that fractures are concentrated in high densities throughout the study area and are oriented in many trends, but in most cases, in zones of deformation (such as fault zones) and fold crests as can be seen along the road cuts in stations (2, 3 and 6).

The major trends NW-SE, NNW-SSE and N-S with other minor trends, ENE-WSW and E-W dominate the study area. The number of joint sets at each station is variable ranging from one set (e.g., stations 6 and 8) to four sets (e.g. station 4). This is due to the local variation of structural position.

To interpret the results easily, rose diagrams for each station were displayed on the geological map (Figure 2). Orientation of all fractures are represented as rose diagrams (Figure 17). All measured strike-slip faults, normal faults, throughgoing fractures, and slickenlines in the study area were also represented separately as rose diagrams and\ or stereoplots (Figure 17).

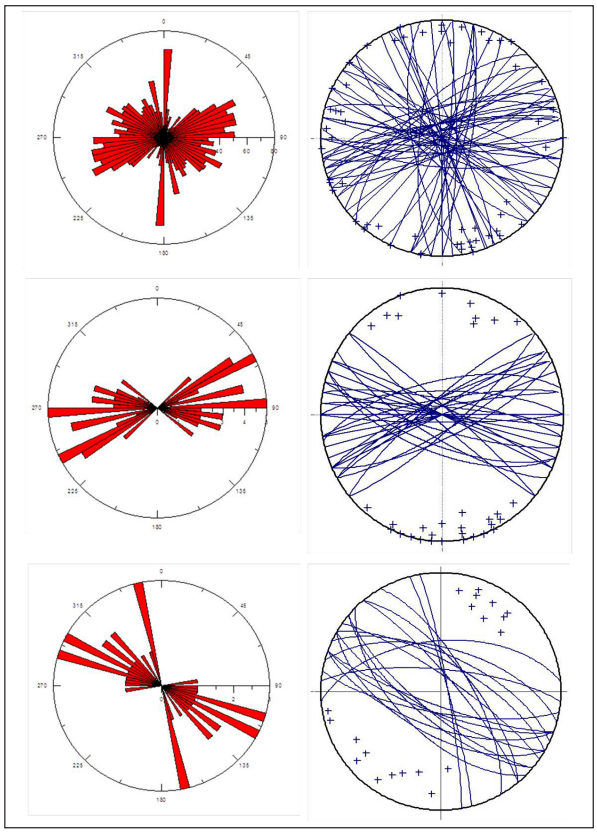

Figure 17. a) Rose diagram and stereoplot of fracture orientation of all stations in the study area. b) Rose diagram and stereoplot of all throughgoing fractures in the study area. c and d) Rose diagram and stereoplot show the orientation of all strike-slip faults in the study area. e and f) Rose diagram and stereoplot of all normal faults in the study area.

Figures (2 and 18) show two dominated trend sets of fractures oriented N-S and NNW to NW in addition to other minor trend sets in E-W, ENE- WSW and WNW-ESE. The N-S and NNW to NW dominant trends represent the range of conjugated, hybrid and extensional fractures.

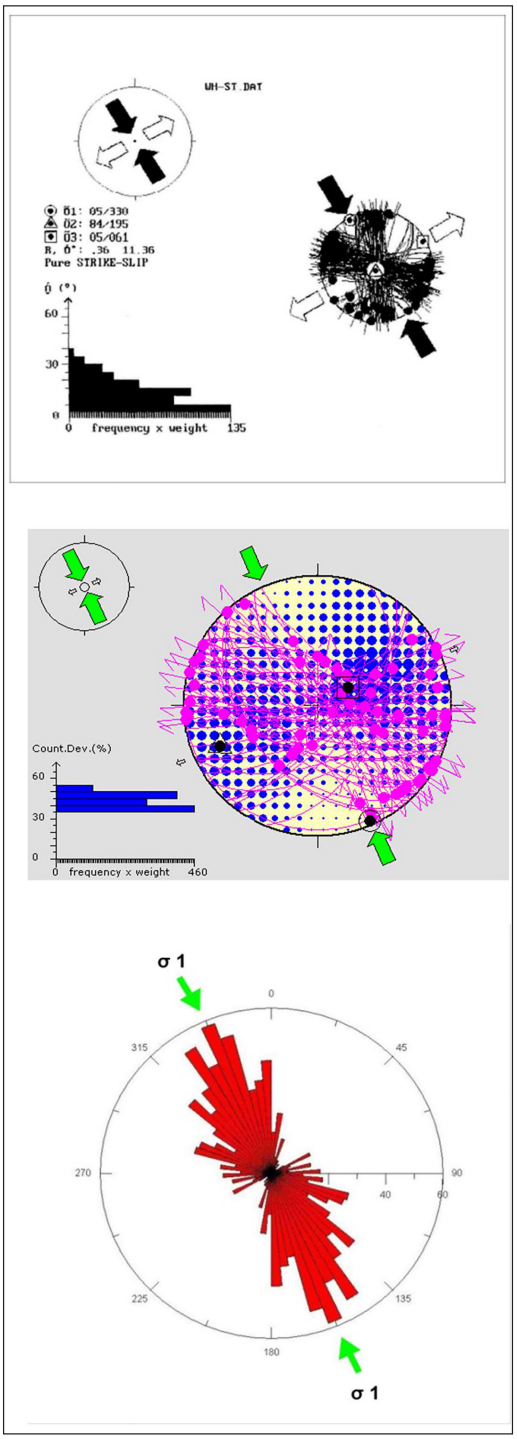

Figure 18. a) Principal stress axes determination by using the TENSOR program and fault- slip data along the Dead Sea transform (DST); inward arrows indicate compression (σ_1), outward arrows indicate tension (σ_3), whereas σ_2 is vertical (Diabat, 1999; Diabat et al., 2004). b) Principal stress axes of 70 fault-slip measurements in northern Jordan; outward ENE arrows indicate tension (σ_3) and inward NNW arrows indicate compression (σ_1), σ_2 is vertical (Diabat, 2013). c) Strike of 740 fracture planes and the deduced SH_{max} from the orientation of extensional fractures in northern Jordan (Diabat, 2013).

The ENE-WSW to E-W trend set of figures (2, 17 a) reflects the majority of fault-slip data analyzed. Plane surfaces of these fractures are mainly coated with calcite steps or slickolites which are of importance as a sense movement indicator, the plunge and azimuth of these structural markings were measured. Investigations show that dextral shear along these fractures have occurred later as a reactivation process. These fault planes are open and calcite curtains or soil staining on their surfaces (Diabat, 2013). Figure (17b) shows no preferred orientation of the throughgoing fractures in the study area, which can be explained as brittle deformation progress. It was more efficient for throughgoing fractures to utilize (reactivate) preexisting fractures rather than to propagate new fracture surfaces in intact rock. This means that they could take the orientation of any preexisting fractures in the study area. Many throughgoing fractures develop subsequent to bed-confined joints, for thin- to medium- bedded rocks, where bed-confined fractures are closely spaced throughgoing fractures are commonly formed by the coalescence of pre-existing joints. Structural geometries indicate a clear temporal order in the formation of the three main fracture populations. Throughgoing fractures were then formed by the coalescence and linkage of selective zones of vertically aligned, preexisting, bed-confined joints. In station 6, there is a contractional tectonic setting, in which the assemblage in the thrust-fold zone indicates that there was a layer-parallel shortening normal to the fold hinge line or axial elongation deformation occurring in a contractional environment. The extensional faults and allied structures in this zone (e.g. boudins) are interpreted as a local product of stretched fold limbs.

6. Conclusions

- Fractures are concentrated in high densities throughout the study area, and are oriented in many trends in most cases, in zones of deformation like fault zones and fold crests as can be seen along the road cuts in stations (2, 3, and 6).

- Many throughgoing fractures develop subsequent to bed-confined joints by the coalescence of pre-existing joints.

- Many joints aligned in vertical to sub-vertical planes. Other throughgoing joint sets are of a parallel trend and are oriented NNW. Joints were enlarged by water solutions forming small cavities.

- The normal fault systems that formed horsts and grabens are thought to be conjugated.

- Many slickensides and slickolites served on fault planes indicate the strike-slip motion.

- This study shows two dominated trend sets of fractures oriented N-S and NNW to NW in addition to other minor

trend sets in E-W, ENE- WSW and WNW-ESE.

References

Abdelhamid, G.H. (1995). The geology of Jarash Area Map Sheet (3154-I), Report of Natural Resource Authority. Geology Directorate, Natural Resources Authority (Ministry of Energy and Mineral Resources) Amman, Jordan.

Abed, A.M. (2000). Geology of Jordan, 1st edition. Jordanian Geologists Association. (In Arabic).

Al-Awabdeh, M., Perez-Pena, J.V., Azanon, J.M., Booth-Rea, G., Abed, A., Atallah, M., Galve, J.P. (2016). Quaternary tectonic activity in NW Jordan: Insights for a new model of transpression–transtension along the southern Dead Sea Transform Fault. Tectonophysics 693: 465-473.

Al-Taj, M., Atallah, M., Abed, A. (2003). Fractures Associated with the Dead Sea Transform in the Jordan Valley, Jordan. Abhath Al – Yarmouk, Series of Basic Sciences and Engineering 12(2B): 633-647.

Atallah, M. (1996). Joint and fault analysis in Al-Husn fold belt - northern Jordan. Abhath Al-Yarmouk, Series of Basic Sciences and Engineering 5: 187-201.

Davis, G.H., Reynolds, S.J., Kluth, C.F. (2011). Structural Geology of Rocks and Regions. 3rd edition. New York, John Wiley and Sons. 864 P.

Diabat, A. (1999). Paleostress and strain analysis of the Cretaceous rocks in the eastern margin of the Dead Sea transform, Jordan. Ph.D Thesis, University of Baghdad.

Diabat, A. (2009). Structural and stress analysis based on fault-slip data in the Amman area, Jordan. Journal of African Earth Sciences 54: 155-162.

Diabat, A. (2013). Fracture systems and dissolution cavities development in hard carbonates, northern Jordan. Jordan Journal of Earth and Environmental Sciences 5 (2): 73-78.

Diabat, A. and Masri, A. (2005). Orientation of the principal stresses along Zerqa- Ma`in Fault. Mu'ta Lil-Buhuth Wad-Dirasat 20: 57- 71.

Diabat, A., Atallah, M., Salih, M.R. (2004). Paleostress analysis of the Cretaceous rocks in the eastern margin of the Dead Sea transform, Jordan. Journal of African Earth Sciences 38: 449-460.

Eyal, Y. (1996). Stress fluctuations along the Dead Sea rift since the Middle Miocene. Tectonics 15: 157-170.

Eyal, Y. and Reches, Z. (1983). Tectonic analysis of the Dead Sea rift region since the Late Cretaceous based on Mesostructures. Tectonics 2:167-185.

Eyal, Y. Gross, M.R. Engelder T., Becker A. (2001). Joint development during fluctuation of the regional stress field in Southern Israel. Journal of Structural Geology 23: 279-269.

Freund, R., Garfunkel, Z., Zak, I., Goldberg, M., Weissbrod, T., Derin, B. (1970). The shear along the Dead Sea rift. Philosophical Transaction of the Royal Society of London 267: 107- 130.

Garfunkel, Z. (1981). Internal structure of the Dead Sea leaky transform (rift) in relation to plate kinematics. Tectonophysics 80: 81– 108.

Gross, M.R. and Eyal, Y. (2007). Throughgoing fractures in layered carbonate rocks. Geological Society of America Bulletin 119: 1387-1404.

Hancock, P.L. (1985). Brittle microtectonics: Principles and Practices. Journal of structural Geology 7: 347 - 457.

Hancock, P.L. and Atiya, M.S. (1979). Tectonic significance of the mesofracture systems associated with the Lebanese segment of the Dead Sea transform fault. Journal of Structural Geology 1: 143-153.

Powell, J.H. (1989). Stratigraphy and sedimentation of the Phanerozoic rocks in central and southern Jordan. Bulletin 11, Geology Directorate, Natural Resources Authority (Ministry of Energy and Mineral Resources) Amman, Jordan. Part B: Kurnub, Ajlun and Belqa Groups. 161 p.

Quennell, A.M. (1951). The Geology and mineral resources of former Transjordan. Colon Geol Min, Resource 2: 85-115, London.

Quennell, A.M. (1983). Evolution of the Dead Sea Rift. A review, First Jordanian Geologic Conference, 460-482.

Radaideh, O.M. and Melichar, R. (2015). Tectonic paleostress fields in the southwestern part of Jordan: New insights from the fault slip data in the southeastern flank of the Dead Sea Fault Zone. Tectonics 34 (9): 1863-1891.

JJEES

JJEES (2020) 11 (3): 174-182
ISSN 1995-6681

Jordan Journal of Earth and Environmental Sciences

Landslide Hazard Zonation Using Multivariate Statistical Models in the Doab Samsami Watershed, Chaharmahal Va Bakhtiari Province, Iran

Ebrahim Karimi-Sangchini*[1], Seyed-Naim Emami[2], Mohsen Shariat-Jafari[3], Farzad Rezazadeh[4], Heidarali Raeisi[5]

[1]*Assistant Professor, Soil Conservation and Watershed Management Research Department, Lorestan Agricultural and Natural Resources Research and Education Center, AREEO, Khorramabad, Iran*
[2]*Soil Conservation and Watershed Management Research Department, Chaharmahal Va Bakhtirai Agricultural and Natural Resources Research and Education Center, AREEO, Shahrekord, Iran.*
[3]*Soil Conservation and Watershed Management Research Institute.*
[4,5]*Natural Resources and Watershed Management Office of Chaharmahal Va Bakhtiari, Iran*

Received 10 December 2019; Accepted 2 April 2020

Abstract

The Doab Samsami watershed is located in the Chaharmahal Va Bakhtiari province, and serves as one of the main tributaries of the Karoon River Basin. Using aerial photos interpretation and field studies, a landslide distribution map for the study area was prepared. Thirty-seven cases of landslide incidents were observed. Nine parameters including elevation, slope, aspect, lithology, distances from fault, stream and roads, land use, and annual precipitation were chosen as landslide determinant factors. Potential landslide hazard maps were prepared using the multivariate stepwise regression model and the logistic multivariate regression model; which were subsequently compared with field data. ROC Index was also considered for the models' accuracy assessment. According to the research results, the logistic multivariate regression model was considered as the superior model for Doab Samsami watershed with an ROC equal to 0.865. Furthermore, the results revealed that about 46% of the watershed area was located in high and very high hazard zones among others. The obtained landslide susceptibility maps may be promising in appropriate watershed management practices and for a sustainable development in the regions characterized by conditions similar to the study area.

Keywords: Landslide hazard, Multivariate statistical model, ROC Index, Doab Samsami.

1. Introduction

Landslides are one of the most important natural hazards, causing enormous financial and life losses on an annual basis worldwide (Kelarestaghi and Ahmadi, 2009). Landslides are amongst the most catastrophic natural hazards in mountainous terrains. The study of landslides has received attentions throughout the world mainly due to the increasing awareness regarding the socio-economic impact of landslides, as well as, the increasing pressure of urbanization on the mountainous landscape (Aleotti and Chowdhury, 1999). Each year, the phenomenon of landslides occurs around many parts of the world including Iran. By the end of September 2007, 4,900 landslides were recorded and the losses resulting from mass movements in Iran were estimated at about 317 million US dollar (Pourghasemi et al., 2013). The burying of Abikar village of the Charmahal Va Bakhtiari Province in the spring of 1997 is one of the most obvious catastrophic examples of landslide damages in the Iran. The volume of material transported by this landslide was 9 million cubic meters. Abikar village with all its 55 residents was buried under the materials of the landslide. Hence, landslide susceptibility mapping can be one of the preliminary steps to minimize such costs (Regmi et al., 2014). Also, landslide susceptibility assessment is found to be a crucial process for the prediction and management of natural disasters. Additionally, it can be considered as a necessary step for integrated watershed management, hazard mitigation, natural and urban planning in government policies worldwide (Dahal et al., 2008; Kayastha et al., 2012). The identification and classification of landslide-prone areas and the susceptibility zonation is a great step in the evaluation of environmental hazards and can make a great contribution to the watershed management (Sakar, 1995). Landslide susceptibility assessment is conducted using three approaches, namely the qualitative, semi-quantitative, and quantitative approaches (Lee and Jones, 2004). Quantitative methods are inspired by mathematical logic, the correlation between factors, and landslide occurrence which include

* Corresponding author e-mail: e.karimi64@gmail.com

bivariate regression analysis (Guzzetti 2002; Nandi and Shakoor, 2009; Yilmaz et al., 2012; Bijukchhen et al., 2013; Jaafari et al., 2014; Youssef et al., 2015b), logistic regression (Ayalew and Yamagishi, 2005; Park et al., 2013; Karimi Sangchini et al., 2014; Karimi Sangchini et al., 2015; Dou et al., 2015a; Dou et al., 2015b), Certainty Factor Model (Dou et al., 2014; Dou et al., 2015a), genetic algorithm (Dou et al., 2015c), fuzzy logic (Gupta et al., 2008; Tangestani 2009; Pourghasemi et al., 2012), and artificial neural network model (Caniani et al., 2008; Pradhan et al., 2010; Zare et al., 2013; Polykretis et al., 2015; Dou et al., 2015b). Qualitative methods are based on expert opinions (Rahman and Saha, 2008; Karimi Sangchini et al., 2011; Karimi Sangchini et al., 2016). Qualitative methods which utilize weighting and rating approaches are known as semi-quantitative methods (Yalcin, 2008). Some examples of such methods are the analytic hierarchy process (AHP) (Yalcin, 2008; Komac, 2006; Rahman and Saha, 2008; Ercanoglu et al., 2008; Akgun and Turk, 2010; Pourghasemi et al., 2012; Awawdeh et al., 2018) and weighted linear combination (Gorsevski et al., 2006; Kouli et al., 2010). Traditionally, the multivariate logistic regression approach has been applied by various researchers (Yesilnacar and Topal, 2005; Nandi and Shakoor, 2009; Felicisimo et al., 2013; Karimi Sangchini et al., 2016). In the previous research works, the abovementioned models had been used in a separate manner. The proposed methodologies use both expert opinions and ground truth simultaneously.

To generate statistics-based susceptibility maps, many modeling approaches for landslide hazard prediction can be applied. Logistic regression and discriminant analysis are the most frequently used models (Brenning, 2005). Logistic regression and statistical models have been developed using the geographic information system (GIS) for landslide hazard zonation (Lee et al., 2010). The multivariate approach was adopted by various practitioners worldwide (Yesilnacar and Topal, 2005; Nandi and Shakoor, 2009; Felicisimo et al., 2013). In the present research, landslide susceptibility mapping with a logistic regression and stepwise multivariate statistical models were used to determine the landslide-prone areas for the sake of landslide hazard management in Doab Samsami watershed.

2. Materials and Methods

2.1. Study Area

Doab Samsami Watershed is spanned over coordinates 421386 to 447042 E and 3550345 3568932 N, covering an area of 276.3 km2 in the Chaharmahal Va Bakhtiari Province, southwest of Iran (Figure 1). This watershed is one of the major sub basins of the Karoon River. The elevation in the study area varies from 1,775 to 3,825 m above sea level. According to the Iran meteorological organization report, the average annual precipitation in the study area is 970 mm. This watershed is nestled in the middle of Zagros Mountains. Subsequent erosion has removed erodible rocks, such as mudstone, and siltstone while leaving behind harder rocks exposed, such as limestone, and dolomite. This differential erosion has formed the linear ridges of the Zagros Mountains. Rangelands account for 66 % of this region and the rest of the area is covered by orchards, forests, agricultural and rocky lands.

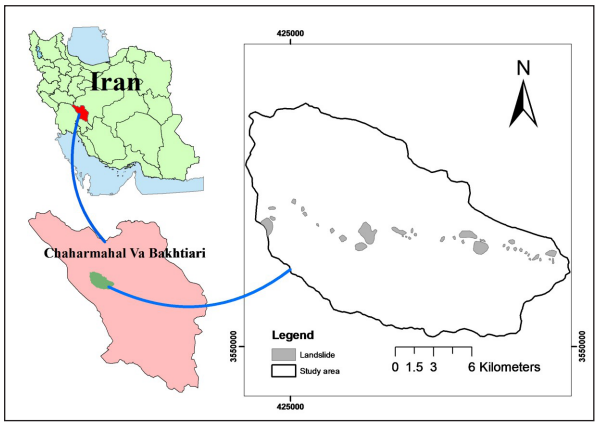

Figure 1. Location map of the study area.

2.2. Landslide Inventory Map

Landslide inventory maps are prepared by gathering the information and data on landslides, or by analyzing the data obtained from remote sensing and GIS techniques. In the current research, a landslide inventory map was prepared using field reconnaissance, local information, and aerial photograph interpretation.

2.3. Selection and Effective Factor Classification

According to the literature review and field conditions of Doab Samsami watershed, a total of nine factors including altitude, slope percentage, slope aspect, lithology, distance from faults, rivers, village and roads, land use, and precipitation amount were chosen as main determinant factors of land sliding. In the next stage, the area and landslide percentage, the density ratio, and landslide density percentage, in each class of these nine landslide factors, were calculated.

2.3.1. Landslide Determinant Factors

Those determinant factors in the occurrence of a landslide are described below (Table 1 and Figure 2). . Vector-type spatial database was extracted through transforming such factors using the ArcGIS 9.3 (ESRI 2008). The resolutions of the girds of the causative factors are 30×30 meters.

2.3.2. Topographical Factors

A digital elevation model (DEM) was created from 20m interval contours and survey base points which were extracted from the 1: 50,000-scale topographic maps (Cartographic Center of Iran, 2003). Based on this DEM, altitude, slope percentage, and slope aspect were prepared.

Altitude was classified into eleven classes with 200 m intervals (Karimi Sangchini et al., 2016). Slope percentage was grouped in six classes of 0-5°, 6-15°, 16-25°, 26-35°, 36-45°, and >45° (Kelarestaghi and Ahmadi, 2009). Slope aspect was classified into eight classes of N, NE, E, SE, S, SW, W, and NW. The slope conditions have received great attention, as slope configuration and steepness play an important role in landslide occurrence (Table 1 and Figure 2 (a-c)).

2.3.3. Lithology

The underlying geology is found to be one of the most substantial factors for landslide modeling. Different geological formations are characterized by various compositions and structures which in turn contribute to the strength of the material. In the current research, a 1: 100,000-scale geological map (Geological Survey and Mineral Explorations of Iran, 1996) was applied to lithology mapping which was then classified according to the lithological units (type) into eleven groups (Table 1 and Figure 2d). Geological formations in this watershed were fossiliferous marly limestones with intercalations of marls and sandy limestones (OM2), white nummulitic limestones, marly limstones and dolomitic limestones (EO), mainly orbitolina limstones, locally evaporites in the lower part (K), shale and marls interbedded with marly limstones containing Ammonites and Inceramuses (K8), marly fossiliferous limestones and thin sandy argillaceous limestones (K7), recent terraces and recent alluviumes (Qal), old terraces deposits (Qt and QR), carbonate-dominated sedimentary package with shale-marl intervals (Pd), and red conglomerates (mainly chert pebbles), sandstones (locally with volcanic intercalations), and silstone with evaporites intercalations (E).

2.3.4. Distance from Faults, Streams, and Roads

A topographical map was used to extract distance to streams, whereas, a distance to faults map was calculated drawing upon the geological map of the study area (Pourghasemi et al., 2012). On the other hand, the distance to roads map was prepared using a road map of the study area. The distance to faults factor was classified into five classes of 0-500, 500-1300, 1300-2300, 2300-3500, and >3500 m. In the case of distance from streams, there were seven classes with 50m intervals. As for the factor of distance from roads, there were six classes of 0-75, 75-150, 150-225, 225-300, 300-500, and >500 m (Table 1 and Figure 2e-g).

2.3.5. Land Use

The land use map was developed using Landsat images provided by Iranian forest, rangeland, and watershed management (http://www.frw.org.ir/pageid/34/language/en-US/Default.aspx). Five classes of rocky land, poor range, medium range, irrigated farming, and dry farming were detected in the study area (Karimi Sangchini et al., 2016) (Table 1 and Figure 2h).

2.3.6. Precipitation

There is no doubt that precipitation is the most important triggering factor in landslides (Naghibi et al., 2015). This factor was mapped using Inverse Distance Weighting (IDW) Interpolation method and classified into five classes of 850-1000, 1000-1200, 1200-1400, 1400-1600, and >1600 mm in the study area (Table 1 and Figure 2i) (Karimi Sangchini et al., 2014).

Table 1. Calculation of the final susceptibility value of each identified land unit

Data layers	Total area (ha)	% of total area (A)	area of Landslide	% of area landslide (B)	Area density value
Aspect					
N	1719.99	6.23	30.38	4.79	-5.32
NE	7715.25	27.93	262.21	41.30	11.01
E	2518.976	9.12	125.04	19.70	26.66
SE	2455.739	8.89	49.94	7.87	-2.64
S	4798.129	17.37	85.43	13.46	-5.17
SW	4676.126	16.93	59.57	9.38	-10.24
W	1370.671	4.96	0.00	0.00	-22.98
NW	2372.664	8.59	22.29	3.51	-13.58
Elevation (m)					
1775-1900	461.9037	1.67	57.97	9.13	102.53
1900-2100	2932.099	10.61	289.84	45.65	75.87
2100-2300	5057.21	18.30	172.11	27.11	11.05
2300-2500	4882.323	17.67	25.45	4.01	-17.77
2500-2700	4593.758	16.63	53.76	8.47	-11.28
2700-2900	3952.74	14.31	35.73	5.63	-13.94
2900-3100	2929.929	10.61	0.00	0.00	-22.98
3100-3300	860.752	3.12	0.00	0.00	-22.98
3300-3500	1532.477	5.55	0.00	0.00	-22.98

Data layers	Total area (ha)	% of total area (A)	area of Landslide	% of area landslide (B)	Area density value
3500-3700	382.009	1.38	0.00	0.00	-22.98
3700-3825	43.83642	0.16	0.00	0.00	-22.98
Slope (%)					
0-5	201.0076	0.73	21.17	3.33	82.34
6-15	2119.803	7.67	59.33	9.35	5.01
16-25	4522.01	16.37	244.67	38.54	31.13
26-35	2157.286	7.81	112.02	17.65	28.95
36-45	492.5005	1.78	7.39	1.16	-7.97
>45	18136.12	65.65	190.28	29.97	-12.49
Geology units					
OM2	449.9949	1.63	3.30	0.52	-15.63
E	190.4042	0.69	0.18	0.03	-22.04
EO	11334.27	41.03	27.59	4.35	-20.54
QR	1297.833	4.70	179.93	28.34	115.66
K	5018.204	18.16	10.84	1.71	-20.82
Qal	201.7005	0.73	46.45	7.32	207.33
Pd	898.8312	3.25	114.50	18.03	104.41
Qt1	542.9987	1.97	85.34	13.44	134.18
Qt2	399.7744	1.45	14.76	2.33	13.95
K8	2948.512	10.67	150.77	23.75	28.16
K7	3555.478	12.87	1.21	0.19	-22.64
distance from fault (m)					
0-500	2463.077	8.92	94.81	14.93	15.51
500-1300	3740.476	13.54	192.53	30.33	28.49
1300-2300	4152.376	15.03	141.37	22.27	11.07
2300-3500	6133.214	22.20	114.22	17.99	-4.35
>3500	11139.89	40.32	91.94	14.48	-14.72
distance from stream (m)					
0-50	2092.495	7.57	51.84	8.17	1.80
50-100	2011.261	7.28	52.52	8.27	3.14
100-150	1942.973	7.03	51.18	8.06	3.36
150-200	1882.406	6.81	47.21	7.44	2.10
200-300	3563.991	12.90	84.96	13.38	0.86
300-450	4803.816	17.39	106.37	16.76	-0.83
>450	11331.47	41.02	240.77	37.92	-1.73
distance from road (m)					
0-75	1583.822	5.73	140.51	22.13	65.74
75-150	1372.74	4.97	125.47	19.76	68.42
150-225	1234.877	4.47	109.28	17.21	65.52
225-300	1134.911	4.11	92.53	14.57	58.55
300-500	2622.979	9.49	121.87	19.20	23.49
>500	19679.09	71.23	45.20	7.12	-20.68
Land use					
Rocky land	5512.351	19.95	0.59	0.09	-22.87
Rainfed agriculture	1645.76	5.96	10.04	1.58	-16.88
Irrigated agriculture	2214.199	8.01	155.03	24.42	47.04
Poor range	12072.93	43.70	391.81	61.72	9.48
Medium range	6183.487	22.38	77.39	12.19	-10.46
Precipitation (mm)					
780-900	10589.69	38.33	539.27	84.94	27.95
900-1000	7996.283	28.94	69.14	10.89	-14.33
1000-1100	6078.483	22.00	26.45	4.17	-18.63
1100-1200	2292.567	8.30	0.00	0.00	-22.98
1200-1260	671.9949	2.43	0.00	0.00	-22.98

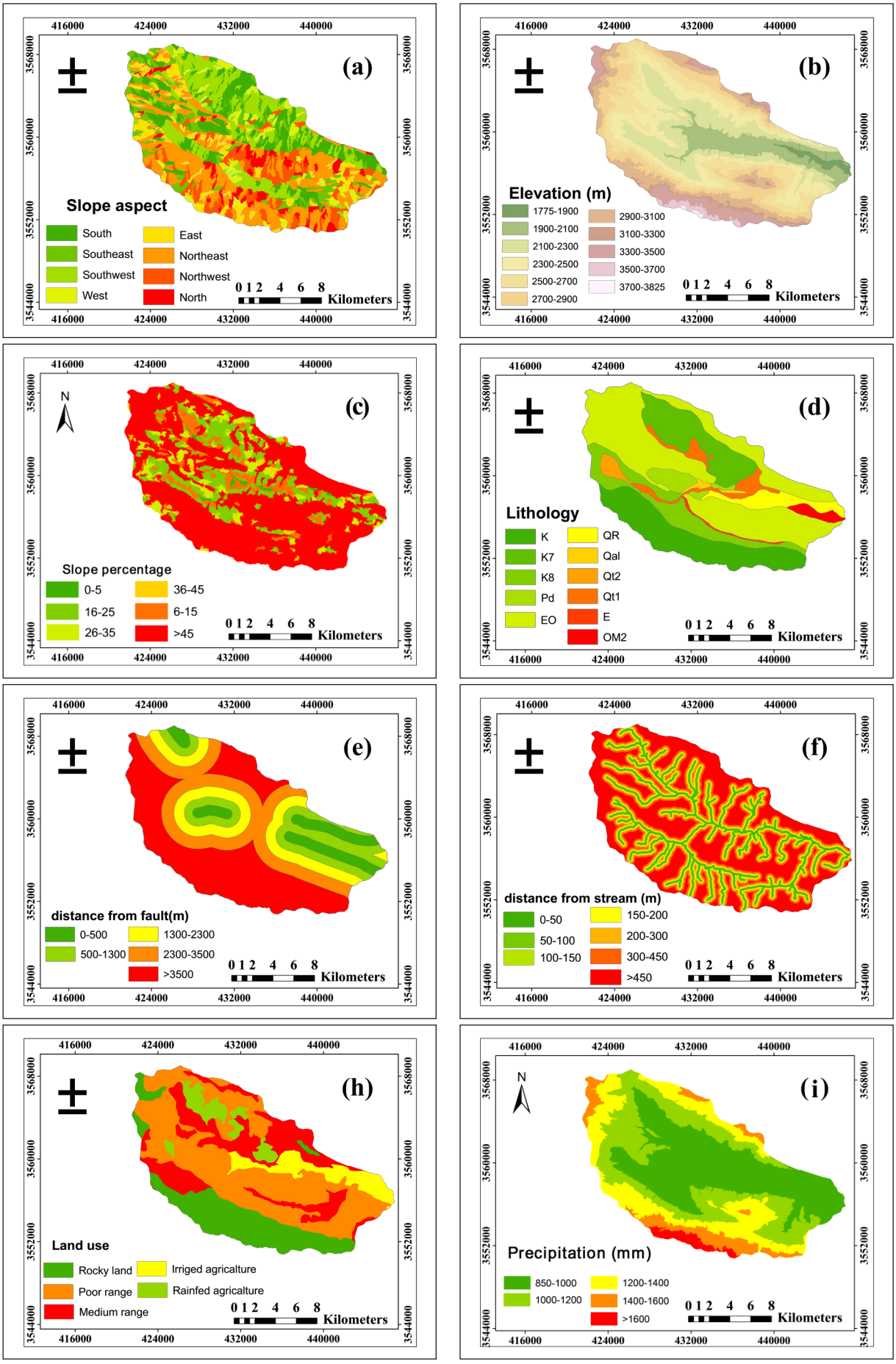

Figure 2. Landslide conditioning factors; **a** aspect, **b** elevation, **c** slope percentage, **d** lithology, **e**, **f** and **g** distance from fault, stream and road respectively, **h** land use, **i** precipitation.

2.4. Landslide Susceptibility Mapping Using Logistic Regression

Model In order to determine the zonation of landslide susceptibility using logistic statistical regression, the landslide density in each class of the nine causative parameters was calculated. To this end, through integrating maps of several factors, a homogeneous units' map was prepared. Homogeneous units were created by combining all the maps of effective factors, and had a unit value in terms of the characteristics of the effective factors. After overlying the homogeneous units' map on the landslide distribution map, the units of the landslide were specified, and all of the homogeneous landslide units were scored by the code (1), and all those with no landslide units were scored by the code (0). The absence or presence of landslide in the homogeneous units being a dependent variable, and the landslide density percentage in each class of the nine parameters in units being an independent variable were entered in the R statistical software. Logistic regression equation is as follows according to Ayalew and Yamagishi (2005):

$$Y = Logit(p) = \ln\left(\frac{p}{1-p}\right) = C_0 + C_1X_1 + C_2X_2 + \cdots + C_nX_n \quad ....(1)$$

where p is the probability of independent variable (Y), p/(1-p) denotes the so-called odds or the likelihood ratio, C_0 is the intercept, C_1, C_2,….C_n are coefficients (which measure the size and the contribution of independent factors (X_1, X_2, ... and X_n) in a dependent variable). Using the density of factors as independent variables, and the presence or absence of landslides as the dependent variable, is an attempt to determine the best equation as follows that is meaningful at 0.01 % error level. Using the resulting model, the landslide susceptibility map was produced and classified into very low, low, medium, high, very high classes.

*Y=(- 2.097 +(0.0074)*Aspect +(0.012)*
**Precipitation +(0.061)*Elevation +(0.0055)*
**Geology -(0.0288)*Fault -(0.1875)*Stream)* ....(2)

2.5. Landslide Susceptibility Mapping Using Stepwise Regression Model

To determine the numerical value of qualitative factors in different parameters (aspect, land use, and lithology), AHP was utilized, and the parameters were weighted according to slippage (landslide) rate in the factors' different classes, and the weight of each factor was assessed after making paired comparisons between classes (show the matrix of AHP). The nine layers were integrated together in a GIS environment, and the map of homogenous units was produced.

After that, the map of homogenous units was cropped with the landslide distribution map and nine factors and the logarithm of the sliding factor (it took place in order to standardize the logarithmic conversion) were, respectively, chosen as independent variables and dependent variable. The most effective factors were determined as elevation, slope, lithology, distance from the fault, distance from the road, land use and annual precipitation using the SPSS software and the stepwise method (Karimi Sangchini et al., 2011). The equation coefficient of determination equals to 67.96 % which is significant at a 95% confidence level.

*Y=(- 1.838 +(0.00059)*Aspect +(0.0692)*Slope*
*+(0.00178)*Elevation +(0.00318)*Geology -(0.000077)*Fault*
*+(0.00167)*Land Use -(0.000163)*Stream -(0.000415)*Road)* .(3)

The landslide hazard intensity mapping was conducted in an ArcGIS 9.3 environment using the abovementioned equation, and the pixels were classified into six classes based on the turning points of the cumulative frequency curve.

2.6. Evaluation of Landslide Hazard Model

Ultimately, the receiver operating characteristics (ROC) curve (Mohammady et al., 2012; Pourghasemi et al., 2012; Naghibi et al., 2015; Karimi Sangchini et al., 2016) was used to determine the accuracy of landslide susceptibility. The ROC curve is a diagram in which the pixel's ratio that correctly-predicted the occurrence or nonoccurrence of landslides (True Positive) is plotted against the corresponding amount that is the pixel's ratio that is wrongly predicted.

3. Results and Discussion

3.1. Performance of the Models

As can be inferred from the results, two models showed a high and a relatively close performance. However, the logistic multivariate regression (AUC= 0.865) was proven to be superior to the stepwise multivariate regression (AUC= 0.792) (Figure 3). AUC is the Area under the ROC Curve.

The main advantage of the logistic regression over the simple multiple regressions is that the former allows using binary dependent variable types in landslide susceptibility mapping. Although the logistic regression is a widely-used quantitative susceptibility mapping method, its major limitation is yielding average parameters for the study area (Erner et al., 2010), which may differ locally across different parts of the study area.

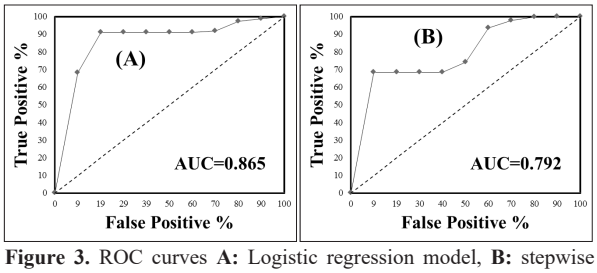

Figure 3. ROC curves **A:** Logistic regression model, **B:** stepwise regression model.

3.2. Landslide Hazard Maps

Landslide hazard maps which were generated by the logistic multivariate regression and stepwise multivariate regression models are illustrated in Figures 4 and 5. The mentioned hazard maps were classified into very low, low, moderate, high, and very high classes based on natural break scheme. The moderate land slide hazard map class derived from the logistic regression model accounts for 40.57 % of

the total area; 4.97, 8.61, 8.88, and 37.04% of the total area are related to very low, low, high and very high HPM zones, respectively (Table 2). As for the stepwise multivariate regression model, very low, low, moderate, high, and very high land slide susceptibility map classes account for 19.34, 33.58, 15.29, 16.38, and 12.41% of the total area, respectively (Table 2). The different results are due to the fact that the two models use different algorithms. The step-by-step multivariate regression model uses a quantitative dependent variable, while the logistics model uses a qualitative dependent variable.

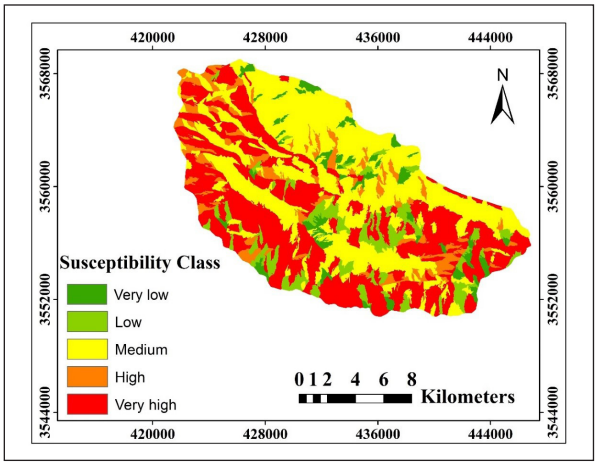

Figure 4. Landslide susceptibility maps based on: Logistic regression model.

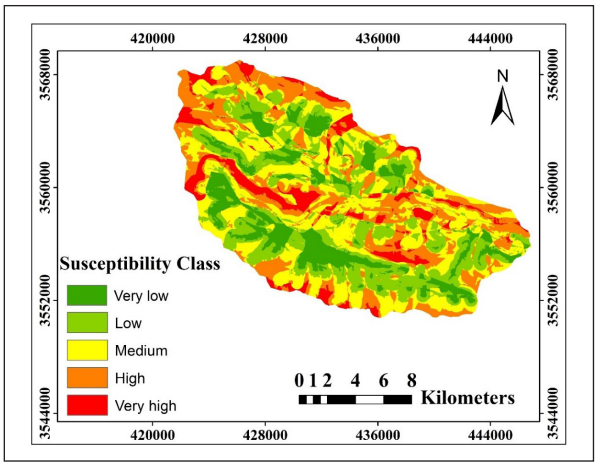

Figure 5. Landslide susceptibility maps based on: the stepwise regression model.

Table 2. The distribution of area in different landslide susceptibility classes.

Logistic regression model			Stepwise regression model		
Hazard class	Area (ha)	% Area	Hazard class	Area (ha)	% Area
Very low	1371.77	4.97	Very low	5340.13	19.34
Low	2377.39	8.61	Low	9271.99	33.58
Medium	11200.63	40.57	Medium	5049.92	15.29
High	2451.98	8.88	High	4521.22	16.38
Very high	10225.19	37.04	Very high	3426.38	12.41
Total	27627.19	100	Total	27627.19	100

3.3 Importance of Landslide Effective Factors

Given the results, the determinant factors such as slope aspect, precipitation, elevation, geology, and land use affect the multivariate logistic regression model function positively (Eq. 2). The highest positive β coefficient is attributed to the precipitation which is 0.00344. On the other hand, distance from faults, distance from stream and distance from roads negatively influence landslide occurrence with β coefficients of -0.000077, -0.000163, and -0.000415, respectively which are consistent with the results of Devkota et al. (2013). Also, distance from roads had the highest negative influence on logistic regression. 'Variance inflation factor' (VIF) and the 'Tolerance' (TOL) are two important indices for multi-collinearity diagnosis (O'Brien, 2007). The tolerance and variance inflation factors were computed for this study, and variables with VIF > 5 and TOL < 0.1 should be excluded from the LR analysis, but there was not any multi-collinearity problem in the landslide effective factors used in this study.

4. Conclusions

Conditions in the Doab Samsami watershed including geology, roughness, geomorphology and tectonic conditions as well as anthropogenic pressure factors such as land use and rural roads' changes have paved the way for landslide occurrence to the point that this phenomenon has occurred in thirty-seven cases with an approximate extent of 635 hectares in the watershed basin. Therefore, in the current study, the stepwise regression and logistic regression models have been used for the sake of mapping landslide hazards in the Doab Samsami Watershed, Chaharmahal Va Bakhtiari Province, Iran. A landslide inventory map and nine landslide effective factors were prepared for this investigation. After that, landslide susceptibility maps were generated using the two aforementioned modelsGiven the superiority of the logistic multivariate regression in landslide hazard mapping in the study area, taking very high susceptible class of landslide hazards produced by this model, which covered 46% of the study area, into account, is of great importance. Determining importance of different landslide effective factors is a necessary step in landslide susceptibility mapping. In several studies logistic regression model has been used in order to determine the importance of effective factors on landslide occurrence (Yesilnacar and Topal, 2005; Ayalew and Yamagishi, 2005; Nandi and Shakoor, 2009; Karimi Sangchini et al., 2016). According to the results, the effective factors such as slope aspect, precipitation, elevation, geology, and land use affect the multivariate logistic regression model function positively. The main advantage of logistic regression over simple multiple regressions is that LR allows the use of

binary dependent variable types in landslide susceptibility mapping. Although logistic regression is a commonly applied quantitative susceptibility mapping method, it has a major limitation of yielding average parameters for the study area (Erner et al., 2010), which may differ locally in different parts of the study area. This implies a high susceptibility to landslide in the watershed basin which is to be considered in the susceptibility management, landslide losses, and land use planning. Finally, the methodology developed in the present study can be generalized in other areas with similar climatic, geological, and topographical conditions in order to facilitate land use planning and hazard management.

References

Akgun, A. and Turk, N. (2010). Landslide susceptibility mapping for Ayvalik (Western Turkey) and its vicinity by multi-criteria decision analysis. Environmental Earth Sciences 61: 595–611.

Aleotti, P. and Chowdhury, R. (1999). Landslide hazard assessment: summary review and new perspectives. Bulletin of Engineering Geology and the Environment 58: 21-44.

Awawdeh, M, ElMughrabi, M., Atallah, M. (2018). Landslide susceptibility mapping using GIS and weighted overlay method: a case study from North Jordan. Environmental Earth Sciences 77(21): 732. Doi: 10.1007/s12665-018-7910-8.

Ayalew, L. and Yamagishi, H. (2005). The application of GIS-based logistic regression for landslide susceptibility mapping in the Kakuda-Yahiko Mountains, Central Japan. Geomorphology 65: 15–31.

Bijukchhen, S.M., Kayastha, P., Dhital, M.R. (2013). A comparative evaluation of heuristic and bivariate statistical modelling for landslide susceptibility mappings in Ghurmi–Dhad Khola, east Nepal. Arabian Journal of Geosciences 6(8): 2727-2743.

Brenning, A. (2005). Spatial prediction models for landslide hazards: review, comparison and evaluation. Natural Hazards Earth Systems Science 5(6): 853–862, Doi: 10.5194/nhess-5-853-2005.

Caniani, D., Pascale, S., Sdao, F., Sole, A. (2008). Neural networks and landslide susceptibility: a case study of the urban area of Potenza. Natural Hazards 45:55–72.

Cartographic Center of Iran. (2003). Cartographical map of Iran (1:25,000-scale series).

Dahal, R.K., Hasegawa, S., Nonomura, S., Yamanaka, M., Masuda, T., Nishino, K. (2008). GIS-based weights-of-evidence modelling of rainfall-induced landslides in small catchments for landslide susceptibility mapping. Environmental Geology 54: 311–324.

Devkota, K.C., Regmi, A.D., Pourghasemi, H.R., Yoshida, K., Pradhan, B., Ryu, I.C., Althuwaynee, O.F. (2013). Landslide susceptibility mapping using certainty factor, index of entropy and logistic regression models in GIS and their comparison at Mugling– Narayanghat road section in Nepal Himalaya. Natural Hazards 65:135–165.

Dou, J., Oguchi, T., Hayakawa, Y.S., Uchiyama, S., Saito, H., Paudel, U. (2014). GIS-Based Landslide Susceptibility Mapping Using a Certainty Factor Model and Its Validation in the Chuetsu Area, Central Japan. Landslide Science for a Safer Geoenvironment 2: 419-424.

Dou, J., Dieu Bui, T., Yunus, A.P., Jia, K., Song, X., Revhaug, I., Xia, H., Zhu, Z. (2015a) Optimization of Causative Factors for Landslide Susceptibility Evaluation Using Remote Sensing and GIS Data in Parts of Niigata, Japan. PLoS ONE 10(7): e0133262. Doi:10.1371/journal.pone.0133262.

Dou, J., Yamagishi, H., Pourghasemi, H.R., Yunus, A.P., Song, X., Xu, Y., Zhu, Z. (2015b). An integrated artificial neural network model for the landslide susceptibility assessment of Osado Island, Japan. Natural Hazards 78: 1749–1776.

Dou, J., Chang, K.T., Chen, S., Yunus, A.P., Liu, J.K., Xia, H., Zhu, Z. (2015c) Automatic Case-Based Reasoning Approach for Landslide Detection: Integration of Object-Oriented Image Analysis and a Genetic Algorithm. Remote Sensing 7: 4318-4342.

Ercanoglu, M., Kasmer, O., Temiz, N. (2008). Adaptation and comparison of expert opinion to analytical hierarchy process for landslide susceptibility mapping. Bulletin of Engineering Geology and the Environment 67:565–578.

Erner, A., Sebnem, H., Duzgun, B. (2010). Improvement of statistical landslide susceptibility mapping by using spatial and global regression method in the case of More and Romsdal (Norway). Landslides 7: 55-68.

ESRI (2008). ArcGIS 9.3 ESRI Inc., Redlands, California.

Geological Survey and Mineral Explorations of Iran. (1996). Geological map of Iran, Shahrekord sheet.

Gupta, R.P., Kanungo, D.P., Arora, M.K., Sarkar, S. (2008). Approaches for comparative evaluation of raster GIS-based landslide susceptibility zonation maps. International Journal of Applied Earth Observation and Geoinformation 10:330–341.

Gorsevski, P.V., Jankowski, P., Paul, P.E. (2006). Heuristic approach for mapping landslide hazard integrating fuzzy logic with analytic hierarchy process. Control and Cybernetics 35(1): 1–26.

Guzzetti, F. (2002) Landslide hazard assessment and risk evaluation: overview, limits and prospective. Proceedings 3rd MITCH Workshop Floods, Droughts and Landslides Who Plans, Who Pays 24–26.

Felicisimo, A., Cuartero, A., Remondo, J., Quiros, E. (2013). Mapping landslide susceptibility with logistic regression, multiple adaptive regression splines, classification and regression trees, and maximum entropy methods: a comparative study. Landslides 10(2): 175-189.

Jaafari, A., Najafi, A., Pourghasemi, H.R., Rezaeian, J., Sattarian, A. (2014). GIS-based frequency ratio and index of entropy models for landslide susceptibility assessment in the Caspian forest, north- ern Iran. International Journal of Environmental Science and Technology11 (4): 909–926.

Karimi Sangchini, E., Ownegh, M., Sadoddin, A., Mashayekhan, A. (2011). Probabilistic Landslide Risk Analysis and Mapping (Case Study: Chehel-Chai watershed, Golestan Province, Iran). Journal of Rangeland Science 2(1): 425-436.

Karimi Sangchini, E., Arami, A., Rezaii Moghadam, H., Khodabakhshi, Z., Jaafari, R. (2014). Risk analysis for landslides in Babaheydar Watershed, Chaharmahal-e-Bakhtiari Province, Iran. Iranian Journal of Earth Science. 6: 121-132.

Karimi Sangchini, E., Nowjavan, M.R., Arami, A. (2015). Landslide susceptibility mapping using logistic regression in Babaheydar Watershed, Chaharmahal-e-Bakhtiari Province, Iran. Journal of the Faculty of Forestry Istanbul University 65(1): 30-40. Doi:10.17099/jffiu.52751.

Karimi Sangchini, E., Emami, S.N., Tahmasebipour, N., Pourghasemi, H.P., Naghibi, S.A., Arami, A., Pradhan, B. (2016). Assessment and comparison of combined bivariate and AHP models with logistic regression for landslide susceptibility mapping in the Chaharmahal-e-Bakhtiari Province, Iran. Arabian Journal of Geosciences 9(201): 1-15. Doi: 10.1007/s12517-015-2258-9.

Kayastha, P., Dhital, M.R., De Smedt, F. (2012). Evaluation of the consistency of landslide susceptibility mapping: a case study from the Kankai watershed in east Nepal. Landslides 10(6): 785-799.

Kelarestaghi, A and Ahmadi, H. (2009). Landslide susceptibility analysis with a bivariate approach and GIS in Northern Iran. Arabian Journal of Geosciences 2: 95–101.

Komac, M.A. (2006). Landslide susceptibility model using the analytical hierarchy process method and multivariate statistics in per Alpine Slovenia. Geomorphology 74(1–4):17–28.

Kouli, M., Loupasakis, C., Soupios, P., Vallianatos, F. (2010). Landslide hazard zonation in high risk areas of Rethymno Prefecture, Crete Island, Greece. Natural Hazards 2: 599–621.

Lee, E.M. and Jones, D.K.C. (2004). Landslide risk assessment. Thomas Telford, London.

Lee, S.T., Yu, T.T., Peng, W.F., Wang, C.L. (2010). Incorporating the effects of topographic amplification in the analysis of earthquake-induced landslide hazards using logistic regression. Natural Hazards and Earth System Sciences 10: 2475-2488. Doi: 10.5194/nhess-10-2475-2010.

Mohammady, M., Pourghasemi, H.R., Pradhan, B. (2012). Landslide susceptibility mapping at Golestan Province Iran: a comparison between frequency ratio, Dempster-Shafer, and weights-of evidence models. Journal of Asian Earth Sciences 61: 221–236.

Naghibi, S.A., Pourghasemi, H.R., Pourtaghi, Z.S., Rezaei, A. (2015). Groundwater qanat potential mapping using frequency ratio and Shannon's entropy models in the Moghan watershed, Iran. Earth Science Informatics 8(1): 171-186.

Nandi, A. and Shakoor, A.A. (2009). GIS-based landslide susceptibility evaluation using bivariate and multivariate statistical analyses. Engineering Geology 110:11–20.

O'Brien, R.M. (2007). A caution regarding rules of thumb for variance inflation factors. Quality and Quantity 41(5): 673–690.

Park, S., Choi, C., Kim, B., Kim, J. (2013). Landslide susceptibility mapping using frequency ratio, analytic hierarchy process, logistic regression, and artificial neural network methods at the Inje area, Korea. Environmental Earth Sciences 68(5): 1443-1464.

Polykretis, C., Ferentinou, M., Chalkias, C. (2015). Comparative study of landslide susceptibility mapping using landslide susceptibility index and artificial neural networks in the Krios River and Krathis River catchments (northern Peloponnesus, Greece). Bulletin of Engineering Geology and the Environment 74(1): 27–45.

Pourghasemi, H.R., Pradhan, B., Gokceoglu, C. (2012) Application of fuzzy logic and analytical hierarchy process (AHP) to landslide susceptibility mapping at Haraz watershed, Iran. Natural Hazards 63:965–996.

Pourghasemi, H.R., Pradhan, B., Gokceoglu, C., Mohammadi, M., Moradi, H.R. (2013). Application of weights-of-evidence and certainty factor models and their comparison in landslide susceptibility mapping at Haraz watershed, Iran. Arabian Journal of Geosciences 6(7): 2351-2365.

Pradhan, B., Youssef, A.M., Varathrajoo, R. (2010). Approaches for delineating landslide hazard areas using different training sites in an advanced artificial neural network model. Geo-spatial Information Science 13(2): 93–102.

Rahman, M.D.R. and Saha, S.K. (2008). Remote sensing, spatial multi criteria evaluation (SMCE) and analytical hierarchy process (AHP) in optimal cropping pattern planning for a flood prone area. Journal of Spatial Science 53: 2161–2177.

Regmi, A.D., Chandra Devkota, K., Yoshida, K., Pradhan, B., Pourghasemi, H.R., Kumamoto, T., Akgun, A. (2014). Application of frequency ratio, statistical index, and weights-of-evidence models and their comparison in landslide susceptibility mapping in Central Nepal Himalaya. Arabian Journal of Geosciences 7(2): 725-742.

Sakar, S., Kanungo, D.P., Mehrotar, G.S. (1995) Landslide zonation: A case study Garhwal Hymalia, India. Mountain Research and Development 15(4): 301-330.

Tangestani, M.H. (2009). A comparative study of Demster-Shafer and fuzzy models for landslide susceptibility mapping using a GIS: an experience from Zagros Mountains, SW Iran. Journal of Asian Earth Sciences 35: 66–73.

Yalcin, A. (2008). GIS-based landslide susceptibility mapping using analytical hierarchy process and bivariate statistics in Ardesen (Turkey): comparisons of results and confirmations. Catena 72:1–12.

Yesilnacar, E. and Topal, T. (2005). Landslide susceptibility mapping: a comparison of logistic regression and neural networks methods in a medium scale study, Hendek region (Turkey). Engineering Geology 79: 251–266.

Yilmaz, C., Topal, T., Suzen, M.L. (2012). GIS-based landslide susceptibility mapping using bivariate statistical analysis in Devrek (Zonguldak-Turkey). Environmental Earth Sciences 65: 2161–2178.

Youssef, A.M, Pourghasemi, H.R., El-Haddad, B.A., Dhahry, B.K. (2015a). Landslide susceptibility maps using different probabilistic and bivariate statistical models and comparison of their performance at Wadi Itwad Basin, Asir Region, Saudi Arabia. Bulletin of Engineering Geology and the Environment 75: 63-87. Doi.org/10.1007/s10064-015-0734-9.

Youssef, A.M., Pradhan, B., Pourghasemi, H.R., Abdullah, S. (2015b). Landslide susceptibility assessment at Wadi Jawrah Basin, Jizan region, Saudi Arabia using two bivariate models in GIS. Geosciences Journal. Doi:10.1007/s12303-014-0065-z.

Zare, M., Pourghasemi, H.R., Vafakhah, M., Pradhan, B. (2013). Landslide susceptibility mapping at Vaz watershed (Iran) using an artificial neural network model: a comparison between multi-layer perceptron (MLP) and radial basic function (RBF) algorithms. Arabian Journal of Geosciences 6(8): 2873-2888.

JJEES

JJEES (2020) 11 (3): 183-192
ISSN 1995-6681

Jordan Journal of Earth and Environmental Sciences

Assessment of Rangeland Condition and its Application in Rangeland Management Using Multi-Criteria Analysis

Marzieh Asgari[1*], Ali Ariapour[2], Armin Mashayekhan[3]

[1]Young Researchers and Elite Club, Borujerd Branch, Islamic Azad University, Borujerd, Iran
[2]Department of Range Management, Borujerd Branch, Islamic Azad University, Borujerd, Iran
[3]Young Researchers and Elite Club, Gorgan Branch, Islamic Azad University, Gorgan, Iran

Received 23 December 2019; Accepted 2 April 2020

Abstract

This study is aimed at evaluating the modified four-factor method to determine the condition of rangelands using multi-criteria decision-making methods in two rangelands in Lorestan Province, Iran (Sarabsefid Boroujerd and Lasore Dorod). In this study, range condition was studied using the modified four-factor method. In both rangelands, three transects of 100m were located within the areas. Ten 1m^2 quadrates were randomly and systematically placed along each 100m transect. A total of 150 quadrates were placed in Sarabsefid and Lasore, respectively. The evaluation criteria and questionnaires completed by experts were compared and ranked using the multi-criteria decision-making methods (AHP and TOPSIS) in the AHP Solver and TOPSIS Solver software. The results showed that the percentage of plant cover was the most important criterion in determining rangeland condition in both areas in TOPSIS. In the hierarchical method (AHP), the percentage of plant cover had the highest weight in Sarabsefid and Lasore (0.5576 and 0.5983, respectively). Both multi-criteria analysis methods produced similar results in terms of evaluating the modified four-factor method and prioritizing expert opinions for both rangelands.

Keywords: Rangeland, AHP-TOPSIS, Modified four-factor method, Experts' opinions.

1. Introduction

Rangelands are among the most important renewable resources of every country, and they play an essential role in supporting livestock and supplying protein. To manage these vital resources, it is necessary to use appropriate methods and tools to monitor their health (Herrero et al., 2013). Managers must decide how to manage a rangeland and to adjust their approaches based on the rangeland's condition (Trollope, 1981). Rangeland condition refers to plant conditions in terms of long-term capability. Rangeland condition reflects the health of a rangeland compared with the climax stage and is one of the important factors in evaluating rangeland ecosystems (Ahmadpour et al., 2016). This metric is used to select appropriate strategies for rangeland management (Faramarzi et al., 2010; Mui-How and Minowa, 2005). Rangeland condition represents the history of effects of living and non-living factors on plant and soil. Therefore, analyzing factors influencing rangeland condition is essential to understand how the system reacts in response to wildlife, grazing and the effect of rangeland managers. It is also potentially useful in land-use assessment and in the conservation of natural values (Phelps and Kaplan, 2017; Dwyer, 1978). During the second half of the twentieth century in many countries, new changes and challenges emerged, which required the use of reliable methods that allow us to recognize such new changes and challenges (Getabalew and Alemneh, 2019). Lack of proper understanding of the potential of rangeland ecosystems and the adoption of incorrect management methods are two reasons contributing to the degradation of rangelands. A wide variety of factors, such as climate change, grazing, wildlife, the effect of rangeland managers and livestock producers are most likely affecting rangelands ecosystems' condition (Getabalew and Alemneh, 2019; Faramarzi et al., 2010; Anada and Herath, 2007). Different rangeland conditions require different management practices. For example, in good conditions, management practices try to maintain the prevailing state; in poor conditions, management strategies should be aimed at improving the conditions of the rangeland. For this reason, it is important to identify the condition of rangelands. The study of changes in rangeland condition and knowledge of the processes behind these changes is one of the important issues in planning and applying rangeland management. Most of the methods used to determine rangeland condition, such as the four-factor method, the African method, the six-factor method, etc., the usage of indices such as vigor and vitality of plants, plant composition, and soil conditions (Karami et al., 2014). Most of these approaches are qualitative, and are

* Corresponding author e-mail: marziye.asgari@gmail.com

consequently subject to personal judgement (karami et al., 2014; Dettenmaier et al., 2017). It is very important to use quantitative methods to assess rangeland conditions since these methods are not influenced by personal variations in judgement and measurement. Multi-criteria decision-making methods are an effective way to quantitatively analyze rangeland conditions. Multi-criteria decision-making techniques enable us to select multiple qualitative and quantitative criteria to guide our decision making (Guarini et al., 2018; D'Urso and Masi, 2015; Ghassemi and Danesh, 2012). Two of the most important multi-criteria decision-making methods are the Technique for Order of Preference by Similarity to Ideal Solution (TOPSIS) and Analytic Hierarchy Process (AHP). AHP has become one of the pervasive MCDA tool and has gained immense appreciation in different areas of research because of its computational simplicity, flexibility to be integrated with other techniques irrespective of their limitations (Mukherjee, 2014).

TOPSIS is a multiple criteria method to identify solutions from a finite set of alternatives based upon simultaneous minimization of distance from an ideal point and maximization of distance from a nadir point (Olson, 2004). It is one of the classical MCDM approaches, based on aggregating function to find a solution which is nearest to positive ideal solution (PIS) and farthest from negative ideal solution (NIS); however, it does not consider relative importance of these distances (Opricovic and Tzeng, 2004). It has been reported that hierarchical analysis can reduce human error (Bababeipouya et al., 2017; Xiaoyan et al., 2015; Mardani et al., 2015; Kuselman et al., 2013).

In rangeland and environmental planning, low confidence in variables and large timescales has created a challenge in decision-making. Multi-criteria decision-making methods can respond to these challenges (Penadés-Plà et al., 2016; Anada and Herath, 2007; Šikšnelytė et al., 2018). These methods provide the appropriate decision-making framework for planning and management because they consider contradictory, ambiguous, multi-dimensional, and non-comparable goals (Inotai et al., 2018; Danesh et al., 2017; Danesh et al., 2018; Erdogan et al., 2019; Abubakar et al., 2019; Angelis and Kanavos, 2017). A correct understanding and evaluation of rangelands lead to proper decision making regarding their abilities, capabilities, and constraints. Therefore, it is necessary to develop methods that allow for the evaluation and discovery of these relationships, changes, and their direction (Kornhaber et al., 2016; Cain, 1932). This research is aimed at assessing rangeland condition using multi-criteria decision-making methods, which creates an opportunity for selecting and categorizing indicators and prioritizing expert opinions to find efficient solutions.

2. Materials and Methodology

2.1 Study Site

In this study, two locations in Lorestan province, Iran, were studied. The studied areas had similar climates and plants, which enables the modified four-factor method to determine the rangelands' conditions. The study sites included Sarabsefid Boroujerd with an area of 8580 ha and Lasore Dorod with an area of 2662 ha. The study area is located in 46º36′48″- 48º27′46″ eastern longitudes and 33º53′31″- 33º58′24″ northern latitudes in Lorestan Province of Iran. The elevation range is 1974-3451 m above sea level, and the average elevation is 2641 m. Mean 20 year rainfall of the zone is 450.9 mm. Maximum and minimum annual temperature rates are 39.2 and 11.5 ºC, respectively. This zone is dry for about four to five months a year.

2.2 Methodology and Data Collection

At first, two areas at three different levels of utilization including exclosure (low grazing intensity), key (average grazing intensity) and critical (high grazing intensity) areas were separated from each other. Sampling was carried out by the randomized-systematic method (Mesdaghi, 2008) so that three random transects were established in each plant type, then 10 plots of 1-m^2, were systematically selected along each transect (Cox, 2002). The current rangelands' condition was studied, and rangeland types were identified using field observation and GPS. The range condition was determined using the modified four-factor method. The modified four-factor method for each factor was carried out in the field survey according to the opinions of three experts. All classes were evaluated for all factors, and the rangelands' conditions were determined using the modified four-factor method. Then, the AHP technique and TOPSIS were applied to weigh the various criteria and to rank the alternatives affecting rangeland condition. Plant cover was measured using plot-transects selected by the random-systematic sampling. In this area, sixteen plant types were determined based on field data (Table 1).

Plots with a minimum area of 1 m^2 were used for sampling. At least three transects were selected, perpendicular to the slope. In order to determine the sample size, ten plots were systematically picked in each plant type and the mean and variance of canopy cover were calculated.

Then, the sample size was determined using the Cochran formula.

$$N = \frac{t^2 \times s^2}{P^2 \times \overline{X}^2}$$

N = minimum required number of samples

t = from Student's t-distribution, at 90% confidence level

X = average of initial samples

P = Error range (± 0.1)

$$S^2 = \sum x^2 - \left(\sum x^2\right)\frac{n}{n-1}$$

S^2 = variance of initial samples

n = number of initial samples (10)

Table 1. Types of plants in this area and percentage of each type in all areas

Code	Type Name	Abbreviation	Area (Ha)	Percentage of all
1	Garden-Farm land	Ga-Fa	416.48	7.1
2	Astragalus adscendens-Eryngium noeanum	As.ad-Er.no	1094.09	18.66
3	Astragalus adscendens-Eryngium noeanum	As.ad-Er.no	969.8	16.54
4	Astragalus microcephalus–Annual grass	As.mi-An.gr	261.27	4.46
5	Astragalus microcephalus–Annual grass	As.mi-An.gr	205.67	3.51
6	Astragalus microcephalus-Cousinia jacobsii	As.mi-Co.ja	206.19	3.52
7	Astragalus microcephalus-Cousinia jacobsii	As.mi-Co.ja	491.37	8.38
8	Astragalus microcephalus-Cousinia jacobsii	As.mi-Co.ja	533.49	9.1
9	Astragalus microcephalus -Melica persica	As.mi-Me.pe	122.06	2.08
10	Astragalus microcephalus -Melica persica	As.mi-Me.pe	146.56	2.5
11	Astragalus microcephalus -Melica persica	As.mi-Me.pe	140.91	2.40
12	Astragalus microcephalus-Rhus coriaria	As.mi-Rh.co	269.35	4.59
13	Hordeum bulbosum-Astragalus microcephalus	Ho.bu-As.mi	361.35	6.16
14	Hordeum bulbosum-Astragalus microcephalus	Ho.bu-As.mi	327.6	5.59
15	Hordeum bulbosum-Astragalus microcephalus	Ho.bu-As.mi	116.75	1.99
16	Hordeum bulbosum-Astragalus microcephalus	Ho.bu-As.mi	201.29	3.43
Total			**5864**	**100**

Totally 150 quadrates were placed in Sarabsefid and Lasore, respectively. The hierarchical method (AHP) and TOPSIS were implemented using AHP Solver (version 1) and TOPSIS Solver, respectively (Khedrigharibvand et al., 2018).

An AHP questionnaire was designed to determine the weights of the four sub-attributes: the respondents were asked the following question for each pair of criteria: how important criterion A is compared with criterion B in the region? A nine-point scale was used, one representing equal importance, and nine representing complete dominance of one of the criteria (Saaty, 1980). In a TOPSIS questionnaire, the respondents were asked to score the alternatives against the applied criteria, based on the five-point Likert scale. The criteria were weighed based on the experts' preference values. Then, the consistency ratio was calculated to indicate if the experts compared the criteria with great care (Saaty, 1980). Finally, the TOPSIS was applied to the outcomes of the AHP to explore the most appropriate factors affecting rangeland condition.

2.3 Modified Four-factor Method

Considering the modified four-factor method, the studied factors include soil conditions (soil erosion and conservation), and plant conditions (plant composition, percentage of plant cover, vigor, and vitality of plant); range conditions were classified into five classes.

Using the modified four-factor method, rangeland condition was calculated based on the sum of scores obtained for four factors: soil erosion and soil conservation (in five classes, score of 0-20), percentage of plant cover (in ten classes, score of 1-10), plant composition (in five classes, score of 1-10), and vigor and vitality of plants (in four classes, score of 1-10) and rangeland condition levels involve excellent (45-100 scores), good (38-45 scores), fair (31-37scores), poor (20-30 scores) and very poor (0-20 scores). Scores of each element had been determined, then based on total scores, the range conditions were determined (Moghadam, 1994).

3. Results

3.1 Development of a Set of Decision-making Criteria

The criteria affecting range condition were expanded, and a list of suitable criteria was developed (Table 3). Ultimately, four sub criteria were developed based on the modified four-factor method (Table 2).

3.2 Evaluating the Weight of Criteria by the AHP Technique

The AHP technique was used to organize multiple-choice criteria into a hierarchy, assessing their relative importance, and to calculate the weight of each criterion and the overall weight of the criteria (Tables 11 and 13). The consistency ratio was calculated as 0.1%, which showed that the experts compared the criteria precisely. Although all criteria with high weights were considered effective for range condition, the two highest criteria in the context of the region included: soil erosion and conservation and percentage of plant cover. Plant composition and vigor and vitality of plant were ranked as the lowest sub-criteria respectively (Tables 11 and 13). Figures 1 and 2 illustrate the global weights of the evaluation criteria.

3.3 Ranking of Factors Affecting Range Condition

After assigning weight to each criterion using the AHP, the factors affecting range condition were ranked using the TOPSIS. In a descending order of preference, the factors are presented in Figure 10. The percentage of plant cover was found to the best factor based on the affecting factors,

followed by Soil erosion and Conservation. Compared with the other factors, Plant composition and Plant vigor and vitality were found to have the lowest values.

3.4 Determination of Rangeland Condition by the Modified Four-Factor Method

Rangeland evaluation was conducted by three experts using the modified four-factor method (Table 2).

Table 2. Results of the evaluation conducted by different experts using the modified four-factor method

Rangeland Condition	Score	Factors	experts	Area
Good	15-19	Soil erosion and conservation	Expert1	Lasore Dorod
	9	Percentage of plant cover		
	8	Plant composition		
	10	Plant vigor and vitality		
Good	15-19	Soil erosion and conservation	2 expert	
	9	Percentage of plant cover		
	8	Plant composition		
	7	Plant vigor and vitality		
Medium	10-14	Soil erosion and conservation	3 expert	
	8	Percentage of plant cover		
	6	Plant composition		
	7	Plant vigor and vitality		
Medium	10-14	Soil erosion and conservation	Expert 1	Sarabsefid Boroujerd
	8	Percentage of plant cover		
	4	Plant composition		
	7	Plant vigor and vitality		
Good	15-19	Soil erosion and conservation	2 expert	
	6	Percentage of plant cover		
	6	Plant composition		
	10	Plant vigor and vitality		
Poor	10-14	Soil erosion and conservation	3 expert	
	4	Percentage of plant cover		
	4	Plant composition		
	5	Plant vigor and vitality		

Score: Score of Range condition's estimation method

3.5 Multi-criteria Decision-making Method for the Condition of Sarabsefid Boroujerd Using TOPSIS

The results of TOPSIS analysis according to the experts' opinions are shown in Tables 3 to 6.

Table 3. Normalization of the decision matrix, Sarabsefid Boroujerd

Un-scaled matrix	expert1	expert2	Expert 3
Soil erosion and conservation	2821/0	467/0	4961/0
Plant composition	094/0	1648/0	1654/0
Plant vigor and vitality	1646/0	2747/0	2067/0
Percentage of plant cover	9405/0	8242/0	8269/0

In this step, the scales in the decision matrix were un-scaled. Therefore, each of the values was divided by the vector size of the same index.

Table 4. Normal matrix weighing, Sarabsefid Boroujerd

Weighted matrix	expert1	expert2	Expert 3
Soil erosion and conservation	1411/0	2335/0	2481/0
Plant composition	047/0	0824/0	0827/0
Plant vigor and vitality	0823/0	1374/0	1034/0
Percentage of plant cover	4702/0	4121/0	4134/0

The decision matrix is parametric and needs to be quantified. For this purpose, the decision-maker allocated a weight for each index, and the sum of the weights was multiplied into the normalized matrix.

Table 5. Determination of positive and negative ideal solutions, Sarabsefid Boroujerd

ideal solution	expert1	expert2	Expert 3
+	4702/0	4121/0	4134/0
-	047/0	0824/0	0827/0

The two virtual options are the worst and best solutions.

Table 6. Calculation of closeness to the positive and negative ideal solutions, and the ranking of options, Sarabsefid Boroujerd

Result	closeness coefficient
Percentage of plant cover	1
Soil erosion and conservation	3724/0
Plant vigor and vitality	1077/0
Plant composition	0

The results obtained from Table 5 show that the percentage of plant cover, soil erosion and conservation, plant vigor and vitality, and plant composition were ranked 1st, 2nd, 3rd, and 4th, respectively. After normalizing the opinions in Table (3) and weighing the criteria in Table (4), the distance from the ideal positive and negative solutions as well as the relative closeness to the ideal solution were calculated and are presented in Table (5). Experts' opinions were arranged as expert 1, expert 3, and expert 2.

Finally, decision options were prioritized (Table 5). The ranking of decision options was based on the relative closeness to the ideal solution, so that the closer to 1 a decision option is, the higher its desirability. According to experts' opinions in the modified four-factor method, the rangeland's condition was reported as good, medium or poor. In TOPSIS, priority was given to the medium rangeland condition according to opinion of expert 1.

3.6 Multi-criteria Decision-making Method for Condition of Lasore Dorod Using TOPSIS Method

The results of TOPSIS analysis based on experts' opinions are shown in Tables 7 to 10.

Table 7. Normalization of the decision matrix, Lasore Dorod

Un-scaled matrix	expert1	expert2	Expert 3
Soil erosion and conservation	3543/0	4115/0	3632/0
Plant composition	1667/0	1646/0	1362/0
Plant vigor and vitality	2084/0	144/0	1589/0
Percentage of plant cover	8962/0	8848/0	9079/0

In this step, the scales in the decision matrix were un-scaled.

Table 8. Normal matrix weighing, Lasore Dorod

Weighted matrix	expert1	expert2	Expert 3
Soil erosion and conservation	1772/0	2058/0	1816/0
Plant composition	0834/0	0823/0	0681/0
Plant vigor and vitality	1042/0	072/0	0794
Percentage of plant cover	4481/0	4424/0	454/0

The decision matrix is parametric and needs to be quantified. Therefore, the decision-maker allocated a weight for each index, and the sum of the weights was multiplied into the normalized matrix.

Table 9. Determination of positive and negative ideal solutions, Lasore Dorod

ideal solution	expert1	expert2	Expert 3
+	4481/0	4424/0	454/0
-	0834/0	072/0	0681/0

The two virtual options are the worst and best solution.

Table 10. Calculation of closeness to the positive and negative ideal solutions and the ranking of options, Lasore Dorod

Result	closeness coefficient
Percentage of plant cover	1
Soil erosion and conservation	306/0
Plant vigor and vitality	0364/0
Plant composition	0158/0

The results obtained from Table 10 show that the percentage of plant cover, soil erosion and conservation, plant vigor and vitality, and plant composition were ranked 1st, 2nd, 3rd, and 4th, respectively. After normalizing the opinions in Table (7) and weighing criteria in Table (8), distance from the ideal positive and negative solutions as well as the relative closeness to the ideal solution were calculated and are presented in Table (9). Experts' opinions are arranged as expert 3, expert 1 and expert 2.

Finally, decision options were prioritized (Table 9). The ranking of decision options was based on the relative closeness to the ideal solution, hence the closer to 1 an option scores, the higher its desirability. According to experts' opinions on the modified four-factor method, the rangeland's condition was reported as good and medium. In TOPSIS, priority was given to the medium rangeland condition according to the opinion of expert 3.

3.7 Multi-criteria Decision-making Method for Condition of Sarabsefid Boroujerd Using AHP Method

Determination of the pair matrices and weight calculation for criteria and options are shown in Tables 11 and 12.

Table 11. Weight and rank of criteria in Sarabsefid Boroujerd

Factors	relative weight of factors	rank of factors
Soil erosion and conservation	2594/0	2
Plant composition	0705/0	4
Plant vigor and vitality	1124/0	3
Percentage of plant cover	5576/0	1

Table 12. Experts' opinions and prioritization in determining the condition of Sarabsefid Boroujerd

Condition	Sum of row	Percentage of plant cover	Plant vigor and vitality	Plant composition	Soil erosion and conservation	Indices	
Medium	43714/0	318662/0	035985/0	01763371/0	06485888/0	expert1	Options
Good	386923/0	159331/0	062607/0	03526742/0	12971775/0	expert2	
Poor	175937/0	079666/0	013779/0	01763371/0	06485888/0	expert3	

The results in Table 11 show that the percentage of plant cover, soil erosion and conservation, plant vigor and vitality, and plant composition were ranked 1st, 2nd, 3rd, and 4th, respectively; and the percentage of plant cover had the highest weight (0.5576). Figure 1 shows the same results. Table (12) shows that expert 1 evaluated the rangeland's condition as medium (at a value of 0.43714) with a priority of 1.

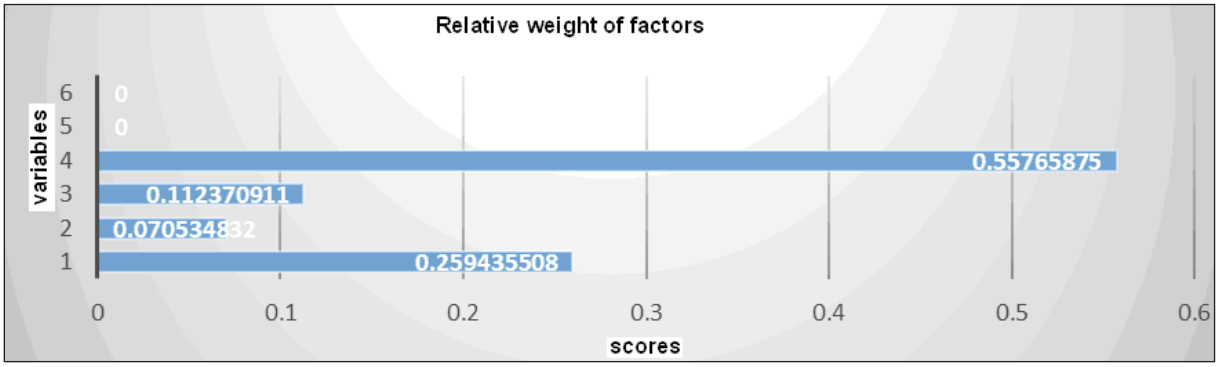

Figure 1. Relative weight of factors in the four-factor method for Sarabsefid Boroujerd using AHP

3.8 Multi-criteria Decision-making Method for Condition of Sarabsefid Boroujerd Using AHP Method

Determination of the pair matrices and weight calculation for criteria and options are shown in Tables 13 and 14.

Table 13. Weight and rank of criteria in Lasore Dorod

Factors	relative weight of factors	rank of factors
Soil erosion and conservation	2686/0	2
Plant composition	0523/0	4
Plant vigor and vitality	0808/0	3
Percentage of plant cover	5983/0	1

Table 14. Experts' opinions and prioritization in determining the condition of Lasore Dorod

Condition	Sum of row	Percentage of plant cover	Plant vigor and vitality	Plant composition	Soil erosion and conservation	Indices	
Good	344632/0	239327/0	040388/0	020927/0	04398956/0	expert 1	Options
Good	230161/0	119664/0	020194/0	010463/0	07984007/0	expert 2	
Medium	425207/0	239327/0	020194/0	020927/0	14475858/0	expert 3	

The results in Table (13) show that the percentage of plant cover, soil erosion and conservation, plant vigor and vitality, and plant composition were ranked 1st, 2nd, 3rd, and 4th, respectively. The percentage of plant cover factor had the highest weight at 0.59832. In addition, Figure 2 shows the same results. Table (14) shows that expert 3 evaluated the rangeland's condition as medium (at a value of 0.4252) with a priority of 1.

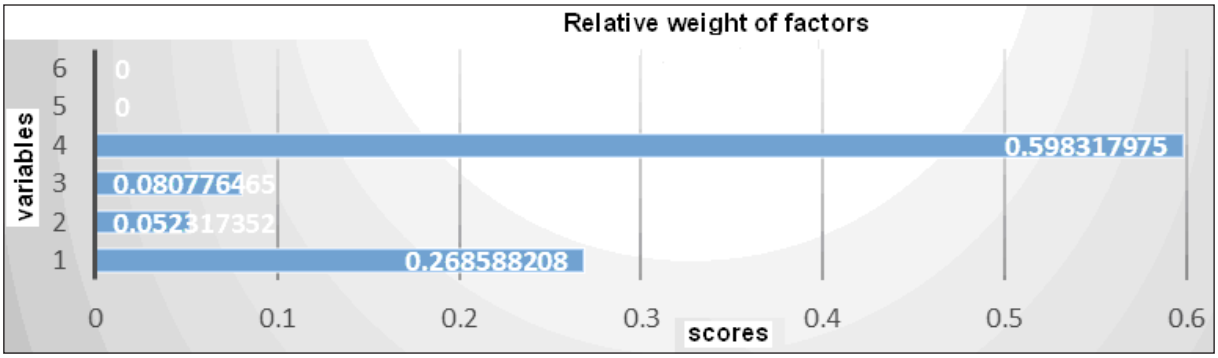

Figure 2. Relative weight of the four-factor method for Lasore Dorod using AHP method

The results of both methods of multi-criteria decision making (TOPSIS and AHP) show that the percentage of plant cover, soil erosion and conservation, plant vigor and vitality, and plant composition were ranked 1st, 2nd, 3rd, and 4th , respectively. Hence, similar results were obtained. The experts' opinions were also ranked according to priorities, and the medium condition was placed in priority 1. Both multi-criteria decision-making methods in this study showed that the percentage of plant cover and soil erosion and conservation were the most important factors among the four factors. The purpose of determining rangeland condition was to identify the extent of plant cover change associated with the changes in soil, as occurs in rangeland communities (14). The prioritization of experts' opinions suggests their different views on rangelands; depending on various factors their opinions may vary. Multi-criteria decision-making methods (TOPSIS and AHP), through prioritizing experts' opinions, showed that the rangeland might have a good condition, but the plant composition and the Soil erosion and conservation might be in a poor state. This disagreement shows that ratings may be made with error. Priority is given to the ideas that have the least error. Depending on experts' opinions, different views have been adopted for determining rangeland condition, leading to significant impacts on rangeland management decisions. Using GIS, two rangeland conditions (medium and poor) of Sarabsefid Boroujerd and Lasore Dorod were determined according to the plant type of the area (Figure 4).

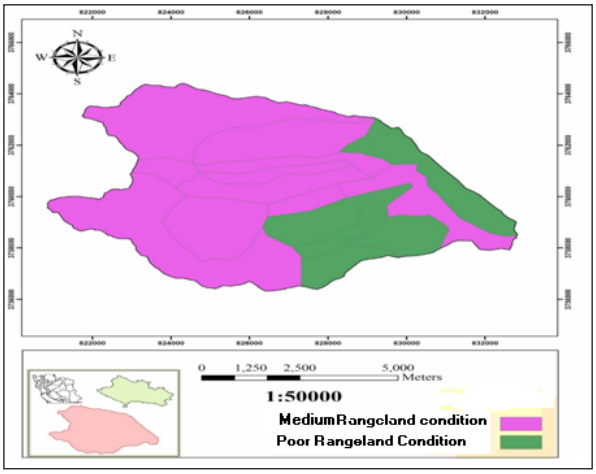

Figure 3. Sarabsefid Boroujerd Rangeland Condition

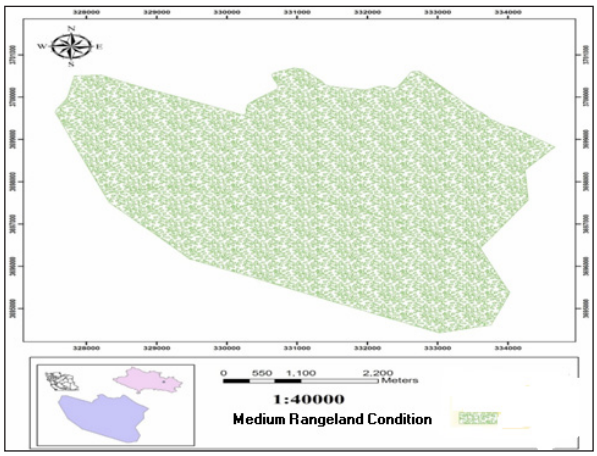

Figure 4. Lasore Dorod Rangeland Condition

The AHP method provides a framework for analyzing and transforming difficult and complex problems into a more logical and simplified hierarchy, through which the planner can easily evaluate the options with the help of criteria and sub-criteria. In TOPSIS method, the percentage of plant cover was the most important criterion in determining rangeland condition in both areas (Sarabsefid Boroujerd and Lasore Dorod). Using the AHP method, the percentage of plant cover had the highest weight in Sarabsefid Boroujerd and Lasore Dorod with 0.55576 and 0.5983 respectively (figures 1 - 2), supported by experts' opinions in the questionnaire (Tables 2, 6, 11 and 13). Multi-criteria decision-making methods produced the same results in prioritizing criteria in this study.

According to the results of prioritization of rangeland conditions, Sarabsefid Boroujerd was evaluated to be in medium condition according to both methods (TOPSIS and AHP; Tables 4 and 11). The medium condition was obtained for Lasore Dorod using both methods (Tables 8 and 13), which was consistent with results of Majiri et al. (2013). Using the multi-criteria methods, it was shown that no area is in good condition in Sarabsefid Boroujerd and Lasore Dorod. According to the estimates made by the Forests, Rangelands and Watershed Management Organization of Iran in 1995 of the 90 million ha of rangelands in Iran, 45.48% are poor to very poor, 41.45% are medium to poor and 10.33% are in a good condition (http://www.frw.org.ir). Currently, there

are no rangelands in the good condition in Iran; or their area is too small to be significant compared to the total area of rangelands. According to plant type, two rangeland conditions (medium and poor) of Sarabsefid Boroujerd were mapped using GIS (figure 4). Rangeland conditions for Lasore Dorod was medium and according to Tables 5, 9, 13, and 16, the evaluation is accurate. The results showed that the determination of rangeland conditions was more accurate using the methods, and emphasized the possibility of updating and forecasting the condition of rangelands. The determination and application of the best management practices for optimal resource management is necessary. The most effective management methods known in the world for integrating possible management practices in rangelands are approaches based on the development of management scenarios. Because each of the possible scenarios will have different and sometimes conflicting consequences, scenarios with priority and highest importance can be predicted using multi-criteria decision-making methods. The main objectives of rangeland management include the promotion of effective cooperation, a balanced and adequate planning and management, and a sustainable use of natural resources.

4. Discussion

The following sections shows the application of the AHP-TOPSIS Approach in Ranking Factors Affecting Rangeland Condition

4.1 Development of Decision-making Criteria

When selecting the factors which affect rangeland condition, specifying a set of factors that measure progress for the sake of having a sustainable range management is important. Due to the increasing complexity in the decision-making process and ensuring the right decision is made, a specific number of factors should be considered (Jalalifar et al., 2009). In the end, four factors affecting rangeland condition were determined using the modified four-factor method.

4.2 Weighting of Factors by the AHP Technique

Through the application of the AHP technique, the factors' weights were obtained. Under the conditions stated in this article, it appeared that the percentage of plant cover was considered more important than other factors. Regarding the factors affecting range condition, studies noted that the percentage of plant cover is essential for determining range condition (Khedrigharibvand et al., 2017; Getabalew and Alemneh, 2019).

4.3 Application of the TOPSIS

After the application of the TOPSIS, the percentage of plant cover was found to be the best factor, followed by soil erosion and conservation, plant vigor and vitality, and plant composition. Thus, the percentage of plant cover factor had the highest weight in rangeland condition determination. In comparison with other factors, plant vigor and vitality, and plant composition had the lowest values; these results deemed them to be affecting rangeland condition the least for a sustainable range management. However, all factors affecting rangeland condition should be considered for sustainable range management in general. In line with this, studies emphasized the importance of four factors affecting range condition for sustainable range management (Khedrigharibvand et al., 2015; Asgari et al., 2018).

5. Conclusions

In this study, to simplify decision-making activities, and make effective decisions and solve real- world problems, it was essential to apply a decision-making procedure (Shih et al., 2007). In line with this, the applications of decision support systems have been expanded in various study area (Khedrigharibvand et al., 2018; Shih et al., 2007; Yue, 2011). Regarding the application of the AHP and TOPSIS approach here, not only were factors affecting rangeland condition by multicriteria decision-making approach, but this was the first study to explore the most appropriate factors affecting rangeland condition. Concerning its applicability in dealing with the factors affecting rangeland condition, this approach (i.e. the AHP-TOPSIS multicriteria decision making approach) could be introduced as a way forward for approaching range management. For range management, the experts ranked the criteria and appropriate factors affecting range condition. The criteria weighing was assigned using the AHP technique. The factors affecting range condition were ranked using the TOPSIS. At the end, the most appropriate factor was extracted. This study concluded that all the factors affecting range condition (soil conditions and plant conditions), including the highest and lowest ranking, are important for approaching range management at the Lorestan province, Iran. This study suggests that the factors affecting range condition with the lowest values (i.e. plant composition and plant vigor and vitality) should still be considered for range management, and that government, institutions and people themselves should be responsible for supporting factors through supportive strategies (Khedrigharibvand et al., 2015). However, the potential of each region for the factors affecting range condition with the highest values should be explored as a priority. This implies that more supports and investments should be allocated for the most appropriate factor (percentage of plant cover). Criteria such as job opportunities were deemed important, and awareness of them was high. Regarding the most appropriate factors, developing non-resource-based factors (hunting, recreation and etc) can greatly reduce pressure on natural resources, and can create new job opportunities and prevent unemployment. Addressing these factors affecting range condition can stabilize the population of each area,

while creating a balance between humans, livestock, and natural resources. In considering these factors, this research demonstrated that the selection of factors affecting range condition was a complex and complicated decision. Thus, the approach presented in this study (AHP-TOPSIS) is suitable for rangeland managers to achieve a sustainable range management. Future studies may consider non-resource-based criteria and more experts randomly. Also, to assess uncertainty in judgments, further research can examine other techniques including ELECTRE, entropy-AHP-TOPSIS, fuzzy-AHP-TOPSIS, AHP-VIKOR, AHP-PROMETHEE. The combination of the AHP-TOPSIS approach and a GIS tool can create sources for additional information for the sake of examining the suitability of each factor.

Acknowledgments

The research team would like to thank the University of Borujerd branch for their valuable insights.

References

Abubakar, A.M., Elrehail, H., Alatailat, M.A., Elçi, A. (2019). Knowledge management, decision-making style and organizational performance. Journal of Innovation and Knowledge 4(2): 104-114.

Ahmadpour, A., Heshmati, G.H., Joulaie, R. (2016). Rangeland condition assessment based on economic criteria. Journal of landscape ecology 9(2): 1-15.

Anada, J. and Herath, G. (2007). Multiattribute Preference Modeling and Regional Landuse Planning. Ecological Economics 65(1): 325-335.

Angelis, A. and Kanavos, P. (2017). Multiple Criteria Decision Analysis (MCDA) for evaluating new medicines in Health Technology Assessment and beyond: The Advance Value Framework. Social Science and Medicine 188 (1): 137-156.

Asgari, M., Mashayekhan, A., Ariapour, A. (2018). Indicator species for Rangeland management by Anp-Dematel method (Case Study: Nahavand Rangeland). Journal of Rangeland Science 8(3): 285-295.

Bababeipouya, A., Hazrati, S., Vosoughi-Niri, M., Habibi, E. (2017). Evaluation human error in control room. Pakistan Journal of Medical and Health Sciences 11(4):1596-1600.

Cain, S.A. (1932). Concerning certain ecological concepts. Ecological Monographs 27(2): 475-508.

Cox, G.W. (2002). General ecology: laboratory manual. Mc Graw- Hill Pub. USA.

D'Urso, M.G. and Masi, D. (2015). Multi-criteria decision-making methods and their applications for human resources. The International Archives of the Photogrammetry. Remote Sensing and Spatial Information Sciences 6(1): 1-7.

Danesh, D., Ryan, M., Abbasi, A. (2017). A Systematic Comparison of Multi-criteria Decision Making Methods for the Improvement of Project Portfolio Management in Complex Organisations. International Journal of Management and Decision Making 16(1):1-11.

Danesh, D., Ryan, M., Abbasi, A. (2018). Multi-criteria decision-making methods for project portfolio management: A literature review. International Journal of Management and Decision Making 17(1):75-86.

Dettenmaier, S.J., Messmer, T.J., Hovick, T.K., Dahlgren, D.k. (2017). Effects of livestock grazing on rangeland biodiversity: A meta analysis of grouse populations. Ecological Evolution 7(19): 7620–7627.

Dwyer, D.D. (1978). Impact of poisonous plants on western U.S. grazing systems and livestock operations. pp. 13-21, In: Keeler, R. J., Van Kampen, K. R., James, L. F. (Eds.), Effects of Poisonous Plants on Livestock. Academic Press. N. Y.

Erdogan, S.A., Šaparauskas, J., Turskis, Z. (2019). A Multi-Criteria Decision-Making Model to Choose the Best Option for Sustainable Construction Management. Sustainability 11(1): 22-39.

Faramarzi, M., Kesting, S., Wrage, N. (2010). Rangeland condition in relation to environmental variables, grazing intensity and livestock owners' perceptions in semi-arid rangeland in western Iran. The Rangeland Journal 32(4): 367-377.

Getabalew, M. and Alemneh, T. (2019). Factors affecting the productivity of Rangelands. Journal of plant sciences and agricultural research 3(1): 1-6.

Ghassemi, S.A. and Danesh, S.H. (2012). Application of fuzzy analitical hierarchy process in determining the optimum alternative of brackish water desalination. Journal of Water and Soil 26(1): 999-1009.

Guarini, M.R., Battisti, F., Chiovitti, A. (2018). A Methodology for the Selection of Multi-Criteria Decision Analysis Methods in Real Estate and Land Management Processes. Sustainability 10(1): 1-28.

Herrero, M., Grace, D., Njuki, J., Jonson, N., Enahoro, D., Silvestre, S., Rufino, M.C. (2013). The role of livestock in developing countries. Animal 7(1): 3-18.

Inotai, A., Nguyen, H.T., Hidayat, B., Nurgozhin, T., Kiet, P.H.T., Campbell, J.D., Németh, B., Maniadakis, N., Brixner, D., Wijaya, K., Kaló, Z. (2018). Guidance toward the implementation of multicriteria decision analysis framework in developing countries. Expert Review Pharmacoeconomics and Outcomes Research 18(6):585-592.

Jalalifar, H., Behaadini, M., Bazzazi, AA. (2009). The optimum rock bolt support system selection by using AHP-Entropy-TOPSIS method. Journal of Mines, Metals and Fuels 57: 251-266.

Karami, E., Ariapour, A., Mehrabi, H.R. (2014). Modeling the Limitative Factors of Forage Production Suitability Using GIS (Case Study: Aliabad Rangelands, Lorestan, Iran). Journal of Rangeland Science 3(4): 1-11.

Khedrigharibvand, H., Azadi, H., Bahrami, H., Tesfamariam, Z., Bazzazi, A.A., Maeyer, P. D., Witlox, F. (2018). Sustainable rangeland management in southwest Iran: application of the AHP-TOPSIS approach in ranking livelihood alternatives. The Rangeland Journal 40: 603-614.

Khedrigharibvand, H., Azadi, H., Teklemariam, D., Houshyar, E., De Maeyer, P., Witlox, F. (2017). Livelihood alternatives model for sustainable rangeland management: a review of multi-criteria decisionmaking techniques. Environment, Development and Sustainability doi:10.1007/s10668-017-0035-5

Khedrigharibvand, H., Azadi, H., Witlox, F. (2015). Exploring appropriate livelihood alternatives for sustainable range land management. The Rangeland Journal 37:345-356. doi:10.1071/RJ15027

Kornhaber, R., Walsh, K., Duff, J., Walker, K. (2016). Enhancing adult therapeutic interpersonal relationships in the acute health care setting: an integrative review. Journal of Multidisciplinary Healthcare. 9(1): 537–546.

Kuselman, I., Pennecchi, F., Fajgelj, A., Karpov, Y. (2013). Human errors and reliability of test results in analytical chemistry. Accreditation and Quality Assurance 18(1):3-9.

Mardani, A., Jusoh, A., Kazimieras, E., Khalifah, Z, Nor, K.M. (2015). Application of multiple criteria decision making

techniques and approachs to evaluating of service quality. A systematic review of the literature. Journal of Business Economics and Management 16(5): 1034-1068.

Mesdaghi, M. (2008). Range management in Iran. 5th Edition. Publications of Imam Reza University, Mashahd, Iran 333p. (In Persian).

Moghadam, M.R. (1994). Rangeland assessment. Booklet of natural resources faculty. Tehran University, Tehran, Iran. (In Persian).

Mui-How, P.H. and Minowa, M. (2005). A GIS-based multi-criteria decision making approach to forest conservation planning at a landscape scale: a case study in the Kinabalu Area, Sabah, Malaysia. Journal of Landscape and Urban Planning 71(1): 207-222.

Mukherjee, K. (2014). Analytical hierarchy process and technique for order preference by similarity to ideal solution: a bibliometric analysis from past, present and future of AHP and TOPSIS. International Journal of Intelligent Engineering Informatics 2(3): 96-117.

Olson, D.L. (2004). Comparison of weights in TOPSIS models. Mathematical and Computer Modelling 40(7–8): 721–727.

Opricovic, S. and Tzeng, G.H. (2004). Compromise solution by MCDM methods: a comparative analysis of VIKOR and TOPSIS. European Journal of Operational Research 156(2): 445–455.

Penadés-Plà, V., García-Segura, T.V., Martí, J., Yepes, V. (2016). A Review of Multi-Criteria Decision-Making Methods Applied to the Sustainable Bridge Design. Sustainability 8(1): 12-25.

Phelps, N. and Kaplan, O. (2017). Land use for animal production in global change studies: Defining and characterizing a framework. Global Change Biology 23(11): 4457–4471.

Saaty, T.L. 1980). The Analytic Hierarchy Process: Planning, Priority Setting, Resources Allocation. (McGraw: New York).

Shih, H.S., Shyur, H.J., Lee, E.S. (2007). An extension of TOPSIS for group decision making. Mathematical and Computer Modelling 45: 801–813.

Šikšnelytė, I., Kazimieras-Zavadskas, E., Streimikiene, D. (2018). An Overview of Multi-Criteria Decision-Making Methods in Dealing with Sustainable Energy Development Issues. Energies 11(10): 27-54.

Trollope, W.S.W. (1981). Application of grassland management principles. In: Veld and Pasture Management in South Africa, University of Natal press.

Xiaoyan, S.U., Mahadevan, S., Xu, Y. (2015). Dependence Assessment in Human Reliability Analysis Using Evidence Theory and AHP. Risk Analysis 35(7): 1296-1316.

Yue, Z. (2011). A method for group decision-making based on determining weights of decision makers using TOPSIS. Applied Mathematical Modelling 35: 1926–1936.

JJEES

JJEES (2020) 11 (3): 193-201
ISSN 1995-6681

Jordan Journal of Earth and Environmental Sciences

Digital Mapping of Soil Properties in the Western-Facing Slope of Jabal Al-Arab at Suwaydaa Governorate, Syria

Alaa Khallouf [1,4], Sami AlHinawi[2], Wassim AlMesber[3], Sameer Shamsham[4],Younis Idries[5]

[1]General Commission for Scientific Agricultural Research (GCSAR), Damascus, Syria
[2]Suwayda Research Center- GCSAR, Suwayda, Syria
[3]Damascus University, Faculty of Agriculture, Department of Soil Science, Syria
[4]Al-Baath University, Faculty of Agriculture, Department of Soil and Land reclamation, Syria
[5]General Organization of Remote Sensing (GORS), Syria

Received 28 December 2019; Accepted 10 April 2020

Abstract

Digital soil mapping has been increasingly used to produce statistical models of the relationships between environmental variables and soil properties. This study aimed at determining and representing the spatial distribution of the variability in soil properties of western face-sloping of Jabal Al-Arab, Suwaydaa governorate. pH, organic matter (OM), total nitrogen (N), phosphorus (P, as P_2O_5), potassium (K, as K_2O), iron (Fe), boron (B) and zinc (Zn) were studied, thus, Forty-five surface soil samples (0 to 30 cm) were collected and analyzed. Descriptive statistics demonstrated that most of the measured soil variables (except pH, $P_2O_{5,}$ and Zn) were skewed and ab-normally distributed, and logarithmic transformation was then applied. Kriging was used- as geostatistical tool- in ArcGIS to interpolate observed values for those variables, and the digital map layers were produced based on each soil property. Geostatistical interpolation recognized a strong spatial variability for pH, P_2O5 & Zn, moderate for OM, N, Fe & B, and weak for K_2O. Exponential for P_2O_5, Fe, & Zn, spherical for pH, OM, & K_2O, and Gaussian for N, and B. Models were fitted to the semivariograms of soil properties. These produced maps permit farmers and decision makers to evaluate farm soils, thus allowing them to make easier and more effective management decisions in order to maintain sustainable productivity.

Keywords: Digital soil mapping, Geostatistical models, Jabal Al-Arab, Kriging, Soil properties

1. Introduction

Digital soil-mapping applications which mean spatial prediction of soil properties at unobserved locations using statistical assumption have increasingly used recently since their early development at the beginning of the 19th century. The introduction of geostatistics tools permits researchers to interpolate the spatial distribution of soil variables (Webster, 1994). Digital soil mapping (DSM) is one of most the modern versions of geostatistical soil mapping, including creation of soil spatial information systems using both laboratory and field methods combined with spatial and non-spatial soil inference systems (Lagacherie et al., 2007; Martı´nez-Graña et al., 2016). The spatial distribution of soil variables is determined by relying on observed samples. These surface observed samples data are interpolated to predict soil variables in non-sampled areas (Sanchez et al., 2009). Traditional methods of soil survey are mostly slow, expensive and demanding. Moreover, the current soil database is not usually detailed or even accurate enough to use soil data efficiently (Malone et al., 2017). The existence of soil nutrients is usually one of the most principal indicators of soil quality; therefore it has a considerable impact on the variability of soil productivity and crop production. Various interpolation techniques are used to map the spatial distribution of soil properties (Cambardella and Karlen, 1999). Like Deterministic and stochastic methods (Myers, 1994). Thiessen, density estimation, inverse-distance-weighted (IDW) and splines are examples for deterministic interpolation methods fitting no assessment of errors. Otherwise stochastic interpolation and Kriging methods do provide prediction of error assessments.

Kriging is a geostatistical interpolation method with confirmed competence for predicting values at non-sampled locations based on observed data. The advantages of this method are: supplying the best linear unbiased estimates and information on the estimation of error distribution; presenting robust statistical characteristics (Wang et al., 2009); reducing filed sampling expenses and laboratory analysis, in addition to providing appropriate soil information that depicts the studied area based on restricted soil samples (Johnson et al., 2012). However, the reliability of produced maps of soil variables relies on satisfactory sampling data and accuracy of spatial interpolation method (Yao et al., 2013).

* Corresponding author e-mail: alaakhallouf@gmail.com

There is a growing tendency to use DSM as a result of the latest advances in technology on Geographic Information Systems (GIS). For instance, Lopez-Granados et al. (2005) used DSM to map soil properties including organic matter (OM), soil reaction (pH) and potassium (K) by using Kriging method. Santos-France´s et al., (2017a) also used Kriging interpolation method for the spatial distribution of heavy metals in north Spain's soils and north Peru (Santos-France´s et al., 2017b). Likewise, Zhang et al. (2010) mapped the spatial variability for some soil fertility nutrients: nitrogen (N), phosphorus (P) and potassium (K) by using Kriging method in northeast China.

In spite of the success and wide application of DSM all over the world, no single study has tested the use of DSM to study the spatial distribution of soil properties in any part of Syria.

In Syria, Fertilizer recommendation is applied as a normal procedure, where the soil is usually analyzed by random sampling and application of fertilizer recommendation based on soil analysis results without taking into consideration the spatial distribution of soil nutrients and their variation from one place to another. As a result, part of the field may receive an extreme amount of fertilizers, while the other may suffer from shortage, adversely affecting productivity levels. This research aims to determine and map the spatial distribution of some basic soil fertility variables and micronutrients in the western facing-slope of Jabal Al-Arab area in Suwaydaa governorate as a preliminary study to be used for improving the efficiency of using the approved fertilizer recommendation.

2. Materials and Methodology

2.1. Site Description

The study area lies in the western region of Suwaydaa governorate in southern Syria between (32°28'15"N, 36°24'18"E and 32°46'44"N, 36°45'15"E; Figure 1) and covers an area of 523 km^2 (52300 hectares). Altitude ranges between 696 m in west and 1795 m above sea level in the east (Tall Qeni). This area is characterized by the Mediterranean wet climate (Csb) in the highest parts with dry and temperate summer and semi-arid climate (Bsk) to cold in the low areas according to Kopin Classification. The mean annual precipitation is between 250-550 mm and more than 80%, falling between October and April. Agricultural land use is about 83.66 % of study area (AlSafadi, 2016).

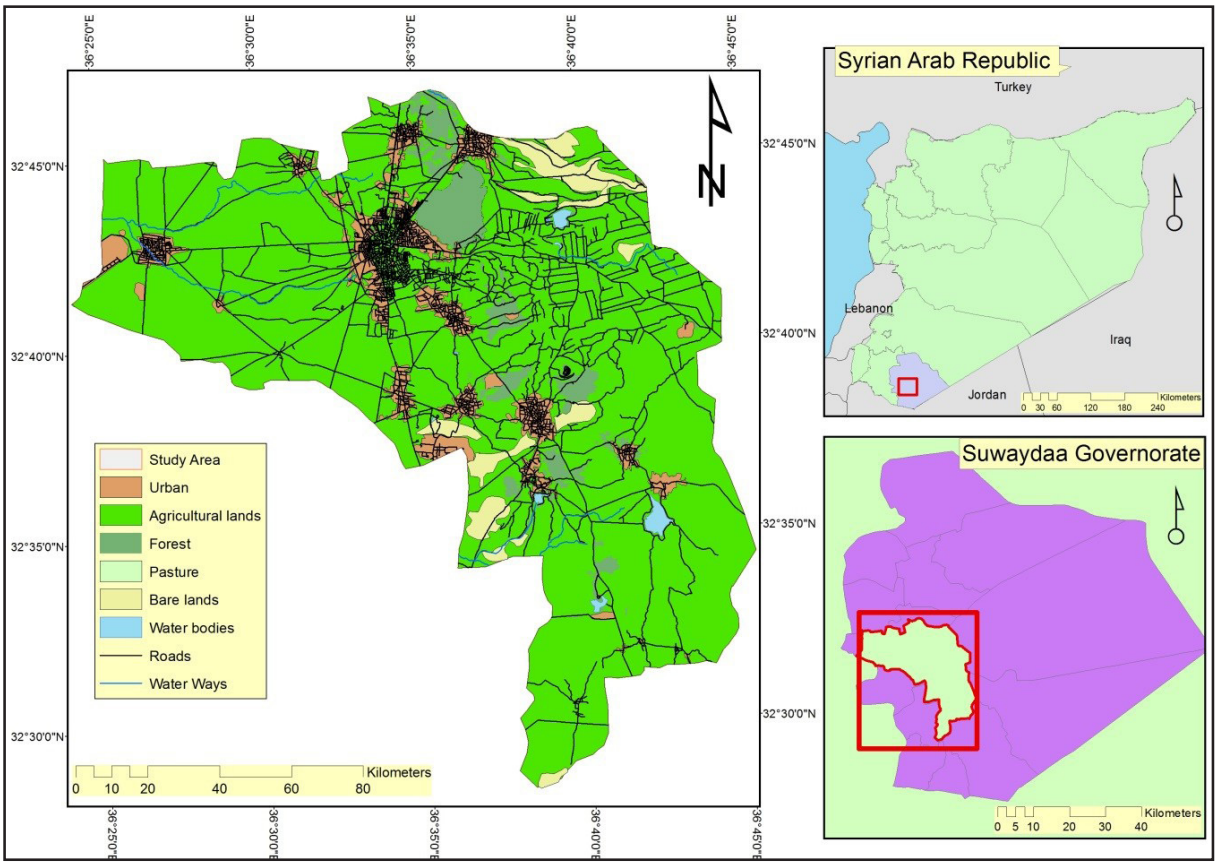

Figure 1. Study area location to Syria and Suwaydaa Governorate

2.2. Soil Sampling and Analysis

Forty-five surface soil samples (0-30cm) were collected during 1-23/4/2016, (Figure 2) and their geographic locations were recorded by using Global Positioning System (GPS). The collected soil samples were air-dried, ground and sieved through a 2mm sieve. The chemical analyses were carried out at Suwaydaa Research Center's laboratory. Organic

matter was measured by wet combustion method (Nelson and Sommers, 1982), pH was determined by using pH-meter in 1:2.5 soil water suspension (Jackson, 1973), total N by Kjeldahl (Bremner and Mulvaney, 1982), available P(P_2O_5) was extracted by using sodium bicarbonate ($NaHCO_3$) and then measured by spectrophotometer (Olsen et al., 1954), available K(K_2O) was extracted by ammonium acetate and determined by flame photometry (Toth and Prince,1949), B was estimated by hot water method(Berger and Truog,1939), Fe and Zn by DTPA extraction and measured by atomic absorption (Lindsay and Norvell, 1978). The measured soil properties were categorized (Table 2) based on soil content according to (Costantini, 2009; GCSAR, 2013).

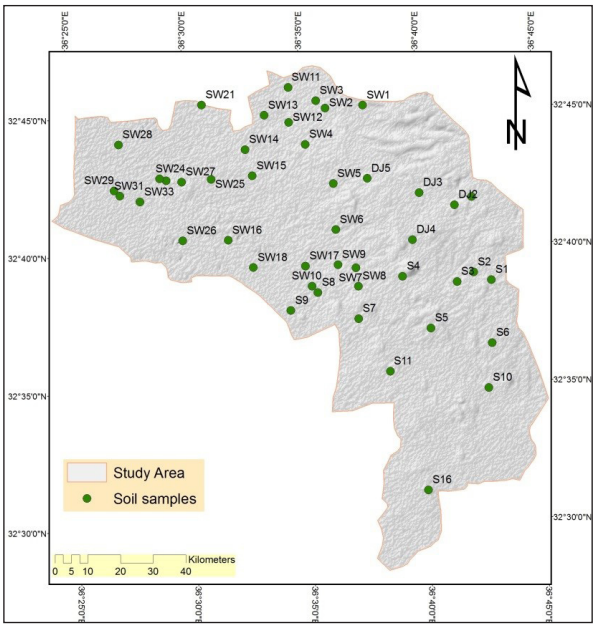

Figure 2. Soil samples locations

2.3. Statistical and Geostatistical Analysis

Descriptive statistics of soil variables (pH ,OM, total N, available P, available K, Fe, B, and Zn) involving mean, minimum, maximum, standard deviation, coefficient of variation, skewness (skew) and kurtosis were calculated by SPSS software. In this study, the ordinary Kriging was used (also called Kriging). Kriging is a linear geostatistical interpolation technique whose theory relies on weighting the sums of adjacent sampled concentrations. Additionally, it is a development over inverse distance weighting (IDW) because prediction estimates in Kriging is less biased and goes along with prediction standard errors. The general formula is formed as a weighted sum of the data:

$$Z(S_0)=\sum_{i=1}^{n} \lambda i\, Z(Si)$$

Where:

$\boldsymbol{Z(s_i)}$ = measured value at *i* location

$\boldsymbol{\lambda_i}$ = unknown weight for the measured value at *i* ocation

$\boldsymbol{s_0}$ = prediction location

N = number of measured values

For any data distribution, Kriging can give the best-unbiased predictor of values at non-sampled locations. The best estimates of probability maps can be produced as data is closer to normal distribution (Tziachris et al., 2017). Therefore, before doing geostatistical analysis, normality of dataset is vital, due to the high skew and presence of outliers. As coefficient of skew was more than 1 (Table1) except for pH, OM, and Zn, the logarithmic transformation was carried out for Kriging analysis to stabilize the variance (Goovaerts, 1999).

Table 1. Summary statistical overview for selected soil properties of study area

Soil variable	Min	Max	Mean	SD	CV%	Skew	Kurtosis	Skew (Tr)	Kurtosis (Tr)
pH	6.37	7.39	6.95	0.275	3.96	0.155	1.84	-	-
OM %	0.47	1.45	0.99	0.203	20.46	-0.30	2.85	-	-
N %	0.03	0.15	0.067	0.029	42.99	1.236	3.87	0.494	2.63
P_2O_5 (mg/kg)	1.7	94.8	15.91	20.23	127.1	2.11	7.03	0.487	2.48
K_2O (mg/kg)	150.3	883.2	440.3	129.1	29.33	1.09	5.87	-0.65	5.65
Fe (mg/kg)	3.5	35.17	14.74	6.96	47.11	1.03	3.81	-0.33	3.4
B (mg/kg)	0.02	0.7	0.18	0.127	70.56	1.96	7.8	-0.36	3.83
Zn (mg/kg)	1.31	7.69	4.02	1.55	38.59	0.289	2.34	-	-

Min: minimum, max: maximum, SD: standard deviation, CV: coefficient of variation, skew: skewness. Skew and Kurtosis: skewness and kurtosis obtained from original data. Skew (Tr) and Kurtosis (Tr) = skewness and kurtosis obtained from log transformed data.

Normality test was conducted after logarithmic transformation for soil variables (N, P_2O_5, K_2O, Fe & B). The transformed data resulted in slight skew as shown in (Table 1).The kriging method uses semivariance to evaluate the spatial distribution structure of soil properties (Zandi et al., 2011; Wang and Shao, 2013). Semivariogram modeling and estimation are crucial for structural analysis and spatial interpolation (Chen and Guo, 2017). Geostatistical parameters were developed, including nugget, structural, sill, and range (Wang and Shao, 2013). The study also takes into consideration the spatial dependency (sp.D) of selected soil variables, i.e. ratio of the nugget to sill variance. If the

ratio is less than 0.25, then the variance will be strong sp.D, whereas the ratio value between 0.25 and 0.75 suggests moderate sp.D. However, it will be weak if the ratio is more than 0.75 (Orman, 2012). To evaluate the best fit of Kriging (spherical, exponential and Gaussian models), two indicators were calculated: mean error (ME) and root mean square error (RMSE) since ME value is closer to 0 referring to unbiased interpolation method. Likewise, the lowest RMSE value implies the best fit to variogram model.

Table 2. Ranges for selected soil properties (Costantini, 2009; GCSAR, 2013)

Range	OM%	N%	P_2O_5 mg/kg	K_2O mg/kg	Fe mg/kg	B mg/kg	Zn mg/kg
Very low	-	0.05<	0-6.9	0-102	2<	0.2<	0.5<
Low	0.86<	0.05-0.1	6.9-18.4	102-180	2-5	0.2-0.5	0.5-1
Medium	0.86-1.29	0.1-0.2	18.4-32.2	180-300	5-20	0.5-1.2	2-10
High	1.29>	0.2-0.4	32.2-46	300-540	20-50	1.2-2	10-20
Very high	-	0.4>	46>	540>	50>	2>	20>

2.4. Data analysis

IBM SPSS software (version 22) was used to carry out the normality test and descriptive statistics for the selected soil variables. In addition, all maps were developed using ArcMap (version 10.3).Spatial and geostatistical analysis tools were principally used. The structure of spatial variability was examined through semivariogram. Finally, spatial pattern distribution was practically identified by using ArcMap and its spatial autocorrelation (Moran's Index) extension.

3. Results and Discussion

3.1. Descriptive statistics for selected soil variables

The descriptive statistics for selected soil variables: pH, OM, total N, available p, available K, Fe, B and Zn are given in Table 1. The variance of soil variables was interpreted using the coefficient of variance (CV) which was classified as: most (CV< 35%) moderate (CV:15 to 35%) and least (CV>15%) (Wilding, 1985). CV ranged from 3.96% (in pH) to 127.1% (in P_2O_5). Different degrees of heterogeneity

It was also observed that some soil properties (N, P_2O_5, K_2O, Fe and B) were abnormally distributed due to high values of both skew and kurtosis. In order to reduce these values, the logarithmic transformation was used as shown in Table 1, and the transformed values were then used in the spatial analysis. among soil properties were noticed by different CV ranges. The pH values ranged from 6.37 to 7.39 with a mean of 6.95. The soil content of organic matter ranged from low (>0.8%) to moderate (0.8 to 1.45%) with a mean of 0.99%. The macronutrients (N, P, K) were also described in Table 1, showing that total N as very low (0.045-0.05%), low (0.05-0.09%) and moderate (0.09-0.15%) with a mean of 0.067%. Available P (P_2O5) ranged from very low (1.7-10 mg/kg) to high (55-94.1 mg/kg). Available K (K_2O) can be described as high (334-500 mg/kg) to very high (500-883.2 mg/kg) with a mean of 440.3 mg/kg. Three micronutrients were also measured (Fe, B, and Zn). The results revealed Fe from moderate (7.12-20 mg/kg) to high (20-35) with a mean of 14.74 mg/kg. Boron (B) also ranged between very low (0.02 -0.2 mg/kg), low (0.2-0.5 mg/kg) and moderate (0.5-0.7 mg/kg). Finally, the soils of the studied area have moderate zinc (Zn) (1.31-7.69 mg/kg) with a mean of 4.02 mg/kg.

3.2. Kriging-based digital soil maps

Digital maps of selected soil properties were developed by using Kriging method. The results are shown in (Figures 2 through 9). They were grouped into many classes based on Table 2. The estimated area of each class is presented in Table 3.

3.2.1 Soil reaction pH

Soil reaction (pH) varied from slight acid (6.1-6.5) in 1.74% to slight alkaline in 8.01% of the total study area, whereas the rest (90.52%) was neutral soil reaction (Table 3, Figure 3). These results are in agreement with Habib's study (2006), who claimed that slight acid pH reflects the nature of soil components leaching soil process, especially $CaCO_3$. Though it was reported that it could be an indication for further pH decrease in the future. Lulu (1980) reported that the majority of soils in the study area tend to be neutral (pH: 6.6-7.3) which is favorable for most crops and soil management.

3.2.2. Soil organic matter

The results demonstrated that all the studied lands (100%) have low organic matter content (0.8-1.15%). (Table 3 and Figure 4). The low organic carbon content in soil can be generally attributed to lack of organic matter sources in the study area and rapid mineralization due to high soil and air temperature or low huminification rate (Habib, 2006).

3.2.3. Total nitrogen N

Nitrogen is the most important soil nutrient that affects crop growth, quality and yield. The geostatistical results showed that more than 91% of the total area had low N content (Figure 5) with values (0.05-0.0812%), while that of the remained area (8.97%) was very low (>0.05%). These results are in agreement with Al-Hinawi (2012). The differences in N content in different parts of the study area are due to soil management, and application of organic manures and mineral fertilizers to the previous crops.(Sherchan and

Gurung, 1995). The severe shortage of nitrogen can be explained by low organic matter of soil, increased organic matter mineralization rates, inefficient use of nitrogen fertilizers on grown crops, which are depleted by crops in the study area (Vasu et al., 2017).

3.2.4. Available phosphorus

The available P_2O_5 varied from very low (2.32-6.9 mg/kg) with 18.95% to very high (<46 mg/kg) with 0.11 % of the total area (Figure 6). However, most soils had low P_2O_5 (6.9-18.4 mg/kg) with 60.38% of the area. The low levels of available P_2O_5 may be explained by low organic matter content in soils. In contrast, the high levels of available P_2O_5 may be due to dissolution of Ca-P under neutral pH (Pal et al., 2012). The amount of available P_2O_5 is affected by soil reaction pH, soil content of organic matter, and amount of applied phosphorus fertilizer. However, it is lost from soils by surface runoff and erosion (Panday et al., 2018).

3.2.5. Available potassium

The majority of soils in the study area had high levels of available K_2O (300 -540 mg/kg) in 91.39% of the total area (Table 3, Figure 7), whereas 8.61% of the area had very high K_2O (<540 mg/kg). These high levels of K_2O were also found by Al-Hinawi (2012). Soil reaction pH has a great effects on K_2O availability, since pH is greater than 7 (most of the area pH <7). Ca cations displaced K cations on the clay surfaces (exchange K by Ca), increasing K_2O concentration in soil solution. Another possible reason is the clay mineral type as the presence of smectite and mica was reported by Al-Hinawi (2012) which are the key sources of exchangeable K.

3.2.6. Micronutrients Fe, B, and Zn

The results showed that most of the study area was medium in Fe and Zn and very low in B (Table 3, Figures 8-10). These results were in agreement with studies conducted by Habib (2006) and Al-Hinawi (2012). The low levels of micronutrients may be explained by the low concentration of these substances in parent materials and low organic matter in the soils. On the other hand, the intensive cropping patterns resulted in high uptake of micronutrients by crops. In spite of sufficient levels of Fe (relatively high in some areas) (Table 3), plants root may not absorb Fe because of the dominant phosphate inion P_2O_5 in soil solution (Habib, 2006; Al-Hinawi, 2012).

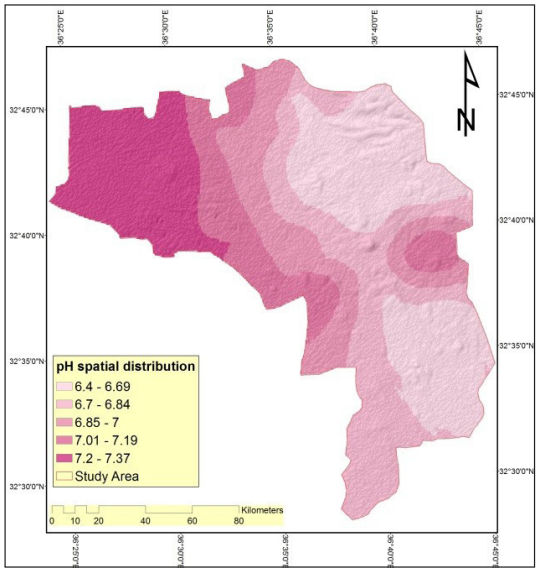

Figure 3. pH spatial distribution.

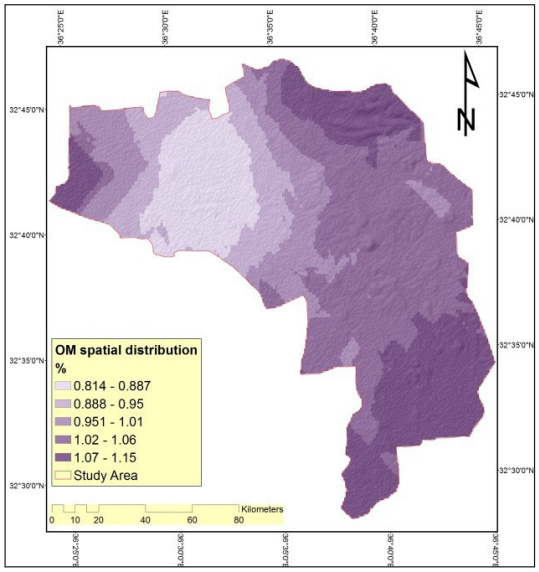

Figure 4. Organic matter spatial distribution.

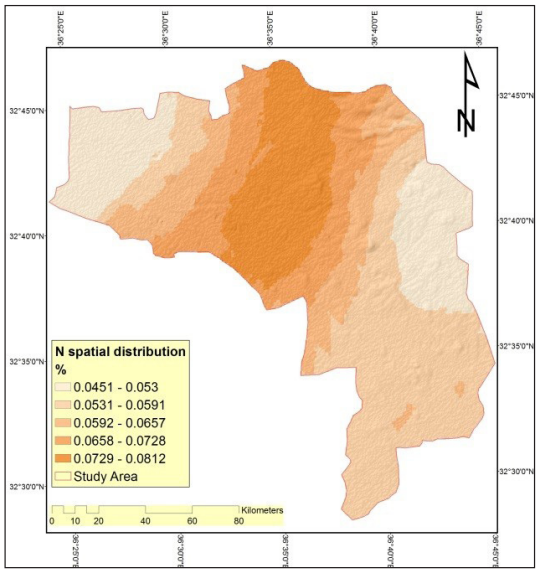

Figure 5. N spatial distribution.

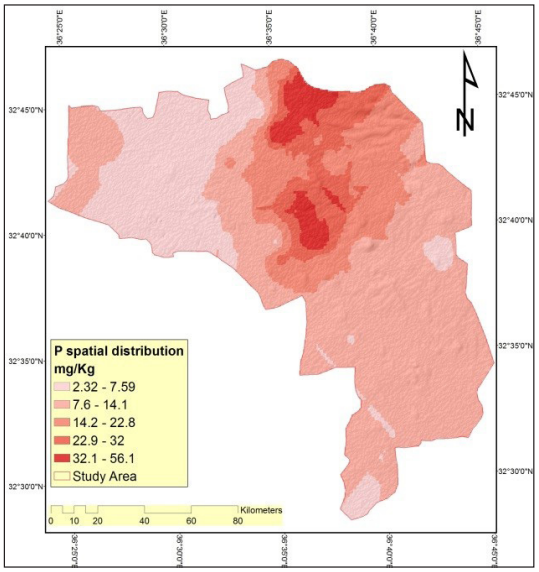

Figure 6. P(P_2O_5) spatial distribution.

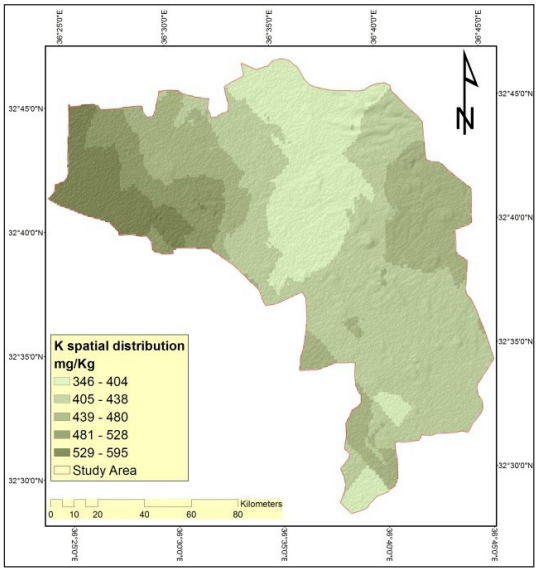

Figure 7. K(K_2O) spatial distribution

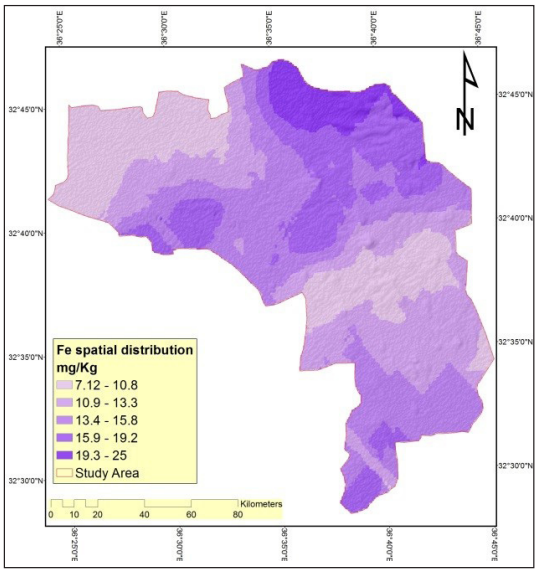

Figure 8. Fe spatial distribution.

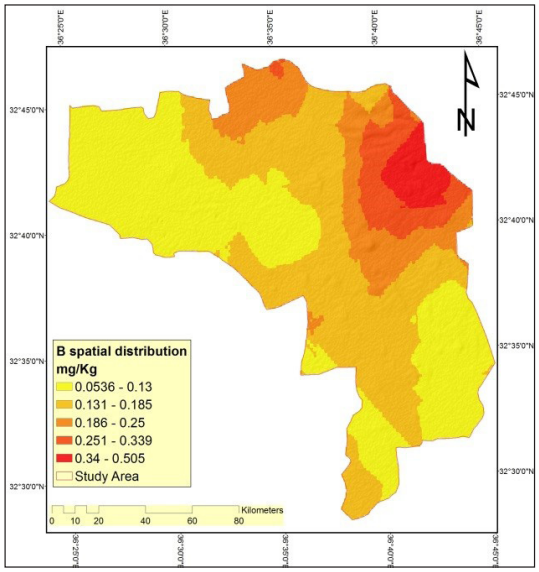

Figure 9. B spatial distribution

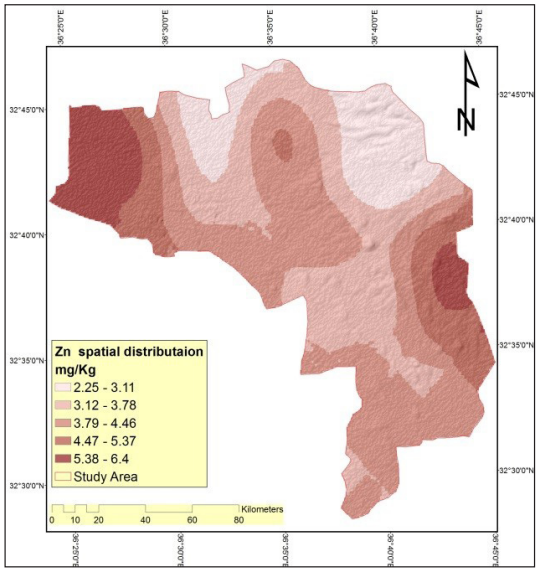

Figure 10. Zn spatial distribution

3.3. Geostatistics for selected soil properties

3.3.1 Semivariogram analysis

Some geostatistical parameters and semivariogram model analysis are shown in Table 4. According to the lowest root mean square (RMSE), three theoretical semivariogram models (spherical, exponential, and Gaussian) were examined for the significant fit of soil properties. (Robertson, 2008)

The results showed that spherical model provided the best fit to semivariogram for pH, OM and available K(K_2O), whereas exponential model was the best fit to semivariogram for available P (P_2O_5), Fe, and Zn. Finally, Gaussian model was the best fit to total N, and B. Because of its ability to explain the maximum variability (Venteris et al., 2013). Many findings recommend exponential model for estimating spatial soil distribution (Lark, 2000; Tripathi et al., 2015).

Spatial dependency (Sp. D) ranged from 0 in pH to 0.92 in available K. Clearly, Sp. D was strong (in pH, available P and Zn), and moderate (in OM, N, Fe and B) versus weak in available K. These results may be counted to external factors such as variable rates of applied K fertilizers in the study area. Spatial dependency ranges were large and varied between 3551 m in available P and B and 15208 m in total N, indicating that the optimum sampling interval varies greatly among different soil properties. The range values give an idea about the correlation between different soil sampling locations, along with the maximum spatial dependency distances between them (Akpa et al., 2014).

Table 4. Semivariogram analysis of spatial structure in soil properties

Soil parameter	ME	RMSE	Model	Range	Lag size	Nugget	Partial	sill	Sp.D	DES Sp.D
pH	0.142	0.147	S	1871	989	0	0.065	0.065	0	ST
OM	0.2	0.19	S	12067	1718	0.34	0.071	0.15	0.32	M
N	0.026	0.027	G	15208	1798	0.11	0.056	0.169	0.65	M
$P(P_2O_5)$	29.2	16.2	E	3551	407	0.135	0.947	1.082	0.12	ST
$K(K_2O)$	143.92	127.38	S	6957	580	0.085	0.006	0.091	0.92	W
Fe	7.7	6.36	E	7085	590	0.11	0.126	0.236	0.46	M
B	0.13	0.104	G	3551	446	0.187	0.171	0.351	0.53	M
Zn	1.38	1.344	E	7350	1628	0.507	1.89	2.397	0.21	ST

ME: mean error, RMSE: root mean square error, E: Exponential, G: Gaussian, S: Spherical, ST: strong, M: Moderate, and W: Weak. Unit for range and lag size, m. Sp.D: spatial dependency, DES. Sp.D: descriptive of spatial dependency.

Table 5. Areas of different soil groups based on soil parameters classes

Parameter	Unit	Rating	Existing class	Area(h)	% of total area
pH	-	6.1-6.5	Slightly acidic	766.62	1.47
		6.5-7.3	Neutral	46913.4	90.52
		7.3-7.8	Slightly alkaline	4619.89	8.01
OM	%	0.86-1.26	Low	52300	100
N	%	0.05<	Very low	5114.24	8.97
		0.05-0.1	Low	47185.46	91.04
P (P_2O_5)	mg/kg	0-6.9	Very low	9824.16	18.95
		6.9-18.4	Low	31299.36	30.38
		18.4-32.2	Medium	8695.23	16.77
		32.2-46	High	1965.82	7.79
		46>	Very high	45.8	0.11
K (K_2O)	mg/kg	300-540	High	47359.23	91.39
		540>	Very high	4461.762	8.61
Fe	mg/kg	6-20	Medium	49524.42	95.55
		20-50	High	2301.9	4.45
B	mg/kg	0.2<	Very low	42050.39	81.13
		0.2-0.5	Low	9738.97	19.79
		0.5-1.2	Medium	510.64	0.08
Zn	mg/kg	2-10	Medium	52300	100

3.3.2 Spatial autocorrelation

It is assumed, at the beginning of the study, that the spatial pattern of soil properties distribution is random. Therefore, the Moran`s index was calculated by using ArcMap to identify the spatial pattern, which varies depending on the feature locations and value of soil properties between dispersed, random and clustered samples (Moran, 1950). According to ESRI (2017), the spatial pattern does not reflect random distribution if the p-value is less than 0.05 and Z-score is either (very high) < 1.96 or (very low) > -1.96. As presented in Table 5 and according to the test of significant values, most of the studied soil chemical properties (pH, OM, N, P_2O5, and B) had clustered distribution, whereas the spatial pattern of K_2O, Fe, and Zn was not different at p-value less than 0.05 from random distribution.

Table 5. Test of significance for the spatial pattern of studied soil properties

soil parameter	Moran`s index	Variance	p-value	Z-score
pH	0.385	0.0020	0.00	8.65
OM	0.065	0.0021	0.057	1.89
N	0.107	0.0021	0.004	2.819
P_2O_5	0.08	0.0019	0.01	2.410
K_2O	-0.01	0.0020	0.701	0.261
Fe	0.02	0.0021	0.350	0.93
B	0.12	0.0019	0.00	3.48
Zn	0.004	0.0021	0.55	0.589

It is assumed, at the beginning of the study, that the spatial distribution is close to random. On the other hand, positive Moran`s index value indicates neighboring values are similar, referring to spatial dependency, while the negative Moran`s index value implies that neighboring values are dissimilar, referring to the opposite of spatial dependency. Also, the zero Moran`s index value points out shortage of spatial pattern (Lloyd, 2010; Al-Ahmadi and Al-Zahrani, 2013). As showen in the Table, except $K_2O$, most of the selected soil properties demonstrated positive Moran`s index values that indicate spatial dependency.

4. Conclusions

The application of geostatistical approach involving descriptive statistics and semivariogram analysis improved the description of spatial variability for soil chemical properties at 0 to 30 cm deep. The descriptive statistics showed that most of measured soil variables were skewed and abnormally distributed, and the available K_2O data were highly variable (338 to 595 mg/kg). Geostatistical interpolation identified that exponential, spherical or Gaussian models provided the best fit to semivariograms, depending on the soil chemical variable, showing in general strong, moderate or weak spatial dependency for all variables.

Kriging maps of soil variables were found effective in interpreting the distribution of soil properties in non-sampled locations based on sampled data. These maps help farmers in making efficient management decisions based on their proper understanding of the conditions of existing farm soils. These results show that Kriging-geostatistical analysis is an effective prediction tool for exploring the spatial variability of soil nutrients. Generally speaking, this tool is recommended for future soil sampling campaigns in Syria.

References

Akpa, S., Odeh, I., Hartemink, A. (2014). Digital mapping of soil particle-size fractions for Nigeria. Soil Science Society of America Journal 78: 1953–1966.

Al-Ahmadi, K. and Al-Zahrani, A. (2013). Spatial autocorrelation of cancer incidence in Saudi Arabia. International Journal of Environmental Research and Public Health 10: 7207–7228. https://doi.org/10.3390/ ijerph10127207 PMID: 24351742.

Al-Hinawi, S. (2012). Characterization and Evaluation of Some Soils from Swaida Province Using Remote Sensing Techniques. PhD thesis Faculty of Agriculture, Damascus University.

AlSafadi, K.J. (2016). Climate and its Impact on Cultivation of Apple and Grapes Crops in Alswuydaa Governorate-Syria, (Unpublished master's thesis In Arabic) Alexandria University, Alexandria, Egypt.

Berger, K.C. and Truog, E. (1939). Boron determination in soils and plants. Industrial and Engineering Chemistry. Analytical Edition 11: 540–545.

Bremner, J.M. and Mulvaney, C.S. (1982) Nitrogen-Total. In: Page, A.L., Miller, R.H. Keeney, D.R. (Eds.), Methods of soil analysis. Part 2. Chemical and microbiological properties, American Society of Agronomy, Soil Science Society of America, Madison, Wisconsin, 595-624.

Cambardella, C.A. and Karlen, D.L. (1999). Spatial analysis of soil fertility parameters. Precision Agriculture 1: 5–14.

Chen, S. and Guo, J. (2017). Spatial interpolation techniques: their applications in regionalizing climate-change series and associated accuracy evaluation in Northeast China. Geomatics, Natural Hazards and Risk 8(2): 689–705.

ESRI. The principles of geostatistical analysis (3) 2010 [Internet]. 2017. http://maps.unomaha.edu/ Peterson/gisII/ ESRImanuals/Ch3_Principles.pdf.

Goovaerts, P. (1999). Geostatistics in soil science: state-of-the-art and perspectives. Geoderma 89(1–2): 1–45.

Habib, H. (2006). Pedological study of soil topo sequence in Jabal Alarab Sowaida Governorate. Damascus University Journal for Agricultural Sciences 22(1): 181-206.

Lagacherie, P., McBratney, A.B, Voltz, M. (2007). Digital soil mapping: an introductory perspective. Developments in soil science. Elsevier publication, The Netherlands.

Lark, R.M. (2000). Estimating variograms of soil properties by the method-of-moments and maximum likelihood. European Journal of Soil Science 51: 717–728.

Lindsay, W.L. and Norvell, W.A. (1987). Development of a DTPA soil test for zinc, iron, manganese, and copper. Soil Science Society of America Journal 42: 421–428.

Lloyd, C.D. (2010). Nonstationary models for exploring and mapping monthly precipitation in the United Kingdom. International Journal of Climatology 30: 390–405.

Lopez-Granados, F., Jurado-Exposita, M., Pena-Barragan, J.M., Garcia-Torres, L. (2005). Using geostatistical and remote sensing approaches for mapping soil properties. European Journal of Agronomy 23(3): 279–289.

Lulu, A. (1980). Classification of Jabal Al-Arab Soils – Swaida Governorate. Ministry of Agriculture and Agrarian Reform, Damascus, Syria.

Malone, B.P., Minasny, B., McBratney, A.B. (2017). Using R

for digital soil mapping. Springer International Publishing, Switzerland.

Martı´nez-Graña, A.M., Goy, J.L., Zazo, C., Silva, P.G. (2016). Soil map and 3D virtual tour using a database of soil forming factors. Environmental Earth Sciences 75(21): 1402.

Moran, P.A. (1950). Notes on continuous stochastic phenomena. Biometrika 37: 17–23.

Myers, D.E. (1994). Spatial interpolation: an overview. Geoderma 62(1–3): 17–28.

Olsen, S.R., Cole, C.V., Watanabe, F.S., Dean, L.A. (1954). Estimation of available phosphorus in soils by extraction with sodium bicarbonate. In: Banderis, A.D., Barter, D.H., Anderson, K. (Eds.), U. S. Department of Agriculture Circular No. 939. Agricultural and Advisor.

Orman, E.E. (2012). Improving the prediction accuracy of soil mapping through geostatistics. International Journal of Geosciences 3: 574–590.

Pal, D.K., Wani, S.P., Sahrawat, K.L. (2012). Vertisols of tropical Indian environments: Pedology and edaphology. Geoderma 189–190: 28–49.

Panday, D., Ferguson, R.B., Maharjan, B. (2018). Flue Gas Desulfurization (FGD) Gypsum as Soil Amendment. In: Rakshit, A, Sarkar, B, Abhilashis, P.C. (Eds.), Soil Amendments for Sustainability: Challenges and Perspectives. CRC Press, FL, pp 199–208.

Robertson, G.P. (2008). Geostatistics for the environmental sciences. Gamma Design Software, Plainwell, Michigan USA, pp 165.

Sanchez, P.A., Ahamed, A., Carre, F., Zhang, G. (2009). Digital soil map of the world. Science 325(5941): 1-680. https://doi.org/10.1126/science.1175084 PMID: 19661405.

Santos-France´s, F., Martı´nez-Graña, A., Alonso, Rojo, P., Garcı´a Sa´nchez, A. (2017b). Geochemical Background and Baseline Values Determination and Spatial Distribution of Heavy Metal Pollution in Soils of the Andes Mountain Range (Cajamarca-Huancavelica, Peru). International journal of environmental research and public health 14(8): 859.

Santos-France´s, F., Martı´nez-Graña, A., Zarza, C.A., Sa´nchez, A.G., Rojo, P.A. (2017a). Spatial Distribution of Heavy Metals and the Environmental Quality of Soil in the Northern Plateau of Spain by Geostatistical Methods. International journal of environmental research and public health 14(6): 568.

Sherchan, D.B. and Gurung, B.D. (1995). An Integrated Nutrient Management System for Sustaining Soil Fertility: Opportunities and Strategy for Soil Fertility Research in the Hills. PP 50-62. In: Schreier, H., Shah, P. B., Brown, S. (Eds.), Challenges in Mountain Resource Management in Nepal. Processes, Trends and Dynamics in Middle Mountain Watersheds. Proceedings of a Workshop held in Kathmandu, Nepal 10-12 April, 1995 .ICIMOD/IDRC/UBC, Kathmandu, pp. 50-62.

Toth, S.J. and Prince, A.L. (1949). Estimation of CEC and exchangeable Ca, K, and Na content of soil by Flame photometer technique. Soil Science 67: 439–445.

Tripathi, R., Nayak, A.K., Shahid, M., Raja, R., Panda, B.B., Mohanty, S., Kumar, A., Lal, B., Gautam, P., Sahoo, R.N. (2015). Characterizing spatial variability of soil properties in salt affected coastal India using geostatistics and kriging. Arabian Journal of Geosciences 8(12): 10693–10703.

Tziachris, P., Metaxa, E., Papadopoulos, F., Papadopoulou, M. (2017). Spatial Modelling and Prediction Assessment of Soil Iron Using Kriging Interpolation with pH as Auxiliary Information. ISPRS International Journal of Geo-Information 6(9): 283.

Vasu, D., Singh, S.K., Sahu, N., Tiwary, P., Chandran, P., Duraisami, V.P. (2017). Assessment of spatial variability of soil properties using geospatial techniques for farm level nutrient management. Soil and Tillage Research 169: 25–34.

Venteris, E.R., Basta, N.T., Bigham, J.M., Rea, R. (2013). Modeling spatial patterns in soil arsenic to estimate natural baseline concentrations. Journal of Environmental Quality 43(3): 936–946.

Wang, J.F., Li, L.F., Christakos, G. (2009). Sampling and kriging spatial means: efficiency and conditions. Sensors 9(7): 5224–5240. https://doi.org/10.3390/s90705224 PMID: 22346694.

Wang, Y.Q. and Shao, M.A. (2013). Spatial variability of soil physical properties in a region of the Loess Plateau of PR China subject to wind and water erosion. Land Degradation and Development 24(3): 296–304.

Webster, R. (1994). The Development of Pedometrics. Geoderma 62(1–3): 1–15.

Wilding, L.P. (1985). Spatial Variability: its documentation, accommodation, and implication to soil surveys. In: Nielsen, D.R. and Bouma, J. (Eds.), Soil Spatial Variability. Proceedings of a workshop of the ISSS and the SSSA, Las Vegas, USA. 30 Nov.–1 Dec. 1984. Wageningen, The Netherlands pp. 166–189.

Yao, X., Fu, B., Lu, Y., Sun, F., Wang, S., Liu, M. (2013). Comparison of four spatial interpolation methods for estimating soil moisture in a complex terrain catchment. PLoS One 8(1): e54660. https://doi.org/10. 1371/journal.pone.0054660.

Zandi, S., Ghobakhlou, A., Sallis, P. (2011). Evaluation of spatial interpolation techniques for mapping soil pH, 19th International Congress on Modeling and Simulation, Perth, Australia, 12–16 December 2011, pp.1153–1159.

JJEES

JJEES (2020) 11 (3): 202-210
ISSN 1995-6681

Jordan Journal of Earth and Environmental Sciences

Heavy-Metal Contamination and Distribution within the Urban Soil Cover in Mutah and Al-Mazar Municipal Area

Tayel El-Hasan[1*] and Amjad Al-Tarawneh[2]

[1]Mutah University, Faculty of Science, Department of Chemistry, Mutah; Jordan.
[2]Mutah University, Prince Faisal Center for Dead Sea, Environmental and Energy Research, Mutah; Jordan.

Received 13 October, 2019; Accepted 15 April 2020

Abstract

Thirteen sites allocated on grid bases covering the urban soil of Mutah – Al-Mazar municipal area (south of Al-Karak province) were collected. The collection was designed to cover inhibited or open areas and all occupational activities. The sites were investigated for their heavy-metal content to delineate the polluted areas and determine the potential pollution sources. The results show no or limited downward mobility of the heavy metals as there is no big difference in average heavy-metal contents between lower and upper soils. This might be due to high soil alkalinity and low rainfall quantities. Besides, it shows that traffic is the main source for pollution which was approved using the correlation coefficient and index of pollution (IP) techniques. Furthermore, the ratio of index of pollution for most of the sites are <1; few are >1 but not reaching 2, which indicates that a low extent of pollution prevails in the study area, because of the absence of heavy industrial firms and high density highways. The correlation coefficient results show that the upper soil differs from lower soil; in upper soils Cu correlated positively with Fe, Cr, Co, Mn, Zn, Ni, and Pb, whereas in the lower soil, it correlated with Fe, Cr, Co and Ni, which indicates a different source of contamination or an anthropogenic source that contains Zn, Mn, and Pb.

Keywords: Urban soil, Heavy metals, Soil pH, Contamination, Anthropogenic

1. Introduction

The detection of soil pollution that could result from heavy metals (HM) has become increasingly important. Heavy metals occur naturally, but rarely at toxic levels. Anthropogenic activities and the use of synthetic products (e.g. pesticides, paints, batteries, and industrial waste) can result in heavy-metal contamination of urban and agricultural soils (Jiries et al., 2017). Moreover, traffic activities on roads can contribute to increasing the levels of heavy metals in these environments through fossil fuel combustion, wear and tear of many parts of the automobile (Alloway and Ayres, 1997).

Soil environmental pollution due to heavy metals in urban areas is extremely urgent, therefore, the following heavy metals (i.e. Cd, Zn, Cu, Ni, Fe, Cr, Mn and Pb) were chosen for analysis due to their effects on human and environmental components. Generally, heavy metal distribution is influenced by the nature of parent materials, climate and their relative mobility, as well depending on soil parameters such as pH, mineralogy, and texture (Jiries et al., 2017). The concentration of these metals in soil is related to the presence of humus and clay minerals which serve as adsorbents of heavy metals (Huisman et al., 1997, Vermeulen et al., 1997, Garnaud et al., 1999; Birke and Rauch, 2000). Many workers have investigated the pollution of soil by heavy metals. El-Hasan (2002) found that heavy metals are concentrated on the surface of soils in the city of Sahab in central Jordan, but they decrease in the lower parts, without representing serious pollution problems. However higher Cu, Pb, Zn, and Cd concentrations in the soils might be attributed to anthropogenic inputs. The influence of urbanization and industrialization as a major cause for heavy-metal contamination either in the dust, sediments, soils, or plants was observed by many authors (e.g. Claridge et al., 1994; Vermeulen et al., 1997; Kim et al., 1998; Wilcke et al., 1998; Garnaud et al., 1999; Brike and Rauch, 2000). Urban geochemistry is a newly developed field that combines the basic knowledge of geochemistry with the urbanization development and its environmental consequences. It serves as environmental implication of known geochemical methods of survey. It was used in many areas around the world, e.g. for Hong Kong city, Ho and Tai (1988), for the city of Prague (Czech Republic), Duris and Zimova (1994), for the urban soil of Bankok city, Wilcke et al., 1998; and Li et al., 2001, and for Berlin metropolitan area, Birke and Rauch (2000). Detecting and characterizing heavy-metal pollution in different areas in Al-Karak province have been done previously by many workers using several proxies

* Corresponding author e-mail: tayel@mutah.edu.jo

such as soil (El-Hasan and Lataifeh, 2003; El-Hasan and Lataifeh, 2013), Wadi sediment (El-Hasan and Jiries, 2001), dry deposition (El-Hasan et al., 2008), lichens by (Jiries et al., 2008) and plants by (El-Hasan et al., 2002).

1.2 Aims of the Study

Henceforth, this work aims at obtaining a comprehensive picture of the soil geochemistry in urban areas with respect to their natural composition and the secondary contamination (anthropogenic). Also, it aims at delineating the distribution and mobilization of heavy metals within soil profile. Moreover, this study aims at investigating the factors which affect heavy- metal concentrations and mobility in soil profile such as pH, conductivity, soil composition, and wind direction as well as determining the various anthropogenic sources. Consequently, this work will assess the environment in terms of heavy-metal contamination. Therefore, it would provide a base-line data for future environmental assessment and monitoring of the soil contamination in the urban area of Mutah and Al-Mazar. To this purpose, the following objectives must be achieved:

1. Determining the concertation of some heavy metals (Cd, Zn, Cu, Ni, Fe, Cr, Mn, and Pb) in the surface soil cover in the Mutah and Al-Mazer area using Atomic Absorption Spectrometry (AAS).

2. Establishing a reliable database for heavy-metal concentrations in order to monitor any increase in their concentrations in future, which pose alarming threats to the health and environment sector in the area when these elements exceed the permissible limits,

1.3 Study Area Settings

The study area includes Mutah and Al-Mazar towns which belong to one municipality. The study area is located in the southern part of Al-Karak governorate, in central Jordan to the east of the Dead Sea. The study area and the sampling sites are shown in (Figure 1). This area has a predominantly Mediterranean climate that is characterized by hot-dry summers and cold-wet winters ((Department of Metrology of Jordan, 2016).). The temperature exhibits large seasonal and diurnal variation. More frequently, seasonal mean temperatures vary from 6°C in January to 22°C in July, reaching a maximum of 38.5°C in summer and a minimum of – 4°C in winter with an average temperature of 22°C in summer and 8°C in winter (Department of Metrology of Jordan, 2016)). The investigated area is about 1000-1200 m high above the sea level. The site is located in the rolling and rounded limestone plateau with phosphorite, which is referred to in the geology of Jordan as Al-Hisa Phosphorite Unit (AHP) (Powell, 1988).

Therefore, the activities vary depending on the area of Mu'tah and Mazar. These are two of the rapidly developing and attractive areas for the population in the Al-Karak governorate, as a result of the population mobilization stations, the increase in transport, the movement of automobiles, and because of the activities of construction and factories. Activities such as industrial zones and fuel stations are also increasing. All this affects the environment of the region by means of increasing the load of heavy elements such as iron, lead, zinc, chromium, manganese and nickel in the soils. Since these factors have an impact on human health, this study is conducted to determine heavy metals' concentration as a basis for future monitoring.

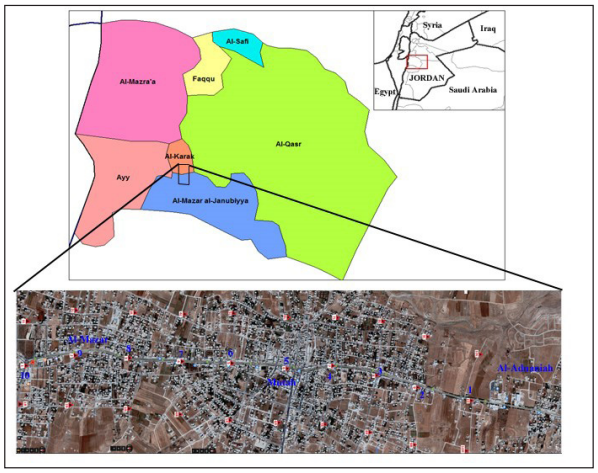

Figure 1. Distribution of sampling sites along the 5 km Al-Mazar city to Al-Adnanieh Street.

2. Materials and Methodology

2.1. Soil Sampling

All soil samples were collected from thirty sites along the highway from Al-Mazar city to Al-Adnanieh village through Mutah, which is 5 km long. Two samples were collected from each site; at the depth of 10 and 20 cm. The soil samples were representatively collected by homogenizing soils from each depth. The distribution of the sampling sites was as follows: ten sites from the margins of the main street, ten sites from a distance of 500 meters to the right of the street, and ten sites from a distance of 500 meters to the left of the street. Therefore, the distance between any two samples in all directions was approximately 500 m (Figure 1).

The total area of investigation is around 10 km^2; it was divided into 500 m× 1000 m grid. A total of forty-eight sample sites were assigned on the google map of Mutah and Al- Mazer towns. The sample density is five samples per km^2. The sampling sites were allocated using the GPS system (Garmin GPS II Plus), with ± 10-meter accuracy. The sampling campaigning duration was three months (Feb-April 2016).

The soil samples were collected from two depths; the upper soil (0–10 cm) hereafter referred to as (A), and the lower soil (10–20 cm) hereafter referred to as (B). The soil samples were dried at room temperature for seventy-two

hours, and were then stored using plastic tools into sealed plastic bags.

The collected samples from the upper and lower soils (A, B) were left to dry up at room temperature. The samples were then sieved to less than 2 mm; then they were sieved again using ordinary stainless steel sieves 150 and 63 um and were divided into two sizes as follows: coarse (150–63 um) referred to as (C) and fine (<63 um) referred to as (F). As a result, each collected soil sample was divided into four samples (AC, AF, BC and BF); the sieved samples were kept in plastic sealed pages and stored for further analysis.

2.2. Soil Sampling

All of the sixty soil samples were collected in sealed plastic bags, sieved to < 2 mm grain size and air-dried for seventy-two hours. They were then kept in plastic bags until analysis. The soil acidity (pH) and electrical conductivity (EC) were analysed by mixing 1:5 ratios of soil and de-ionized water following the procedure of (Blakemore et al., 1987).

2.2.1 Soil Sample Digestion and Analysis

In order to find the best experimental setting that would produce a higher yield of elements from the leached soil samples, the following orientation test was executed: four parameters were tested to find their effect on the digestion process, those are (Temperature (25 and 70°C); Solvent used (2 M HNO_3 and 2M aqua regia 1HNO_3: 3HCL v/v); Incubation time and type were as follows (i.e. 2 and 24 hours for the mechanical shaking) and the sonication time was (i.e. 30 and 120 minutes). Two elements (Pb and Fe) were chosen for this test. To statistically find the best settings, the matrix of the obtained data was treated using Minitab Program software. All samples were digested according to the best results obtained from the previous orientation test, which showed that the mechanical shaking for twenty-four hours with 2M aqua regia at 70°C and 150 rpm gave the higher elemental yield. Thus, the samples were digested using these settings.

The soil leaching procedure was achieved using the method of (Fialova et al., 2006) by which 2 g of the soil sample were mixed with the assigned solution mentioned above, Later, all samples were centrifuged at 3000 rpm for five minutes. The supernatant was collected, and the precipitate was then washed with 10 ml Deionized water. Then the supernatant was collected again and mixed with the first collected supernatant in a 50ml volume flask. Finally, the collected supernatant was diluted up to 50 ml. All samples were filtered using a syringe filter of a 0.45 µm pore size and were kept in polyethylene vials for analysis. Then, the samples were analyzed by means of Flame Atomic Absorption Spectrophotometer (AA-7000, Shimadzu Scientific Instruments, Japan) according to the Standard Method 3111 B. Finally, the result was evaluated and recalculated to be expressed in mg/kg soil. The solution was then transferred into 25-ml polyethylene bottles, filled up with distilled water exactly to 25-ml, then stored in the refrigerator until analysis time. The concentrations of heavy metals (Zn, Ni, Pb,Cu, Co, Cr, Fe, and Mn) in the soil samples were determined using the Flame Atomic Absorption Spectrophotometer (AA-7000, Shimadzu Scientific Instruments, Japan).

2.2.1.1. Soil pH

The pH values of all soil samples were measured according to the standard method SM 4500 H+B (Eaton et al., 2005) by preparing 1:5 (Soil: Deionized Water) suspensions. The suspensions were prepared by shaking 10 g of air-dried soil < 2 mm in 50 mL of deionized water in a rotating shaker for one hour at 15 rpm. The obtained pH values (pH meter 315i, WTW GmbH, Weilheim, Germany) were recorded when the equilibrium (stability in the reading) was reached while stirring with a mechanical stirrer (Rayment and Higginson, 1992).

2.2.1.2. Electrical Conductivity (EC)

The EC values of all soil samples were measured according to the standard method SM 2510 (Eaton et al., 2005). The soil EC was determined by shaking a 1:2.5 (w/w) ratio of soil and deionized water. The mixture was homogenized for thirty minutes at 15 rpm using a horizontal shaker, and was then left at room temperature until the soil settled down before EC measurement. The conductivity of the supernatant liquid was determined using the conductivity meter without disturbing the settled soil (Conductivity meter 4310, JENWAY, UK) (Chapman and Pratt, 1974).

2.3. Mineralogical Analysis of the Soil Samples.

Eight urban soil samples were selected. Each soil sample collected was powdered in an agate mortar for the XRD analyses. Organic tissues were previously removed to avoid the noise that organic matter produces in the XRD signal. XRD patterns were acquired by an automated PANalytical X'pert Pro diffractometer equipped with the X'Celerator detector, with the following measurement conditions: 5.01-69.98° 2θ angular range, 0.0170° step-size, Ni-filtered Cu Kα1 radiation (λ = 1.54060 Å), operating at 40 kV and 40 mA.

3. Results and Discussion

3.1. Soil Mineralogy

The XRD patterns of all samples are quite similar and mainly formed by quartz and calcite with subordinate contents of dolomite, clay minerals and feldspars. Quartz and calcite are identified by several peaks (Figure 2) whereas dolomite, plagioclase and K-feldspar can be recognized just by their strongest peaks at about 30.8°, 27.9° and 27.5° 2θ, respectively. Quartz and calcite relative proportions vary

from one sample to another, as highlighted by the intensities of their strongest peaks (XRD patterns were collected under the same measurement conditions).

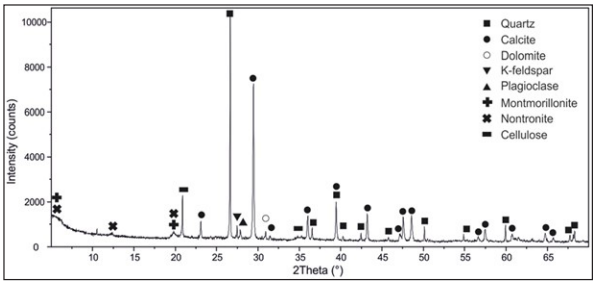

Figure 2. XRD pattern of a representative urban sample from upper soil.

In all XRD patterns of both lower and upper soils, the presence of two or three small peaks at low angles, between 8.9° and 12.4° 2θ have been detected. The peak at 12.4° 2θ (~ 7.15 Å) is always found and is attributed to kaolinite; a small peak, rarely found at 8.9° 2θ (~ 9.94 Å) is attributed to illite; other peaks, commonly occurring within this range cannot be precisely attributed due to the chemical and structural variability of clay minerals but can be assigned to montmorillonite or saponite and/or nontronite. In addition to the mineral phases, the signature of cellulose is clearly observed in all samples as testified by the (002) peak at about 20.8° 2θ and by the large, poorly-defined (040) peak in the 34.5-35.5° 2θ range.

3.2. Soil Chemistry

As for the soil chemistry, Tables (1 and 2) represent the analytical results of heavy metals, pH and EC for both the upper soil (i.e. 0-10cm and the lower soil (i.e. 10-20 cm) in the study area. Additionally, the texture analysis for the selected soil samples from the area shows that it belongs to the Vertisol type of silty sand texture, this is similar to (Hararah et al., 2011), (Table 3).

In order to determine the chemical enrichment and depletion of the heavy metal, the correlation coefficient relationships were used. The correlation coefficient for both soils is presented in Tables (4-5). From these matrices, it can realize that a similar correlation coefficient relationship existed between Fe and other HM in both soils, the only obvious difference was that in upper soils there was a positive correlation between Cu and Pb and Zn, whereas in the lower soils, co correlation existed. In the upper soils Cu has a very positive correlation with all HM, whereas it is only correlated to Cr, Co and Ni in the lower soils. Moreover, there was a quite clear positive correlation between Cu and Mn, Pb and Zn in the upper soils, but no correlation between Cu and Zn and Pb was observed in the lower soils. Mn, Pb and Zn are positively correlated to each other; only Cu was in the upper soils. This suggests a different source of contamination or an anthropogenic source that produces the Zn, Mn and Pb, which is most likely to be traffic-related. Another difference between upper and lower soils in the behavior of pH and EC is that they have a clear negative correlation with all HM in the lower soils, but they have a neutral correlation with HM in the upper soils. This means that EC and pH are relatively higher in the upper soils, due to the effect of the higher evaporation and lower rainfall in the area.

Table 1. The analytical results of the upper soil; heavy metals (mg/kg), pH and EC (µs/cm).

Sample ID upper	pH	EC [µs/cm]	Fe [mg/kg]	Cu [mg/kg]	Cr [mg/kg]	Co [mg/kg]	Mn [mg/kg]	Zn [mg/kg]	Ni [mg/kg]	Pb [mg/kg]
1R	8.24	78.9	20255	13.7	26.8	6.7	530.2	183.8	21.0	20.3
1	8.21	95.1	19744	12.3	14.5	3.0	213.6	223.1	12.5	31.2
1L	8.12	68.1	26483	17.2	36.5	14.2	1255.6	111.8	37.6	16.8
2R	8.31	82	23992	15.6	36.0	9.6	660.1	78.2	27.1	20.3
2	8.17	140	24615	15.6	36.7	9.6	643.9	57.0	26.9	19.0
2L	8.13	69.9	27768	15.7	38.6	11.9	952.5	135.8	30.5	20.1
3R	8.22	121.6	21228	11.8	31.4	9.1	757.6	82.0	24.9	23.9
3	8.16	169.2	29014	30.1	39.1	13.7	1309.7	316.3	35.7	35.0
3L	8.24	117.2	27223	14.8	40.8	10.4	844.2	101.2	28.4	23.1
4R	7.97	97.9	26795	14.6	37.4	11.8	841.5	120.4	32.1	12.1
4	8.12	113.4	23408	13.8	30.8	11.2	920.0	195.3	28.8	15.3
4L	7.99	104	24537	15.8	30.8	13.0	1139.2	69.5	31.3	13.2
5R	7.94	120.4	22863	13.8	27.1	8.9	833.4	91.6	25.5	15.3
5	8.24	149.2	17763	13.1	17.4	6.7	665.6	66.6	17.4	18.1
5L	8.17	126	21481	11.1	17.9	8.0	852.3	74.3	23.1	15.6
6R	8.1	97.8	19243	12.9	11.3	7.8	947.0	199.1	23.2	15.6
6	8.25	149.9	14260	9.3	6.6	6.1	768.4	28.2	16.7	7.6
6L	8.1	92.5	16868	13.0	10.8	8.5	486.9	78.2	25.0	12.4

7R	8.26	75.3	16226	8.2	17.0	5.8	486.9	130.0	17.7	13.1
7	8.26	91.3	11515	9.2	11.2	3.9	346.2	182.8	13.7	17.1
7L	8.13	132.7	19301	17.9	44.6	5.9	508.6	162.6	28.0	12.8
8R	8.18	120.2	24770	12.0	32.1	9.7	898.3	87.8	28.3	11.8
8	8.22	81.9	23972	11.3	27.6	10.4	868.5	43.6	28.1	10.9
8L	8.16	73.4	24517	10.7	31.0	7.8	800.9	125.2	24.8	13.1
9R	8.22	95.8	24031	10.0	28.0	8.5	941.6	117.5	24.8	12.0
9	8.2	107.4	17977	8.8	21.4	6.3	752.2	101.2	20.3	15.6
9L	7.9	76	26950	12.4	49.6	10.1	703.4	135.8	29.3	7.9
10R	8.07	73.1	18231	9.2	18.2	6.2	589.8	59.0	20.1	10.3
10	8.11	89.7	13948	7.6	16.3	4.4	351.6	124.2	16.7	16.8
10L	8.11	48.1	25627	11.3	28.0	10.1	776.5	74.3	28.5	6.5
Maximum	8.31	169.2	29014	30.0	49.6	14.2	1309.7	316.3	37.6	35.0
Minimum	7.9	48.1	11515	7.6	6.6	3.0	231.6	28.3	12.5	6.5
Mean	8.15	101.9	21820	13.1	27.2	8.6	754.9	118.5	24.9	16.1
σ	0.1	27.9	4541	4.1	11.1	2.8	252.5	61.8	6.1	6.3

Table 2. The analytical results of the lower soil; heavy metals (mg/kg), pH and EC (µs/cm).

Sample ID lower	pH	EC [µs/cm]	Fe [mg/kg]	Cu [mg/kg]	Cr [mg/kg]	Co [mg/kg]	Mn [mg/kg]	Zn [mg/kg]	Ni [mg/kg]	Pb [mg/kg]
1R	8.27	82	20527	13.5	27.7	7.0	541.1	94.5	21.9	20.7
1	8.17	88.3	19160	15.1	22.5	2.9	156.7	150.2	17.0	26.5
1L	8.17	73.9	28274	16.9	36.8	14.0	1269.1	120.4	37.5	16.7
2R	8.4	78.4	25335	17.7	35.1	9.5	687.2	128.1	26.2	20.3
2	8.1	96.3	23525	15.7	34.5	9.8	673.7	97.4	25.9	22.2
2L	8.12	84	29052	15.9	40.0	12.5	1017.4	162.6	30.7	20.4
3R	8.27	116.4	23544	12.4	33.1	9.5	790.1	72.4	25.6	23.2
3	8.46	166.4	23213	12.8	35.8	10.8	838.8	68.6	25.7	24.2
3L	8.36	102.6	26055	16.4	33.4	10.8	681.8	105.0	31.1	13.7
4R	7.98	79.2	30142	30.3	51.2	12.8	925.4	168.4	35.5	12.1
4	8.14	103.3	25666	15.1	32.4	11.7	987.6	101.2	30.3	14.3
4L	8.12	113	25627	15.7	30.1	12.3	1120.3	206.8	31.3	14.3
5R	8.05	98.5	23544	13.9	25.7	9.7	982.2	101.2	27.7	14.5
5	8.19	116.2	18192	13.5	17.5	7.0	781.9	85.8	19.1	22.2
5L	8.22	109.7	23174	13.1	16.8	10.2	1101.3	97.4	26.1	15.6
6R	8.17	105.8	17841	12.4	9.0	6.9	936.2	97.4	21.7	15.9
6	8.32	120.2	15856	9.8	7.2	5.9	828.0	179.0	16.9	15.6
6L	8.2	80.3	24809	14.3	11.9	10.4	768.4	52.2	29.3	12.1
7R	8.27	76.1	14649	7.9	14.9	5.3	468.0	180.9	16.4	12.4
7	8.12	83.3	9686	6.5	9.5	3.2	332.7	203.0	11.2	15.4
7L	8.26	106	19184	17.9	46.5	6.0	535.6	237.5	28.3	12.4
8R	8.21	110.2	26386	12.5	33.8	10.0	971.4	87.8	29.3	11.2
8	8.11	107.5	25004	11.3	28.0	9.7	849.6	72.4	27.0	11.8
8L	8.26	71.3	22941	11.0	31.9	7.7	879.4	107.0	25.3	12.4
9R	8.31	91	24868	11.1	32.2	9.7	657.4	59.0	27.3	9.9
9	8.21	143.2	15895	8.3	20.4	5.7	725.1	94.5	18.6	16.0
9L	7.97	53.9	26678	12.9	44.4	10.6	687.2	93.5	28.8	8.4
10R	8.13	65.3	18308	9.2	19.7	6.3	578.9	85.8	19.2	10.1
10	8.09	76.2	12313	7.7	14.3	4.5	370.5	107.0	17.1	14.0
10L	8.18	55.3	27456	11.2	29.7	9.8	806.3	105.0	28.7	8.1
Maximum	8.46	166.4	30142	30.3	51.2	14.0	1269.1	237.5	37.5	26.5
Minimum	7.97	53.9	9160	6.5	7.7	2.9	156.7	52.2	11.2	8.1
Mean	8.19	95.1	22230	13.4	27.5	8.7	765.0	117.4	16.1	15.6
σ	0.11	24.5	5095	4.4	11.5	2.9	246.5	49.1	6.1	4.8

Table 3. Soil texture analysis for selected soil samples from the study area.

Sample	Sand %	Clay %	Silt %
4L	61	20	19
7R	68	8	24
9L	53	18	29
10L	70	14	16

Table 4. Correlation coefficient matrix for the heavy metals, pH and EC in upper soil. n=30; at 95% confidence level (P<0.05).

upper	Fe	Cu	Cr	Co	Mn	Zn	Ni	Pb	EC	pH
Fe	1.0	0.54	0.81	0.89	0.77	-0.03	0.91	-0.02	0.03	0.03
Cu		1.00	0.56	0.62	0.54	0.51	0.67	0.57	0.43	0.32
Cr			1.00	0.65	0.43	0.12	0.78	0.11	-0.04	-0.02
Co				1.00	0.86	-0.02	0.94	0.04	0.13	-0.02
Mn					1.00	0.04	0.79	0.03	0.40	0.16
Zn						1.00	0.05	0.60	0.21	0.19
Ni							1.00	-0.05	0.08	0.00
Pb								1.00	0.44	0.42
EC									1.00	0.44
pH										1.00

Table 5. Correlation coefficient matrix for the heavy metals, pH and EC in lower soil. n=30; at 95% confidence level (P<0.05).

lower	Fe	Cu	Cr	Co	Mn	Zn	Ni	Pb	EC	pH
Fe	1.0	0.57	0.69	0.95	0.73	-0.27	0.93	-0.25	-0.12	-0.38
Cu		1.00	0.67	0.58	0.33	0.20	0.69	0.12	0.09	-0.34
Cr			1.00	0.61	0.26	0.08	0.74	-0.04	-0.05	-0.33
Co				1.00	0.80	-0.23	0.92	-0.13	-0.03	-0.41
Mn					1.00	-0.16	0.69	-0.13	0.09	-0.35
Zn						1.00	-0.12	-0.01	-0.03	-0.02
Ni							1.00	-0.22	-0.10	-0.46
Pb								1.00	0.42	0.40
EC									1.00	0.15
pH										1.00

The comparison in heavy metal distribution between the upper and lower soils was investigated using the 1:1 ratio charts and is shown in Figure (3). This type of charts is previously used to distinguish the enrichment and depletion of elements between two layers, (Jiries et al., 2004). This figure shows that Fe has a slightly higher content in the lower soil. This was mainly in the samples located in unused or unoccupied areas (i.e. background). These are characterized as red soils without any human activities. This slight enrichment could be explained by the aggressiveness of the acid mixture used in the soil sample digestion process which resulted in attacking the internal mineral composition of the soil mineral lattice in addition to the adsorbed metals on the soil surface, thus increasing the element content.

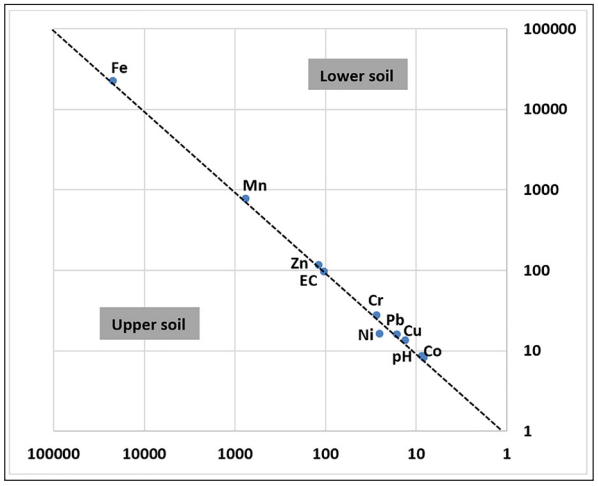

Figure 3. 1:1 ratio plot showing no difference between the upper and lower soils.

3.3 Source of Pollution

The heavy metal distribution within the surface soil samples was investigated to delineate the areas with pollution and to allocate the major source/s of pollution. To this purpose, the samples were classified according to the occupied activates into four categories: Background (open areas without activities); Housing (areas mainly occupied by normal houses); Traffic (sites dominated by high traffic density); and Industry (sites that are in areas which has certain industrial or semi-mechanical warehouses). These categories with average HM contents are illustrated in Table (6) and Figure (4).

Table 5. Surface soil samples categories, and there average heavy metal contents

Sample ID	Background	Houses	Traffic	Industry
No. Samples	5	14	7	4
pH	8.21	8.2	8.1	8.2
EC (µs/cm)	106.7	95.8	106.5	109.5
Fe (mg/kg)	15489	21749	24537	25228
Cu (mg/kg)	9.4	12.5	14.9	16.5
Cr (mg/kg)	14.0	28.3	31.5	32.2
Co (mg/kg)	4.7	8.3	10.8	10.8
Mn (mg/kg)	486.4	700.7	929.3	974.8
Zn (mg/kg)	131.9	104.7	107.2	170.1
Ni (mg/kg)	16.0	24.7	29.3	29.4
Pb (mg/kg)	17.7	14.6	16.4	18.6

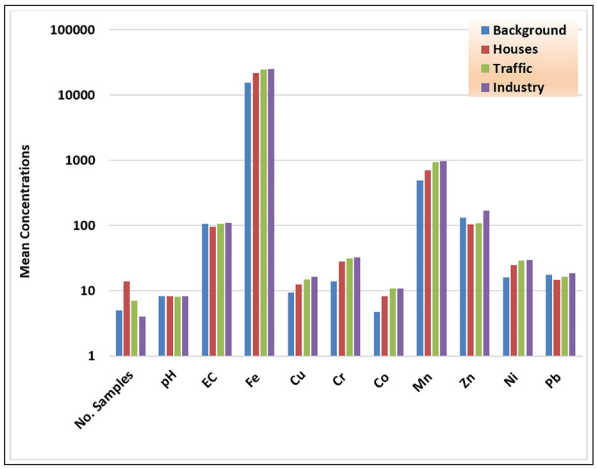

Figure 4. The average HM, pH and EC for the four categories in the study area.

3.4 Index of Pollution

For the purpose of the environmental evaluation of the HM and to elucidate the extent of their pollution in the surface soils of the study area, Index of Pollution (IP) was used. This statistical technique, that was first introduced by (Chester et al., 1985), and was used then by many in Al-Karak area, was used to delineate the pollution in the Wadi sediments (El-Hasan and Jiries, 2002; Jiries et al., 2004). It depends on soil sample categorization based on the occupied activities in the specific soil sampling site (i.e. Background, Domestic, Traffic or Industrial). The prime step of this method is the assigning of the Artificial Background Samples (ABS), which were chosen from the background sampling sites that have the lowest HM concentrations to establish the base line that reflects a non-polluted area. The first step was to calculate the threshold using equation (1) (Saffarini and Lahawani, 1992).

$$\text{Threshold} = X + 2\sigma \quad \ldots\ldots\ldots\ldots\ldots (1)$$

where X is the mean, σ is the standard deviation.

Secondly, individual samples should show lower heavy-metal concentrations relative to other samples, (Chester et al., 1985). The chosen ABS samples are shown in (Table 1). The new threshold was then calculated using the following equation (2):

$$\text{Threshold} = X_{ABS} + 2\sigma_{ABS} \quad \ldots\ldots\ldots\ldots\ldots (2)$$

where X ABS is the mean of ABS samples, σ (ABS) is the standard deviation of ABS.

Finally, the IP was then calculated using the following equation (3).

$$IP = \text{Conc. } E / (X_{ABS} + 2\sigma_{ABS}) \quad \ldots\ldots\ldots\ldots\ldots (3)$$

where (Conc. E) is the concentration of any element in the sample, and the (X ABS +2σ ABS) is the ABS threshold of that element. Whenever IP >1.0, it indicates that additional pollutant input has been introduced to the sample.

The results are shown in Table (7). It is obvious that the degree of soil contamination by heavy metals is very low in the study area as it has no massive industries and high density traffic. Most of the upper soils at the sampling sites have IP < 1, which means no additions of HM were incremented to the soil. Meanwhile; only few sites which belong to the Traffic and Industrial categories have an IP >1, which means additional anthropogenic HM sources are presented affecting these site. The values and the distribution of sites, with an IP>1, reflect a low pollution extent and a very scarce dispersion. The Mutah and Al-Mazar areas have become the most attracting areas in Al-Karak province for the population because of the relatively higher work opportunities and the fast growth in urban development and the relatively good commercial situation. Thus an increase in traffic and more middle-size industrial firms are expected to be established in the coming few years, which will, therefore, be reflected on the size and type of pollution generation. Therefore, monitoring HM contamination is essential as a precautionary tool for enhancing the sustainable environmental conditions.

Table 7. Index of Pollution (IP) values for the heavy metals within the surface soil samples.

	pH	EC	Fe	Cu	Cr	Co	Mn	Zn	Ni	Pb
1R	0.99	0.50	0.92	1.06	1.07	0.88	0.53	0.65	0.95	0.58
1	0.99	0.61	0.89	0.95	0.58	0.39	0.21	0.79	0.56	0.90
1L	0.98	0.43	1.20	1.33	1.46	1.87	1.26	0.40	1.70	0.48
2R	1.00	0.52	1.08	1.21	1.43	1.26	0.66	0.28	1.23	0.58
2	0.98	0.89	1.11	1.21	1.46	1.27	0.64	0.20	1.22	0.55
2L	0.98	0.45	1.26	1.22	1.54	1.56	0.95	0.48	1.38	0.58
3R	0.99	0.77	0.96	0.92	1.25	1.20	0.76	0.29	1.13	0.69
3	0.98	1.08	1.31	2.34	1.56	1.80	1.31	1.12	1.62	1.01
3L	0.99	0.75	1.23	1.15	1.63	1.36	0.85	0.36	1.29	0.66
4R	0.96	0.62	1.21	1.13	1.49	1.55	0.84	0.43	1.45	0.35
4	0.98	0.72	1.06	1.07	1.23	1.47	0.92	0.69	1.30	0.44
4L	0.96	0.66	1.11	1.23	1.23	1.71	1.14	0.25	1.42	0.38
5R	0.96	0.77	1.03	1.07	1.08	1.17	0.83	0.32	1.15	0.44
5	0.99	0.95	0.80	1.01	0.69	0.89	0.67	0.24	0.79	0.52
5L	0.98	0.80	0.97	0.86	0.71	1.05	0.85	0.26	1.05	0.45
6R	0.98	0.62	0.87	1.00	0.45	1.03	0.95	0.71	1.05	0.45
6	0.99	0.95	0.64	0.72	0.26	0.81	0.77	0.10	0.76	0.22
6L	0.98	0.59	0.76	1.01	0.43	1.12	0.49	0.28	1.13	0.36
7R	1.00	0.48	0.73	0.64	0.68	0.76	0.49	0.46	0.80	0.38
7	1.00	0.58	0.52	0.71	0.44	0.51	0.35	0.65	0.62	0.49
7L	0.98	0.85	0.87	1.39	1.78	0.77	0.51	0.58	1.27	0.37
8R	0.99	0.77	1.12	0.93	1.28	1.28	0.90	0.31	1.28	0.34
8	0.99	0.52	1.08	0.88	1.10	1.36	0.87	0.15	1.27	0.31
8L	0.98	0.47	1.11	0.83	1.24	1.03	0.80	0.44	1.12	0.38
9R	0.99	0.61	1.09	0.77	1.11	1.12	0.94	0.42	1.12	0.34
9	0.99	0.68	0.81	0.68	0.85	0.83	0.75	0.36	0.92	0.45
9L	0.95	0.48	1.22	0.96	1.97	1.33	0.70	0.48	1.33	0.23
10R	0.97	0.47	0.82	0.72	0.72	0.82	0.59	0.21	0.91	0.29
10	0.98	0.57	0.63	0.59	0.65	0.58	0.35	0.44	0.76	0.48
10L	0.98	0.31	1.16	0.87	1.11	1.33	0.78	0.26	1.29	0.19

4. Conclusions

This study has used the urban soil cover as a tool in determining heavy-metal contamination in relation to various anthropogenic occupational activities. The studied area bears low additional inputs of heavy metals as it has no massive industrial firms or high-density transportation infrastructures. Few sites have an index of pollution of IP>1 in areas with traffic activities and, therefore, traffic seems to be the only source of pollution by heavy metals in the study area. The prevailing climatic conditions in terms of high evaporation, low rainfall, and the lower pedogensis process are reflected in higher EC and pH values at the upper soils. Moreover, this study shows different patterns of distribution of heavy metals between the upper and the lower soils, which might be attributed to the soil mineralogy, high alkalinity, and low rainfall. In conclusion, the heavy-metal pollution in the study area is not as severe as it is in many other cities in Jordan or elsewhere in the world. However, precautionary environmental requirements, as quick as possible, are needed due to the rapid growth rate in the area especially that the results of this study do confirm the rapid effects of the human-related activities in changing the chemistry of the environment of the study area.

References

Alloway, B.J. and Ayres, D.C. (1997). Chemical principles of environmental pollution. 2nd edition. New York: Blackie Academic and Professional.

Blakemore, L.C., Searle, P.L., Daly, B.K. (1987). Methods for the chemical analysis of soils. New Zealand Soil Bureau Scientific Report 80.

Birke, M. and Rauch, U. (2000). Urban Geochemistry: investigation in the Berlin metropolitan area. Environmental Geochemistry and Health 22: 233-248.

Chapman, H.D. and Pratt, P.T. (1974). Methods of analysis for soil, plant and water. University of California, Division of agricultural Sciences P 309.

Chester, R., Kudoja, W.M., Thomas, A., Towner, J. (1985). Pollution reconnaissance in stream sediments using non-residual trace metals. Environmental Pollution (series B) 10: 213–238.

Claridge, G.G.C., Campbell, I.B., Powell, H.K.J., Amin, Z.H., Balks, M.R. (1995). Heavy metal contamination in some soils

of the McMurdo Sound region, Antarctica. Antarctic Science 7 (1): 9-14.

Department of Meteorology of Jordan (2016). Annual Report. Unpublished report.

Duris, M. and Zimova, M. (1994). Gochemicko-ekologicke mapovani prazske aglomerace, Obovod Praha 7. Cesky Geologicky ustav (in Czech).

Eaton, A.D., Clesceri, L.S., Franson, M.A.H., Rice, E.W., Greenberg, A.E. (Eds.), (2005). Standard methods for the examination of water and wastewater 21. American Public Health Association. Washington, D.C.

El-Hasan T. and Jiries, A. (2001). Heavy metal distribution in valley sediments in Wadi Al-Karak catchment area, South Jordan. Environmental Geochemistry and Health 23: 105–116.

El-Hasan, T. (2002). Urban Geochemistry: Heavy Metals Distribution on the Soils of Relatively Heavy Industrial City of Sahab, Central Jordan. Mu'tah Lil-Buhuth wad-Dirasat, Pure Sciences 17 (3): 49-67.

El-Hasan, T. and Lataifeh, M. (2003). Environmental Magnetism: The Implication of Initial Magnetic Susceptibility and Saturation Magnetization for Detecting Roadside Pollution in Arid Regions. Dirasat, Pure Sciences 30 (2):191-202.

El-Hasan, T. and Lataifeh, M. (2013). Field and Dual Magnetic Susceptibility Proxies Implication for Heavy Metal Pollution Assessment in the Urban Soil of Al-Karak City, South Jordan. Environmental Earth Sciences 69(7): 2299-2310.

El-Hasan, T., Al-Omari, H., Jiries, A., Al-Nasir, F. (2002). Cypress Tree (Cupressus Semervirens L.) Bark as an Indicator for Heavy Metal Pollution in the Atmosphere of Amman City, Jordan. Environment International 28(6): 513-519.

El-Hasan, T., Momani. K., Al-Nawayseh, J., Al-Nawayseh, K. (2008). The influence of Dead Sea on the chemistry and mineralogy characteristics of the dry deposition fallen over the eastern highlands, central Jordan. Environmental Geology 54(1):103-110.

Fialova, H., Maier, G., Petrovsky, E., Kapicka, A., Boyko, T., Scholger, R. (2006). Magnetic properties of soils from sites with different geological and environmental settings. Journal of Applied Geophysics 59:273–283.

Garnaud, S., Mouchel, J.M., Chebbo, G., Thevenot, D.R. (1999). Heavy metal concentrations in dry and wet atmospheric deposits in Paris district: comparison with urban runoff. The Science of the Total Environment 235: 235-245.

Hararah, M.A., Al-Nasir, F., El-Hasan, T. Al-Muhtaseb, A.H. (2011). Zinc adsorption-desorption isotherms: Possible effects on the calcareous vertisol soils from Jordan. Environmental Earth Sciences 65: 2079-2085.

Ho, Y.B. and Tai, K.M. (1988). Elevated levels of lead and other metals in roadside soil and grass and their use to monitor aerial metal deposition in Hong Kong. Environmental Pollution 49: 37-51.

Huisman, D.J., Vermeulen, F.J.H., Baker, J., Veldkamp, A., Kroonenberg, S.B., Klaver, G.T.h. (1997). A geological interpretation of heavy metal concentrations in soils and sediments in the southern Netherlands. Journal of Geochemical Exploration 59(3): 263-174.

Jiries, A., Al-Nasir, F., El-Hasan, T. (2017). Pasture land in a desert area at Al-Karak province, Jordan. In: Abou-Elnaga and Aydin (Eds.), Proceedings of the regional workshop: Solutions to water challenges in MENA region. April 25-30 – 2017; Cairo-Egypt. 10-17.

Jiries, A., Batarseh, M., El-Hasan, T., Ziadat, A., Al-Naser, F. (2008). Lichens (Rhizocarpon geographicum) as Biomonitor for Atmospheric Pollution in Amman City, Jordan. Environmental Bioindicators 3(2): 106-113.

Jiries, A., El-Hasan, T., Al-Hiwati, M., Seiler, K.P. (2004). Evaluation of the Effluent Water Quality Produced from Phosphate Mines in Central Jordan. Mine Water and the Environment 23 (3): 133-137.

Kim, K.W., Myung, J.H., Ahn, J.S., Chon, H.T. (1998). Heavy metal contamination in dusts and stream sediments in the Taejon area, Korea. Journal of Geochemical Exploration 64 (1-3): 409-419.

Li, X., Poon, C., Liu, P.S. (2001). Heavy metal contamination of urban soils and street dusts in Hong Kong. Applied Geochemistry 16:1361-1368.

Powell, J.H. (1988). The geology of Karak area. Map sheet No. 3152 II. Geology Directorate, Natural Resources Authority (Ministry of Energy and Mineral Resources) Amman, HK.

Saffarini, G.A. and Lahawani, Y. (1992). Multivariate statistical techniques in geochemical exploration applied to Wadi sediments data from an arid region:Wadi Dana, SW Jordan. Journal of African Earth Sciences 14(3): 417–427. Rayment, G.E. and Higginson, F.R. (1992). Australian laboratory handbook of soil and water chemical methods. Intaka Press, P 330.

Vermeulen, F.J.H., Baker, J., Veldkamp, A., Kroonenberg, S.B., Klaver, G.T.h. (1997). A geological interpretation of heavy metals concentrations in soils and sediments in the southern Netherlands. Journal of Geochemical Exploration 59(3): 163-174.

Wilcke, W., Muller, S., Kanchanakool, N., Zech, W. (1998). Urban soil contamination in Bankok: heavy metal and aluminum portioning in surface soils. Geoderma 86 (3-4): 211-228.

JJEES

JJEES (2020) 11 (3): 211-224
ISSN 1995-6681

Jordan Journal of Earth and Environmental Sciences

Susceptibility of Agricultural Land to Soil Degradation by Rainfall Using Aggregates' Stability Indices in Parts of Abia State, South Eastern Nigeria

Ubuoh Emmanuel Attah*, Onwughara Izuchukwu Joshua, Odey Emmanuel

Michael Okpara University of Agriculture, College of Natural Resources and Environmental Management, Department of Environmental Management and Toxicology, Nigeria

Received 22 December 2019; Accepted 17 April 2020

Abstract

This study determines the dynamics in soil aggregate stability within agricultural land in Abia State, Nigeria at three physiographic positions: Upper, middle and lower slopes. The soil samples were collected at 0–25cm and 25-50cm of soil depths along the slopes. The parameters assessed were aggregate stability (AS) and mean- weight diameter (MWD), size distribution of water stable aggregates (WSA): >2.00mm, 2-1mm, 1-0.50mm, 0.50-0.25 mm and <0.25mm. Class and severity indices were used as critical limits for soil aggregate stability. The results of the physical parameters indicate significant differences ($p \leq 0.05$), but there was no significant difference among the chemical parameters ($p \leq 0.05$) in the gully sites respectively. MC correlated with hydraulic conductivity (r = -0.490). Clay correlated positively with sand, aggregate stability and MWS (r=-0.957, r=0.412, r=0.432) respectively. Silt correlated negatively with sand (r=-0.608), sand was negatively correlated (MWD) (r=-0.552) and aggregate stability correlated positively with MWD (r=0.938). The recorded aggregate stability status based on 2mm, 1mm, 0.5mm and 0.25mm in USL was as follows: stable 17%, moderate 41.7%, unstable 66%, MWD 44.05%, MSL: very unstable 8%, stable 17%, medium 25% and unstable 50%, MWD 54.4% and LSL: severe moderate 33%, very severe 67% and MWD 59.04% respectively. The soil aggregate stability status along the slope gradients was the same at the $p \geq 0.05$ significant level. Soil aggregate structural deformation is influenced by soil moisture, hydraulic conductivity, textural characteristics and soil organic matter. It is recommended that the soil surface coverage must be improved on slopes which could lead to the stabilization of soil aggregates to avert soil erosion problems in the area.

Keywords: Gully Erosion, Soil Aggregate Stability, Runoff, Land degradation

1. Introduction

The stability of soil aggregates describes their resistance to breakdown under disruptive forces. It is a key soil characteristic affecting ecosystem processes, such as carbon storage (Quanchao et al., 2018), nutrient availability (Wang et al., 2001), and the resistance of soils to erosion (Barthès and Roose 2002; Frei et al., 2003). In severely- eroded ecosystems, such as Badlands characterized by many active gullies and high level of disturbance, aggregate stability of soil is an emerging indicator of their ecological restoration status (Burri et al., 2009). The plant community composition dynamics through succession change, occurring on the eroded ecosystems, is a major factor of restoration (Walker and Del Moral, 2009), and thus can potentially provide aggregate stability to various soils. Studies showed that soil aggregate stability generally increases as succession proceeds (Cheng et al., 2015; Qui et al., 2015); however, the factors leading to these modifications along succession gradients are hardly known. Soil aggregate stability is an effective way of increasing soil quality and also preventing soil erosion and other environmental problems caused by soil degradation (Zhu et al., 2017), associated with the amount and intensity of precipitation and human activities (Ubuoh and Ogbonna, 2018). Higher amounts of precipitation and irregular rainfall events can decrease aggregate stability and increase erosion (Dimoyiannis, 1998). According to Six et al. (2004), it has also been suggested that the dynamics of aggregate formation are closely linked to SOM storage in soils (Golchin et al., 1998; Ubuoh et al., 2016). Soil aggregate stability is the most appropriate indicator in protecting slopes from erosion and shallow mass movements (Kalhoro et al., 2017). The micro aggregates are stabilized against disruption by several mechanisms wherein organo-mineral complexes and soil organic matter act as the main cementing agents in the soil aggregates' development (Denef and Six, 2005; Singh et al., 2017).When organic matter in soil reduces, aggregates breakdown, and the small particles of soils are transferred during soil erosion by water (Bronick and Lal, 2005).

* Corresponding author e-mail: ubuohemmanuel@yahoo.com

In Southeast Nigeria, the soils are naturally prone to erosion due to their fragile nature and ease of leaching being mainly ultisols and alfisols (Oguike and Mbagwu, 2009), especially gully erosion which is predominant in the region (Adekalu et al., 2007). Hence, erosion is a major cause of soil degradation leading to reduction in soil's productivity as the result of leaching out of the soil organic matter and other soil cementing agents which bind the soil particles together (Ubuoh and Ogbonna, 2018), especially in the Southeast Nigeria due to poor aggregation of soil (Onweremadu et al., 2010). Most studies have been carried out on agricultural soils (Idowu, 2003; Milne and Haynes, 2004), and far fewer on soils on steep slopes affected by erosion using indices (Gros et al., 2004 ;Canton et al., 2009). The soils in parts of Abia are particularly not fertile and are prone to leaching because of heavy rainfall, leading to the ecological problems such as sheet and gully erosion. Despite soil erosion on agricultural land, increasing demand for land as a result of population increase and food scarcity has made farmers to farm in marginal lands such as lands susceptible to erosion and flooding (Sanchez et al., 1997; Quansah, 1997; Ubuoh et al., 2017).

Therefore, the study aimed to investigate the relationships between the soil aggregate stability and rainfall along the slope gradient of agricultural land using aggregate stability indices in parts of Abia State, Southeastern Nigeria. The result of the study will reveal environmental conditions that would promote the stability of soil aggregate, which may lead to the development of the sustainable agricultural land to alleviate water erosion and ensure food security for the teeming population.

2. Research Methodology

2.1 Study Area

Abia state is located in the southeastern Nigeria and lies between latitude 5° 31' 59.99" N and Longitude 7° 28' 59.99" E. The state covers an area of about 5,243.7 square kilometres with a population of 2,833,999 (NPC, 2006). The area is dominated by flat and low lying land, but it is also characterized by undulating lands with many hills, generally less than120m above sea level. The mean annual rainfall is about 2200mm in average and the mean temperature is above 27^{0}C (Iheanyi, 2016). Relative humidity reaches about 90% throughout the year. The soils of the area fall within the broad group of ferallitic soils of the coastal plain sand and escarpment; other soil types includes alluvial soils found along the low terrace of Cross river and other rivers (Figure 1).

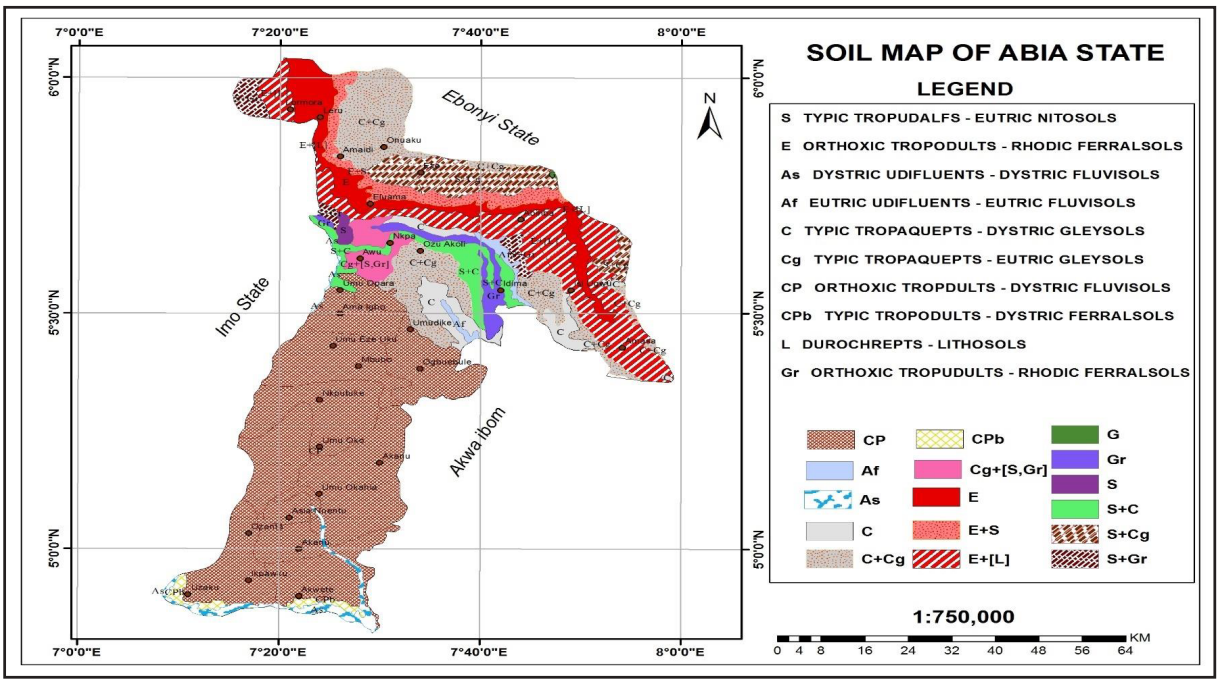

Figure 1. Soil Map of Abia State, Nigeria Source: Ogbonna, Abia State University, Uturu.

2.2 Soil Sample Locations

Soil samples were collected based on the chosen agro-ecological zones (Figure 2) in Abia State as follows:-

i: Bende: Two communities with pronounced gullies were selected to include: Ozuitem Ndiagho designated SSP_1 and OnuIbina-UkwuIgbere designated soil sample point (SSP_2)`

ii: Ohafia: Ohafia designated SSP_3 and Ebem- Ohafia designated SSP_4

iii: Umuneoche: Amuada designated SSP_5 and ObinaoluNgodo designated SSP_6

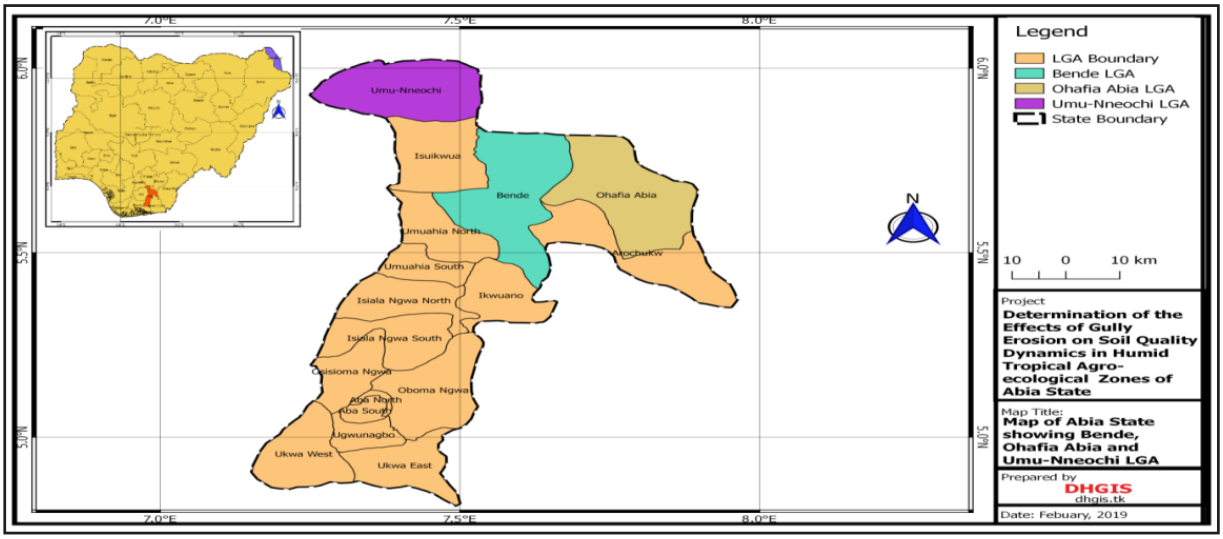

Figure 2. Map of Abia State Showing Sampling Locations

2.3 Soil Sampling Technique

Soil survey method was used to site points for soil sampling in each of the selected sites. Forty-eight soil samples were collected from each site at 0–25 cm, 25-50 cm of soil depths using an auger. From each of the study locations, soil samples were collected from the upper slope (USL), middle slope (MSL) and lower slope (LSL) of the gully and 100m away as controls. The samples were placed in polythene bags, labelled and were taken to the National Soil, Plant and Water Laboratory, Federal Department of Agricultural Land and Climate Change Management Services, Umudike for analysis. Handheld Global Positioning System receiver (Etrex Garmin Ltd. Kansas) was used for the geo-referencing of the sampling points (Table 1).

Table 1. Coordinates of the study Locations

S/No	Agroecological Zones	Coordinates of the study locations
1	BENDE	N 05^0 36.954 , E 07^0 36.423
	100 m away from erosion site	N 05^0 42.569, E 07^0 39.174
2	OHAFIA	N 05^0 38.421, , E 07^0 50.026
	100 m away	N 05^0 38.997, E 07^0 49.587
3	UMUNEOCHE	N 05^0 59.477, E 07^0 24.145
	100 m away	N 05^0 57.902, E 07^0 23.398

2.4 Soil Physical Properties and Analysis

The soil physical properties analysed were the factors presumed to be affecting soil quality. Particle-size distribution was determined by the hydrometer method (Gee and Or, 2002). Soil-bulk density was determined using the core method (Grossman and Reinsch, 2002). Saturated hydraulic conductivity was determined in the laboratory using a constant head permeameter (Young, 2000). The soil moisture content was calculated using the following formula:

$$SMC = \frac{\text{mass at saturation} - \text{oven dried mass}}{mass\ of\ dried\ soil} x100 \quad \text{..... Eq. 1}$$

2.5 Soil Chemical Properties and Analysis

Soil pH was determined with a pH electrode, extracted from 0.01M $CaCl_2$ with a ratio of 1:2.5 (Bao, 2000; Huang et al., 2015). Soil organic matter (SOM) was determined by wet digestion with a mixture of 5 mL of 0.8 mol/L potassium dichromate ($K_2Cr_2O_7$) and 5mL of concentrated sulfuric acid (H_2SO_4) (Kalembasa and Jenkinson, 1973). Organic C was determined by the oxidation of organic matter with a hot mixture of $K_2Cr_2O_7$ and H_2SO_4 using the Walkley and Black procedure (Walkley and Black, 1934). The amount of organic carbon was then determined by titration with 0.05N $FeSO_4$ following the procedure outlined by Nelson and Sommers (1982).

2.6 Soil Aggregate Stability Determinations

2.1.2. Percentage Aggregate Stability and Mean Weight Diameter (MWD)

The percentage of aggregate stability and Mean Weight Diameter (MWD) were computed from size distribution of water stable aggregates. The distribution of water stable aggregates was determined by the wet sieving technique described by Kemper and Rosenau (1986). To separate the water stable aggregate, 25gm of the >2mm air-dried aggregates were put on top of a nest of sieves measuring 1mm, 0.5mm, and 0.25mm, and was pre-soaked for ten minutes in water. The sieves and their contents were oscillated vertically once per second in water twenty times. The resistant aggregates on each sieve were oven-dried at 105°C for twenty-four hours and weighed. The mass of <0.25mm was obtained by calculating the difference between the initial sample weight and the sum of sample weight collected on the 2.00mm, 1.00mm, 0.50 mm, and 0.25mm sieve nests respectively. The percentage ratio of aggregates in each sieve represented the water stable aggregate of size >2.00mm, 2-1mm, 1-0.50mm, 0. 50-0.25 mm and <0.25mm and was computed as follows:

$$WSA = \frac{Mr}{Mt} x\ 100 \quad \text{..... Eq. 2}$$

Where
WSA = Water stable aggregates
Mr = mass of resistant oven–dry aggregates in the size class fraction after wet sieving.
Mt = the total mass of the initial material (25gm)

Percentage of aggregate stability was calculated using this Formula:

$$\%\ \text{Aggregate stability} = \frac{\text{wt.of WSA}>0.50\ mm - wt.of\ sand x100}{\text{wt.of sample} - \text{wt.of sand}} \text{..... Eq. 3}$$

Where
Wt= weight

The mean weighted diameter (MWD) was calculated using the following equation (Oguike and Mbagwu, 2009).

$$\mathbf{MWD} = w_i x_i \quad \text{..... Eq. 4}$$

Where
w_i *= weight of aggregate in the ith aggregate size range as fraction of dry weight of sample.*
w_i *= Mean diameter of any particular size range of aggregates separated by sieving.*

The larger MWD value is a manifestation of a higher distribution of macro-aggregates and, therefore, a higher stability to erosion by water. The aggregation stability index is the ratio between the mass of the total sample and the mass of the sample retained in the 0.212 mm sieve mesh, expressed as a percentage.

2.6.2. Soil Aggregate Stability Index (ASI)

Aggregate stability was determined using the method described by Le Bissonnais (1996). This method included three disruptive tests that correspond to various wetting conditions and energies. Five classes of the soil aggregate stability were identified according to the values of MWD (Table 2).

Table 2. Soil aggregate stability based on the values of MWD

S/N	Classes of MWD/mm	Stability
1	<0.4	Very unstable
2	0.4-0.8	Unstable
3	0. .8–1.3	Medium
4	1.3-2.0	Stable
5	>2.0	Very stable

Source: (Le Bissonnais, 1996).

2.6.3. Severity Index (SI).

Lal (1986) has classified the critical levels of aggregate stability based on the levels of MWD as follows:

a. 0.5<0.1-5 : designating very severe
b. 1- 2 : designating severe moderate
c. 2-2.5: designating low
d. 2.5< designating no limitation respectively.

2.7 Statistical Analysis

The interrelations between the wet and dry stable aggregate indices were determined through a correlation matrix using the SYSTAT9 statistical program (SPSS, 1999) computer package. Also the relationships between the macro-aggregates stability indices along the gully slopes: upper slope (USL), middle slope (MSL), and lower slope (LSL), and soil properties were determined in a correlation matrix.

3. Results and Discussion

Table 3 demonstrates the soil physical properties in the gully affecting the agricultural sites along the three slope profiles. The slope types exhibited significant differences in soil properties (P<0.05).

Table 3. Soil Physical Characteristics in Gully Erosion Prone Sites at the different Slope Gradients in the study area

Slope	Bulk density (%)	Moisture content (%)	Hydraulic conductivity (cm/hr)	Sand (%)	Silt (%)	Clay (%)
Upper slope(USL)	1.77±0.13	5.94±1.58	18.95±2.38	63.58±11.67	10.5±2.90	25.67±8.95
Middle slope(MSL)	1.66±0.04	6.39 ±1.58	10.63±16.2	78.5± 478	4.25±1.53	2.92±3.42
Lower slope (LSL)	1.68±0.06	7.70±3.46	22.36±10.20	81.83±4.0	4.58±0.82	12.5±3.56
Control (Ctrl)	1.94±0.05	13.05±3.36	6.28±1.67	75.08±7.54	6.67±3.07	19±6.13
F- $LSD_{0.05}$	0.1742	1.3117	11.7308	11.593	4.583	6.667
CV	10.49	81.61	93.20	18.16	70.74	61.26
Sig.	SD	SD	SD	SD	SD	SD

Data are expressed as Mean ± SD

From Table 3, the mean bulk density ranged between the mean value of 1.66±0.04 and 1.77±0.13 g/cm^3 with the upper slope being more compacted than the middle slope; the lower slope being the least compacted, but it was found less compacted than the control with 1.94±0.05, having 10.5% of CV more than the mean bulk density values of 1.14 and 1.26 g/cm^3 in the gully sites in Ideato, Imo State (Oyegun et al., 2016). The results of bulk density are also far above the value of 1.0-1.3 g/cm^3 considered for a well-aggregated forest (Ibitoye et al., 2008). The high bulk density suggests that soil erosion is very evident in the selected communities. Ubuoh et al. (2013) reported that dry bulk density and moisture content lead to gully formation in the southeastern part of Nigeria.

The mean moisture content ranged between 5.94±1.58 and 7.70±3.46% with the upper slope having the lowest mean value, followed by the middle slope and the lower slope recording the highest moisture content, but it was less than control with a 13.05±3.36 % moisture content, having 81.61% CV respectively. The present results of moisture content are greater than the results of soil moisture content at the field capacity that ranged from 0.23 to 0.31% in the gully site, Kano (Mallam et al., 2016). Robinson and Dean (1993) and Nyberg (1996) all found that moisture content is inversely proportional to relative elevation.

The mean hydraulic conductivity in the study area ranged between 10.63±16.2 and 22.36±10.20 with the lower slope recording the highest value and the middle slope being the lowest followed by the upper slope being greater than the control with a value of 6.28±1.67 having 93.20 % CV respectively. In soil, Hu (2008) reported that, along the slope, hydraulic conductivities generally decreased downwards, and the soil in this portion of the slope had a higher number of bio pores. Based on the soil particle analyses at the study area, sand ranged between 63.58±11.67 % to 81.83±4.0% with the lower slope having the highest mean value and the upper slope having the least values followed by the middle slope along with the control having 75.08±7.54% with18.16% of CV respectively; this is greater than the gully sand in Umueshi, Imo State with 62.44 -74.05% (Oyegun et al., 2016), within 74.1% reported by Ubuoh et al. (2013) in the Ukpor gully erosion site in Anambra State. Various authors (Ukaegbu et al., 2015; Nwite and Okolo, 2017) have previously reported predominance of sand fraction in soils of different land uses in southeast Nigeria. Accordingly, authors including Liu et al. (2013), Xu et al. (2016) reported that the southeastern part of Nigeria soils are predominantly sandy and is >70%, as a result, this region is more prone to erosion especially with the presence of high rainfall. There was significantly more sand in gully sites than non-gully site. This could be the result of the loss of organic binding agents under the effect of rain, leading to the loss of finer soil particles carried away by the force of erosion and flood water (Olusegun et al., 2011; Uwanuruochi and Nwachukwu, 2012). The clay content in the soil in the study area ranged between 2.92±3.42 and 25.67±8.95 percentage, with the middle slope recording the lowest value to be followed second by the lower slope. The upper slope has the highest clay content along with the control recording 19±6.13 percentage of clay. Silt and clay ranged between 4.25±1.53 to 10.5±2.90 and 2.92±3.42 to 25.67±8.95 respectively, with the middle slope recording the least mean values along with the control at 6.67±3.07, 19±6.13 showing CV70.74% and 61.26% respectively, which is suspected to be due to erosion processes down the slopes Soil physical parameters along the three slopes indicated significant differences at $p>0.05$ level. The result was in tandem with the finding of Hossein et al. (2015) who reported that textural classifications were significantly different among the slope positions and control site ($p>0.05$). This is different from the findings of Salako et al. (2006) who reported a high clay content down the slope of the gully.

Table 4. Correlation between soil physical properties and soil aggregate indicators in the study area.

Parameters	MC	BD	Clay	Silt	Sand	HC	AST.	MWD
Moisture Content	1							
Bulk Density	0.027	1						
Clay	-0.008	-0.386	1					
Silt	-0.352	-0.224	0.304	1				
Sand	0.214	0.368	0.957**	-0.608**	1			
Hydraulic C	-0.490*	-0.096	0.059	0.337	-0.195	1		
Aggregate Stab (AST).	0.255	0.140	0.412*	0.167	-0.441	0.124	1	
MWD	0.190	-0.001	0.432*	0.174	-0.552*	0.208	0.938**	1

***. 0.01 level (2-tailed). *. 0.05 level (2-tailed).*

Table 4 reveals that MC, correlated negatively, but also weakly, with hydraulic conductivity (r = -0.490) at the significant level p <0.05. This inverse relationship may be attributed to the low soil infiltration rates due to soil compaction. Accordingly, Infiltration rates decreased with an increase in the bulk density and with a reduction in the air-filled porosity. Clay correlated positively, but strongly, with sand fraction (r=-0.957) at the significant level p<0.01. The relationship may be attributed to the fact that sand soils of humid tropical southeastern Nigeria will effectively depend on reliability of determination of clay and coarse sand contents of the soils (Chinedu et al., 2012). Clay correlated positively, but weakly, with aggregate stability and MWD (r=0.412, 0.432) at the p<0.05 significant level respectively. This implies that clay content increased with the decrease in aggregate stability/MWD respectively. Since clay in the soil is weakly correlated with aggregate stability (MWD), hence aggregate stability is highly susceptible to erosion. Therefore, aggregate formation and stabilization are affected by different factors such as clay content (Denef and Six, 2005). The indication was that mean weight diameter increased as clay contents increased resulting in a better aggregation of the soil (Uzoma and Onwuka, 2018). Silt correlated negatively, but strongly, with sand (r=-0.608) at the significant level p<0.01, Sand correlated negatively, but moderately, with weight diameter (MWD) (r=-0.552) at the p< 0.05 significant level. This indicates that the increase in sand particles decreased the soil micro aggregation. Aggregate stability correlated positively with MWD (r=0.938) at the significant level p<0.01.

Table 5. Soil Chemical Characteristics in Gully Erosion Prone Sites at the study Area

Slope Profile	pH (H_2O)	E/C (ds/cm)	OM(%)	OC (%)
Upper Slope (USL)	5.43±0.25	0.97±0.23	4.25±1.02	3.65±0.14
Middle slope (MSL)	5.59±0.25	10.0±0.23	4.18±1.09	3.05±0.58
Lower slope (LSL)	5.60±0.23	1.08±0.28	4.28±1.33	3.04±0.50
control (Ctrl)	5.68±0.30	0.89±0.24	4.37±1.42	2.68±0.53
F.$LSD_{0.05}$	0.925	0.865	0.1935	0.3696
CV	4.804	29.167	25.293	20
Sig	NSD	NSD	NSD	NSD

From Table 5, the results of the soil pH ranged between 5.43±0.25 at the upper slope indicating strong acid conditions and 5.60±0.23; this is lesser than the control 5.68±0.30 which indicates moderate acid conditions (5.6-6.0) respectively (Shehu et al., 2015). Soil pH distribution in the study area was in the increasing order of: USL (5.43±0.25) ≤ MSL (5.59±0.25) ≤ LSL (5.60±0.23) ≤Ctrl: (5.68±0.30) indicating strong acid conditions (5.0-5.5), moderate acid conditions (5.6-6.0) for the middle slopes, the lower slopes, and the control respectively, and these values were similar to the overall mean values of soil pH (5.4) obtained from the three gully profiles in Kano State (Mallam et al., 2016). The mean value of soil electrical conductivity (EC) ranged from 0.97±0.23 to 10.0±0.23, which is greater than the control with 0.89±0.24 mm/S. However, the present results of EC are in tandem with the results of EC obtained by Ubuoh and Ogbonna (2018) from soils affected by human-induced environmental hazards in Imo State. The mean values of soil organic matter obtained in this study were between 4.18±1.09% for MSL and 4.28±1.33% for LSL which are less than control with the value of4.37±1.42%. The overall results of OM were at the decreasing order starting with the control with the values of 4.37±1.42≥ LSL: 4.28±1.33≥ USL: 4.25±1.02≥ and MSL: 4.18±1.09 with CV of about 25.3 indicating no significant difference in the level of OM along the three slopes and the control at the p>0.05 level. The significantly lower values of SOM along the slopes may have been caused by the removal of plant residues by water erosion (Shinjo et al., 2000). The ecreased aggregate stability in this study is suspected to be mainly driven by the

lack of the soil organic-matter accumulation along the three slopes sequence as confirmed by Obalum et al. (2011). The soil Organic carbon ranged between 3.04±0.58 and 3.65±0.14 which is greater than the control value 2.68±0.53. The SOC was in the decreasing order of USL: 3.65±0.14≥MSL: 3.05±0.58≥ LSL: 3.04±0.50 ≥ and Ctrl: 2.68±0.53 showing a CV value of 20%, with no significant difference. The results are higher than the SOC values of (0.22% and 0.96%) in part of Imo State (Oyegun et al., 2016). The result from this study is different from the finding of Erktan et al. (2015), who observed that soil aggregate stability increased along the succession gradient, which is mainly driven by soil organic carbon accumulation. Thus, rainfall might have initiated the extent of the gully erosion (Ajaero and Mozie, 2011). Authors believed that the emphasis on high rainfall and topography can be attributed to the high rainfall in the humid tropics while the steep slopes in the area might have also aided the high speed of surface runoff leading to the rapid washing away of the soil surface and the weakening of soil strata.

Table 6. Correlation of the selected soil chemical properties with MWD and aggregate stability in the study area.

Variables	pH (H_2O)	E/C	Soil organic carbon	Soil organic matter	MWD	Agg. Stab.
pH (H_2O)	1					
E/C	0.233	1				
OC	-0.362	-0.134	1			
OM	-0.261	-0.295	0.022	1		
MWD	0.394	0.319	0. 757*	0.691**	1	
Agg. Stab.	0.555**	0.369	0.302	-.211	-0.938**	1

***. 0.01 level (2-tailed). *. 0.05 level (2-tailed).*

According to table 6, pH (H_2O) correlated positively, but moderately, with soil aggregate stability ((r= 0.56) at the significant level p<0.01. The weak positive association could be attributed to the moderate acidic pH level of the soil due to human activities such that accelerated soil erosion. Soil organic carbon correlated negatively, but strongly, with MWD (r= -0.76.). This implies that the decrease in soil organic carbon also led to the decrease in MWD leading to the susceptibility of the soil along with erosion by constant rainfall. This result is in line with the report by FAO (2019) which shows that most tropical soils are structurally fragile and are easily susceptible to many forms of erosion. Soil organic matter (SOM) correlated positively, but strongly, with MWD at r=0.69. This implies that reduction in soil organic matter leads to a decrease in the mean weighted diameter. MWD correlated negatively, but strongly, with aggregate stability (r= -0.94), signifying a low value of MWD. These low values of MWD could lead to quick dispersion of the soil during rainfall events leading to severe rill or inter-rill erosion and finally gully. In line with these results, it was suggested that wetting by rapid immersion for the measurement of dried aggregate stability had led to aggregate breakdown by slaking, while the slaking process may not occur in the measurement of wetting aggregate stability. As Ternan et al. (1996) and Unger (1997) suggested, the slaking process played a major role in the breakdown of surface soil aggregates in a semiarid region where intermittent rainfall causes rapid wetting of the relatively dry soil surface (Shinjo et al., 2000). However, Amezketa et al. (1996) showed that the combined use of MWD in various forms and the soil-slaking index could be useful in assessing soil erosive behavior. The results have further proven the important contributions of SOM and SOC in binding soil particles together into large macro aggregates to improve the aggregate stability of the soil (Yang, 2017). Oguike and Mbagwu (2009) observed that soils with low MWD have the potential to erode faster than those with higher MWD, and soils with good structures and high MWD resist aggregate breakdown during rainstorms (Ubuoh et al., 2013; Okon et al., 2016).

Table 7. MWD and Soil Aggregate Stability classes in Upper Slope in Gully Erosion Site regarding soil depth and particle size

LGA/ COMMUNITY	UPPER SLOPE (US)	Soil Depth (cm)	2mm	1mm	0.5mm	0.25mm	MWD (mm)	Class	Stability Status
BENDE: OZUITEM NDIAGHO	US	0-25	14.26	13.07	8.24	44.96	1.41	1.3-2.0	Stable
BENDE: OZUITEM NDIAGHO	US	25-50	4.3	10.19	16.2	54.83	0.61	0.4-0.8	Unstable
BENDE: ONUIBINA-UKWU IGBERE	US	0-25	3.23	8.72	10.04	55.34	0.51	0.4-0.8	Unstable
BENDE: ONUIBINA-UKWU IGBERE	US	25-50	3.74	16.1	16.66	52.55	0.68	0.4-0.8	Unstable
OHAFIA: ELU OHAFIA	US	0-25	2.85	11.1	15.84	58.36	0.53	0.4-0.8	Unstable
OHAFIA: ELU OHAFIA	US	25-50	1.34	10.63	19.74	57.82	0.56	0.4-0.8	Unstable
OHAFIA: EBEM OHAFIA	US	0-25	19.9	25.81	17.13	32.32	1.23	0. .8–1.3	Medium
OHAFIA: EBEMOHAFIA	US	25-50	26.86	35.82	16.41	18.37	1.53	1.3-2.0	Stable
UMUNEOCHE: AMUODA	US	0-25	2.92	14.2	16.14	50.66	0.61	0.4-0.8	Unstable
UMUNEOCHE: AMUODA	US	25-50	2.91	20.09	16.14	46.22	0.68	0.4-0.8	Unstable
UMUNEOCHE: OBINAOLU NGODO	US	0-25	12.04	31.22	19.37	31.19	1.09	0. .8–1.3	Medium
UMUNEOCHE: OBINAOLU NGODO	US	25-50	0.49	15.85	20.88	56.31	0.62	0.4-0.8	Unstable
F-$LSD_{0.05}$			21.29	20	7.91	32.75	0.84	-	
CV			106.96	50.84	22.71	27.44	44.05	-	
Sig.			NSD	NSD	NSD	NSD	NSD	-	

The summary of results and classes of soil aggregate stability in the upper slope in the gully erosion sites are presented in Table 7. At 2mm, aggregate stability ranged from 1.34 - 26.86 mm, at 1mm, aggregate stability ranged from 8.72 - 35.82 mm, at 0.5mm, aggregate stability ranged from 8.24 to 20.88 mm and at 0mm, aggregate stability ranged from 18.37 - 58.36mm respectively. The results imply that the smaller the particle size of the aggregate, the larger the specific surface area, and the greater the adsorption of organic matter. The results of this study demonstrated that the SOC contents of small-sized aggregate fractions were higher than those of coarse grain. This result also confirmed former reports by Arrouays et al. (1995). F-$LSD_{0.05}$ ranged between 7.91- 32.75, CV 22.71-106.96 with MWD 0.84±0.37, 0.84, 44.05 respectively. However, a non-significant ($p \leq 0.05$) effect was observed in the upper slope between 1mm – 0.25mm WSA alongside MWD mm. According to these results, land uses had little effect on dry aggregates in this study. Based on MWD, soil aggregate stability recorded stability constituting 17%, medium stability 17% and unstable 66% in the upper slope of the gully site. The result of unstable soil aggregates is explained by Hitoshi et al. (2012) that as the slope gradient increased, the amount of eroded soil assumed to increase, resulting in the relative increase of sand/ gravel in the soil surface coverage. The increase in the amount of eroded soil, in turn, would reduce the soil rooting depth, which is not suitable for the growth of shrub species whose tap root penetrates very deeply, sometimes 1 m or more, to exploit the limited amount of water (Thalen, 1979).

Table 8. MWD and Soil Aggregate Stability classes at the Middle Slope in the Gully Erosion Site regarding soil depth and particles size

LOCAL GOVERNMENT AREA/COMMUNITY	DISTANCE	Soil Depth (cm)	2mm	1mm	0.5mm	0.25mm	MWD (mm)	Stability status
BENDE: OZUITEM NDIAGHO	Middle Slope (MS)	0-25	14.26	13.07	8.24	44.96	1.41	Stable
OZUITEM NDIAGHO:	MS	25-50	1.26	2.73	3.63	61.28	0.13	Very unstable
ONU IBINA-UKWU IGBERE	MS	0-25	3.23	8.72	10.04	55.34	0.51	Unstable
ONU IBINA-UKWU IGBERE	MS	25-50	1.38	13.71	16.04	54.61	0.46	Unstable
OHAFIA: ELU OHAFIA	MS	0-25	2.85	11.1	15.84	58.36	0.53	Unstable
ELU OHAFIA	MS	25-50	0.61	8.72	12.26	52.12	0.47	Unstable
EBEM OHAFIA	MS	0-25	19.9	25.81	17.13	32.32	1.23	Medium
EBEM OHAFIA	MS	25-50	22.66	33.93	18.75	21.82	1.41	Stable
UMUNEOCHE: AMUODA	MS	0-25	2.92	14.2	16.14	50.66	0.61	Unstable
AMUODA	MS	25-50	11.71	33.22	15.7	30.31	1.08	Medium
OBINAOLU NGODO	MS	0-25	12.04	31.22	19.37	31.19	1.09	Medium
OBINAOLU NGODO	MS	25-50	1.38	15.2	14.33	50.74	0.57	Unstable
MEAN			7.85±7.91	17.64±10.61	13.96±4.63	45.31±13.01	0.79±0.43	
F-LSD0.05			19.6	22	12.01	28.17	0.84	
CV			100.7643	60.14739	33.16619	28.71331	54.43038	
Significant			NSD	NSD	NSD	NSD	NSD	

From the results of MWD in Table 8, it is observed that Ozuitem Ndiagho at the soil depth of 25-50cm (middle slope) recorded the lowest value of 0.13 and at 0.25cm recorded the highest value of 1.41 (Ozuitem Ndiagho) and Ebem Ohafia at the depth of 25-50cm respectively . From these results, all the study locations were affected by gully erosion on aggregate stability with an intensity ranging between severe moderate constituting 41.7% to very severe constituting values up to 58.3%. This implies that the aggregate stability of the soil has contributed to gully erosion ranging between 41.7 -58.3% in the selected communities. Table 8 shows the summary of the gully erosion on aggregate stability at the middle slope at the depths 0-25 and 25-50cm respectively. At 2mm, soil aggregates ranged from 0.61 to 22.66 where Elu (0-25cm) recorded the lowest value while Ebem recorded the highest value with the overall mean value of 7.85±7.91, at 1mm, soil aggregates ranged from 2.73 to 33.93 where Ndiagho recording the lowest value, while Ebem (0-25cm) recorded the highest mean value of 17.64±10.61. At 0.5mm, soil aggregates ranged from 8.24 to 19.37 with Ndiagho recording the lowest and highest values at 0-25cm respectively at the mean value of 13.96±4.63. At 0.25mm, soil aggregates ranged from 21.82 to 61.28 with Ngodo recording the lowest value at 0-25cm and Ndiagho showing the highest value at 25-50cm with a mean of 45.31±13.01 respectively. There was no significant difference existing between aggregate stability and MWD of the soil in the middle slope at $p>0.05$ at the different soil depths and various locations. Based on MWD, the recorded soil aggregate stability was as follows: stable at 17%, very unstable at 8%, medium at 25% and unstable at 50% with unstable soil aggregate stability showing the highest percentage.

Table 9. Critical levels for aggregate stability based on levels of Mean weighted diameter in the middle slope

S/No	Local Government Area/Community	Soil Depth (cm)	MWD (mm)	Critical limit	Description	Symbol
1	BENDE: Ozuitem Ndiagho	0-25	1.41	1- 2	severe moderate	SM
		25-50	0.13	0.5<0.1-5	Very severe	VS
2	Onu Ibina-Ukwu Igbere	0-25	0.51	0.5<0.1-5	Very severe	VS
		25-50	0.46	0.5<0.1-5	Very severe	VS
3	OHAFIA: Elu Ohafia	0-25	0.53	0.5<0.1-5	Very severe	VS
		25-50	0.47	0.5<0.1-5	Very severe	VS
4	Ebem Ohafia	0-25	1.23	1- 2	severe moderate	SM
		25-50	1.41	1- 2	severe moderate	SM
5	UMUNEOCHE: Amuoda	0-25	0.61	0.5<0.1-5	Very severe	VS
		25-50	1.08	1- 2	severe moderate	SM
6	Obinaolu Ngodo	0-25	1.09	1- 2	severe moderate	SM
		25-50	0.57	0.5<0.1-5	Very severe	VS

According to the results of the MWD in Table 9, Ndiagho recorded the lowest value of 0.128955 at the soil depth of 0-25 cm, while at the depth of (25-50 cm), Ndiagho recorded the highest value of 1.41045 with the mean value of 0.79±0.43. The levels for aggregate stability based on levels of MWD ranged from severe moderate (41.7%) to very severe (58.3%), indicating that locations situated in the middle slope are affected by gully erosion that ranges between severe moderate to very severe.

Table 10. MWD and Soil Aggregate Stability classes at the Lower Slope in Gully Erosion Site regarding soil depth and particle size

LOCAL GOVERNMENT AREA/ COMMUNITY	Soil Depth (cm)	2mm	1mm	0.5mm	0.25mm	MWD (mm)	Stability Status
BENDE: OZUITEM NDIAGHO	0-25	14.26	13.07	8.24	44.96	1.4	Stable
	25-50	1.89	14.34	6.55	55.62	0.52	Unstable
ONU IBINA-UKWU IGBERE	0-25	3.23	8.72	10.04	55.34	0.51	Unstable
	25-50	2.06	6.39	8.98	51.51	0.42	Unstable
OHAFIA: ELU OHAFIA	0-25	2.85	11.1	15.84	58.36	0.53	Unstable
	25-50	0.56	9.38	15.24	55.82	0.48	Unstable
EBEM OHAFIA	0-25	19.9	25.81	17.13	32.32	1.23	Medium
	25-50	2.78	9.92	16.12	58.95	0.57	Unstable
UMUNEOCHE: AMUODA	0-25	2.92	14.2	16.14	50.66	0.61	Unstable
	25-50	2.59	12.82	18.79	54.17	0.61	Unstable
OBINAOLU NGODO	0-25	12.04	31.22	19.37	31.19	1.09	Medium
	25-50	28.86	22.82	9.35	24.36	2.00	Stable
Mean		7.83±9.00	14.98±7.61	13.48±4.51	47.77±11.89	0.83±0.49	
CV		114.94	50.8	33.46	0.25	59.04	
F-LSD		18.75	19.5	10.07	29.4	1.042	
REMARK		NSD	NSD	NSD	NSD	NSD	

Table 10 shows the summary of the gully erosion on aggregate stability at the lower slope at the depths 0-25 and 25-50 cm respectively. At 2 mm, soil aggregates at the lower slope ranged from 0.56 to 14.26 with Elu (25-50cm) recording the lowest value and Ndiagho (25-50) recording the highest values with the overall mean value of 7.83±9.00. At 1mm, soil aggregates at the lower slope ranged from 6.39 to 31.22 and UkwuIgbere recorded the lowest value while Ngodo (0-25cm) recorded the highest values with the mean value of 14.98±7.61. At 0.5 mm. Soil aggregates at the lower slope ranged from 6.55 to 19.37 with Ndiagho (25-50) recording the lowest value and Ngodo recording the highest at 0-25cm respectively with the mean value of 13.48±4.51, and at 0.25mm. Soil aggregates at the lower slope ranged from 24.36 to 58.95 with Ngodo recording the lowest value at 0-25cm and Ebem having the highest value at 25-50cm with the mean value of 47.77±11.89 respectively. The coefficient of variance ranged from 0.25 to 114.94 (0.25-2 mm), and F-LSD ranged from 10.07 to 19.5 (0.5-1 mm) at 0.05%. Statistically, there was no significant difference at (p-value <0.05), indicating that soil aggregate stability in the lower course of the slope has no significance differences existing among the sampled communities. There was no significant difference existing between aggregate stability and MWD of the soil in the three sampled slopes at p>0.05 of the different soil depths at various locations. Uwanuruochi and Nwachukwu (2012) reported that when comparing aggregate stability of eroded and non-eroded soils, there was no statistical difference at 0.6 mm and 1.0mm, but there was a highly significant reduction of aggregate stability in eroded soils at 2mm aggregate size. Based on MWD, the recorded soil aggregate stability was shown as stable in Ndiagho and Ngodo constituting 17%, there was medium stability in Ebem and Ngodo with 17%, while the rest of the locations being unstable recording 66% of soil aggregate stability in the lower slope of the study area (Table 11). Above all, aggregate stability decreases with increasing the water content at aggregates with a diameter of 0.25mm fraction and affecting the three slopes within the agricultural land leading to a very poor soil quality (Figure 3).

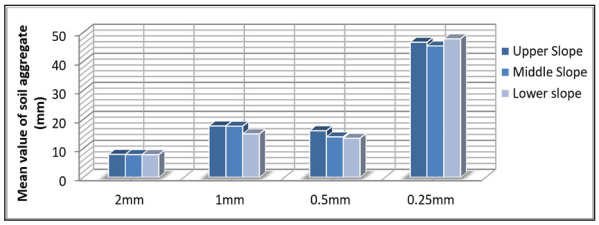

Figure 3. Water content at soil aggregate mean diameter fractions along the slopes.

Table 11. Critical levels for aggregate stability based on levels of Mean weighted diameter in the lower slope

Local Government Area/Community	Soil Depth(cm)	MWD (mm)	Critical limit	Description	Symbol
BENDE: Ozuitem Ndiagho	0-25	1.41	1- 2	Severe moderate	SM
	25-50	0.53	0.5<0.1-5	very severe	VS
Onu Ibina-Ukwu Igbere	0-25	0.51	0.5<0.1-5	very severe	VS
	25-50	0.42	0.5<0.1-5	very severe	VS
OHAFIA: Elu Ohafia	0-25	0.53	0.5<0.1-5	very severe	VS
	25-50	0.48	0.5<0.1-5	very severe	VS
Ebem Ohafia	0-25	1.23	1- 2	Severe moderate	SM
	25-50	0.57	0.5<0.1-5	very severe	VS
UMUNEOCHE: Amuoda	0-25	0.61	0.5<0.1-5	very severe	VS
	25-50	0.61	0.5<0.1-5	very severe	VS
Obinaolu- Ngodo	0-25	1.09	1- 2	Severe moderate	SM
	25-50	2.00	1- 2	Severe moderate	SM

The effect of location on the MWD revealed no significant difference from the results of mean weight diameter. Elu at the soil depth of 25-50cm recorded the lowest value of 0.48, while Ndiagho (25-50cm) recorded the highest value of 2.00 with the mean value of 0.83±0.49, with 59.04 CV and F-LSD 1.042 signifying that there is no significance difference among the communities in terms of mean weight diameter (MWD) in the lower slope at a 0.05% significance level. From the results obtained, the three studied slopes were susceptible to gully erosion leading to severe moderate (33%) to very severe (67%) based on the critical limit suggested by Lal (1986), implying that the sampled location recorded low aggregate stability with intensity ranging between severe moderate to very severe stability based on levels of Mean weighted diameter in the three slopes. Above all, the indices of macro aggregate stability in the gully sites and control showed that stability was lower, though lesser than control, which is thought to be decreasing the OC content and dominant sand in the gully-affected agricultural lands. The result is in agreement with Olusegun et al. (2011), who explained that the loss of organic binding agents through rain action resulted in the loss of finer soil particles to erosion and floodwater respectively. The low MWD values of the soils were attributed to low clay and organic-matter contents resulting in the weak aggregation of the soils along the slopes. The continued wetting and drying at the lower landscape position could lead to a decreased macro-aggregate stability, which is supported by Caron and Kay (1992), and Malgwi and Abu (2011). In addition, considering the translocation of the disintegrated aggregates along the slopes, the gentler the lower slopes, the larger the amount of disintegrated aggregates on the upper slopes can be added to the lower slopes, resulting in the increase of the amount of unstable aggregates on gentler slopes. This assumption was supported by previous results by Shinjo et al. (2000), showing that the gentler slope yielded a soil loss comparable to that on the steeper slope during the monitoring of water erosion over two rainy seasons.

4. Conclusions

The results of the soil physical and chemical parameters along the three slopes show high soil moisture and high bulk density which cause excessive drainage. The higher bulk density recorded along the three slopes were attributed to the coarse texture, low soil organic-matter content, and poorly-structured coarse particles dominated by the sand content, and low soil pH indicating acidity along the slopes. This finding suggests that the soil surface coverage can enhance the soil aggregate stability through the increasing of the organic-matter content, and that the slope gradient can increase the translocation of unstable aggregates, leading to the stabilization of soil in gully prone sites.

Acknowledgement

The authors are grateful to the staff of Nigeria Erosion and Watershed Management Project (NEWMAP), Abia State, during the course of the field work. The authors thank the laboratory Technicians of the Department of Environmental Management and Toxicology, Michael Okpara University of Agriculture, Umudike, Abia State who provided field assistance during the soil survey exercise in the study area.

References

Adekalu, K.O., Olorunfemi I. A., and Osunbitan, J. A. (2007). Grass mulching effect on infiltration, surface runoff and soil loss of three agricultural soils in Nigeria. Bioresource Technology, 98 (4), pp. 912-917.

Ajaero, C.K., and Mozie, A.T. (2011). The Agulu- Nanka Gully Erosion Menace In Nigeria: What Does the Future Hold for the Population at Risk? Climate Change and Migration: Rethinking Policies for Adaptation and Disaster Risk. Institute for Environment and Human Security United Nations University, Studies of the University: Research, Counsel Education publication series of UNU-EHS.No.15 pp74-81.

Amandine, E., Lauric, C., Frank, G. Catherine, R., Cédric, L., and Freddy, R. (2015). Increase in soil aggregate stability along a Mediterranean successional gradient in severely eroded gully bed ecosystems: combined effects of soil, root traits and plant community characteristics. Plant Soil,1104-015-2647-6.

Amezketa, E. M., Singer, J., and Le- Bissonnais, Y.(1996). Testing a new procedure for measuring water-stable aggregation. Soil Sci. Soc. Am. J. 60:888-894.

Arrouays, D., Balesdent, J., Mariotti , A., and Girardin , C. (1995). Modelling organic carbon turnover in cleared temperate forest soils converted to maize cropping by using 13C natural abundance measurements. Plant Soil 173, 191–196.

Bao, S.D. (2000). Soil and Agricultural Chemistry Analysis. China Agriculture Press, Beijing.

Barthès, B., and Roose, E. (2002). Aggregate stability as an indicator of soil susceptibility to runoff and erosion; validation at several levels. Catena 47(2):133–149.

Bronick, C.J., and Lal, R. (2005). Soil structure and management: a review. Geoderma 124, 3–22.

Burri , K., Graf, F., and Böll, A. (2009). Revegetation measures improve soil aggregate stability: a case study of a landslide area in Central Switzerland. For Snow Landsc Res 82(1):45–60.

Canton, Y., Sole-Benet, A., Asensio, C., Chamizo, S., and Puigdefabregas, J. (2009). Aggregate stability in range sandy loam soils: relationships with runoff and erosion. Catena 77, 192–199.

Caron, J., and Kay, B.D. (1992) .Rate of response of structural stability to a change in water content: Influence of cropping history. Soil and Tillage Research , 25 (2–3): pp. 16.

Cheng, M., Xianga, Y., Xueb, Z., An, S., and Darboux , F. (2015). Soil aggregation and intra-aggregate carbon fractions in relation to vegetation succession on the Loess Plateau, China. Catena 124:77–84.

Chinedu, I. O. , Jude , C. O., and Onweremadu , E. U. (2012). Modeling of Permanent Wilting from Particle Size Fractions of Coastal Plain Sands Soils in Southeastern Nigeria. International Scholarly Research Network ISRN Soil Science Vol. 2012, Article ID 198303, 5 pages.

Denef, K., Six J., Merckx, R., and Paustian, K. (2005).Short-term effects of biological and physical forces on aggregate Soil, 246, 185-200.

Dimoyiannis, D.G., Tsadilas, C.D., and Valmis, S. (1998). Factors affecting aggregate instability of Greek agricultural soils. Communications in Soil Science and Plant Analysis 29, 1239-1251.

FAO (2019) . Proceedings of the Global Symposium on Soil Erosion 2019. Rome.

Frei, M., Boll, A., Graf, F. Heinimann, H., and Springmann, S. (2003). Quantification of the influence of vegetation on soilstability. In: Lee CF, Tham LG (eds) Proceedings of the international conference on slope engineering. Hong Kong, China, pp. 872– 877.

Gee, G.W., and Or, D. (2002). Particle Size Analysis. In: Dane, J.H. and Topp, G.C., Eds., Methods of Soil Analysis, Part 4, Physical Methods, Soils Science Society of America, Book Series No. 5, Madison, 255-293.

Golchin, A., Baldock, J. A., and Oades, J. M. (1998). A model linking organic matter decomposition, chemistry, and aggregate dynamics. In: Soil Processes and the Carbon Cycle. pp. 245–266, Lal, R., Kimble, J. M., Follet, R. F., and Stewart B. A., Eds., CRC Press, Boca Raton, FL.

Gros, R., Monrozier, L. J., Bartoli, F., Chotte, J.L., and Faivre, P. (2004). Relationships between soil physico-chemical properties and microbial activity along a restoration chronosequence of alpine grasslands following ski run construction. Applied Soil Ecolog 27,pp. 7–22.

Grossman, R.B., and Reinsch, T.G. (2002). Bulk density and linear extensibility. pp. 201–228. In J.H. Dane and G.C. Topp (ed.) Methods of soil analysis.Part 4. SSSA Book Ser. 5. SSSA, Madison, WI.

Hitoshi, S., Haruhiro, F., Gus, G, . and Takashi, K. (2000). Soil aggregate stability under different landscapes and vegetation types in a semiarid area in northeastern Syria, Soil Science and Plant Nutrition, 46 (1) pp. 229-240.

Hossein, R. , Ali, A. J. , Ahmad, A. , Farzin , S. , and Khalil, V. K. (2015). Effect of Slope Position on Soil Properties and Types Along an Elevation Gradient of Arasbaran Forest, Iran.

Huang, Y.M., Liu, D., and An, S.S. (2015). Effects of slope aspect on soil nitrogen and microbial properties in the Chinese Loess region. Catena 125, 135–145.

Ibitoye, M.O., Ekanade O., Jeje L.K., Awotoye, O.O., and Eludoyin A.O. (2008). Characterization of gully formed in built up area in Southwestern Nigeria. Journal of Geography and Regional Planning , 1(9):pp. 164-171.

Idowu, O.J. (2003). Relationships between aggregate stability and selected soil properties in humid tropical environment. Communications in Soil Science and Plant Analysis 34, 695–708.

Igwe, C.A. (2004). Soil properties influencing stability of structure of B-horizons of Ultisols in semiarid Nsukka, Eastern Nigeria. Arid Land Res. Manag., 18, pp. 185-195.

Iheanyi, E. C. (2016).Assessment of soil properties from selected erosion sites in AbiaState, Southeastern Nigeria. Journal of Global Resources, 3,pp. 146-152.

Kalembasa, S. J., and Jenkinson, D.S. (1973). A comparative study of titrimetric and gravimetric methods for the determination of organic carbon in soil, J Sci Food Agric 24:pp.1085–1090.

Kalhoro, S. A. , Xuexuan, X. , Wenyuan , C. Rui, H., Sajjad, R. D., and Kang, D. (2017). Effects of Different Land-Use Systems on Soil Aggregates: A Case Study of the Loess Plateau(Northern China).Sustainability , 9, pp. 1349.

Kemper, D.W., and Rosenau R.C. (1986). Aggregate stability and size distribution. In: Methods of Soil Analysis, Part 1, (Ed. A. Klute). Am. Soc. Agron., 9, pp. 425-442.

Lal, R. (1986). Methods and Guidelines for Assessing Sustainable Use of Soil and Water Resources in the Tropics. Soil Management Support System, USDANRCS, Washington, DC.

Le Bissonnais, Y. (1996). Aggregate stability and assessment of soil crustability and erodibility: I. Theory and methodology. Eur. J. Soil Sci. 47,pp. 425–437.

Liu, H. U., Zhang, T. Y., Liu, B.Y. Liu, G., and Wilson, G. (2013). Effects of Gully Erosion and Gully Filling on Soil Depth and Crop Production in the Black Soil Region, Northeast China. Environ. Earth Sci., 68: pp. 1723–1732.

Malgwi, W. B., and Abu, S. T. (2011). Variations in some physical properties of soils formed on a hilly terrain under different land use types in Nigerian Savannah. Int. Journal of Sciences . 6 (3): pp. 150 – 163.

Mallam, I. Iguisi E.O., and Tasi'u .Y. R (2016). An Assessment of Gully Erosion in Kano Metropolis, Nigeria . Global Advanced Research Journal of Agricultural Science, 5(1) pp. 014-027.

Milne, R.M., and Haynes, R.J. (2004). Soil organic matter, microbial properties, and aggregate stability under annual and perennial pastures. Biology and Fertility of Soils 39, pp. 172–178.

Nelson, D.N., and Sommers, L.E (1982). Total carbon, organic carbon and matter. In: methods of soil analysis part 2 (Miller, A.D., and Keeney, D.K.M). American Society of Agronomy. pp 539-579.

NPC (2006). National Population Commission, 2006 Population Census Nigeria.

Nwite, J. N. , and Chukwuebuka, C. O. (2017). Organic carbon dynamics and changes in .some physical properties of soil and their effect on grain yield of maize under conservative tillage practices in Abakaliki, Nigeria. African Journal of Agricultural

Research , 12(26), pp. 2215-2222.

Nyberg, L. (1996) . Spatial variability of water content in the covered catchment at Gardsjon, Sweden, Hydrological Processes, 10, pp. 89–103.

Obalum, S. E. Nwite J.C., Oppong, J. Igwe, C.A. and Wakatsuki, T. (2011). Variations in selected soil physical properties with landforms and slope within an inland valley ecosystem in Ashanti region of Ghana. Soil & Water Res. 6: 73-82.

Oguike, P.C., and Mbagwu J.S.C. (2009). Variations in some Physical Properties and Organic Matter Content of soils of Coastal Plain Sand under different Land use types. World Journal of Agricultural Sciences 5 (1)63-69.

Okon, M. A, . Osujieke, D.N., Obi, C. I., Obasi, S. N., and Nkwopara, U.N. (2016). Aggregate Stability of Soils on a Sloppy Terrain in Owerri, Southeastern Nigeria. International Journal of Research in Agriculture and Forestry, 3 (12): 29-33.

Olusegun , O. A., Ogunkunle C O., and Adeniyi S.A. (2011). Assessment of soil quality under various land use practices in a humid agro-ecological zone of Nigeria . African Journal of Plant Sciences 5(10)pp 565-569.

Onweremadu, E.U., Izuogu, O.P., and Akamigbo, F.O.R. (2010) Aggregation and pedogenesis of seasonally inundated soils of the tropical watershed. Chiang Mai J. Sci. 37 (1): 74-84.

Oyegun, C. U., Erekaha, U.N., Eludoyin, O.S. (2016). Gully Characterization and Soil Properties in Selected Communities in Ideato South L.G.A., Imo State, Nigeria. Nat Sci. 14(2):34-50.

Quansah, C. (1997). Approaches to Replenishing Soil Fertility Depletion in Ghana; In Proceeding of International Seminar on Approaches to Replenishing to Soil Fertility in Africa – NGO, Perspectives ICRAF.

Quanchao, Z. Frédéric, D., Cheng, M., Zhaolong, Z., and Shaoshan, A. (2018). Soil aggregate stability under different rain conditions for three vegetation types on the Loess Plateau (China). CATENA, Elsevier, 167, pp.276–283.

Qui. L. Wei, X. Gao , J., and Zhang, X. (2015) . Dynamics of soil aggregate associated organic carbon along an afforestation chronosequence. Plant Soil 391:237–251.

Robinson, M., and Dean, T.J. (1993). Measurement of near surface soil water content using a capacitance probe. Hydrological Processes Joumal7, 77-86.

Salako, F. K., Hauser, S. , Babalola, O. , and Tian, G. (2001.) Improvement of the physical fertility of a degraded Alfisol with planted and natural fallows under humid tropical conditions. Soil Use and Management 17: 41-47.

Sanchez, P. A., Buresh R. J., Kwesiga F.R. , Mokwunye A.U., Ndiritu, C.G. Shepherd, K.D., Soule, M. J. and Woomer, P. L (1997). Soil Fertility Replenishing in Africa: An Investment in Natural Resource Capital pp. 121 – 129. In Proceedings of international Seminar on Approaches to Replenishing Soil Fertility in Africa – NGO Perspectives. ICRAF House Nairobi, Kenya

Shehu B.M., Jibrin J.M., and Samndi A.M. (2015). Fertility status of selected soils in the Sudan Savannah Biome of Northern Nigeria. International Journal of Soil Science, 10:pp.74 – 83.

Shinjo, H., Fujita, H., Gintzburger, G., and Kosaki, T. (2000). Impact of grazing and tillage on water erosion in northeastern Syria. Soil Sci. Plant Nutr., 46, pp. 151-162.

Singh, A.K., Rai, A., Pandey, V., and Singh, N. (2017a). Contribution of glomalin to dissolve organic carbon under different land uses and seasonality in dry tropics. Journal of Environmental Management 192: 142-149

Six, J., Bossuyt, H., Degryze, S. and Denef, K. (2004). A history of research on the link between (micro) aggregates, soil biota, and soil organic matter dynamics. Soil Tillage Res. 79.

SPSS, (1999). SYSTAT 9 statistics I. SPSS Inc.: Chicago, IL. Igwe, C.A., and Nwokoch, D. (2005). Influence of soil properties on the aggregate stability of a highly degraded tropical soil in Eastern Nigeria . . Int. Agrophysics, , 19, pp. 131-139.

Ternan, .L., Williams, A.G., Elmes, A., and Hartley, R. (1996). Aggregate stability of soils in central Spain and the role of land management. Earth Surface Processes and Landforms, 21, 181-193.

Thalen, D. C. P. (1979) Ecology and utilization of desert shrub rangelands in Iraq. Dr. W. Junk. Publishers, The Hague.

Ubuoh, E. A., Akhionbare, W. N., Onweremadu, E. , Onifade , O. A. (2013). Characterization of Soil Quality in Erosion Prone Environment of Ukpor, Nnewi-South L.G.A. of Anambra State, Nigeria. International Journal of Advances in Applied Sciences, 2(1), pp. 1~8.

Ubuoh, E. A., Ufot, U. O., and Ezenwa, L. (2016). Influence of Temperature Dynamics on Phosphorus Availability in Humid Tropical Soils of Southeastern Nigeria. Journal of Basic and Environmental Sciences (JBES) 3:pp.140-147.

Ubuoh, E. A. , and Ogbonna, P. C. (2018). Effects of Some Anthropogenically Induced Environmental Hazards on Soil Fertility Indices, Germination and Growth of Maize and Soyyabeans in Imo State. African Journal of Agriculture Technology and Environment, 7 (2): pp.30-43.

Ubuoh, E. A., Uka, A., and Egbe, C. (2017) . Impact of flood disaster on soil quality dynamics in agro-ecological zone of Ebonyi State, Nigeria. JOFESD , 3 (1): pp.143-153.

Ukaegbu, E. P., Osuaku, S. K. and Okolo, C. C. (2015). Suitability Assessment of Soils Supporting Oilpalm Plantations in the Coastal Plains Sand, Imo State Nigeria . International Journal of Agriculture and Forestry , 5(2): 113-120.

Unger, P. W. (1997). Aggregate and organic carbon concentration interrelationships of a Torrertic Pale Stoll Soil and Till-age Research 42 95-113.

Uwanuruochi, A. O., and Nwachukwu, O. I. (2012).Impact of erosion on selected soil structural indices of four Local Government Areas of Abia State, Nigeria. PAT 8 (2): 127-133.

Uzoma, K. C., and Onwuka, B. M. (2018) . Variations in Aggregate Stability and selected Soil Chemical Properties Under Different Land Use Systems in Ikpe Ikot Nkon, Southeastern, Nigeria . Agri Res & Tech: Open Access J 17 (5): 1-9.

Walker, L. R., and del Moral, R. (2009). Lessons from primary succession for restoration of severely damaged habitats. Appl Veg Sci 12:55–67.

Walkley, A., and Black, A. (1934). An examination of the Detgareff method for determining soil organic carbon, chronic titration method. Soil Sci. 37: 2 – 38.

Wang , X. , Yost, R. S., and Linquist, B.A . (2001). Soil aggregate size affects phosphorus desorption from highly weathered soils and plant growth. Soil SciSoc Am J 65:139–146.

Wang, J. Bojie, F. Yang, Q. and Liding , C. (2001). Soil nutrients in relation to land use and landscape position in the semi-arid small catchment on the loess plateau in China . Journal of Arid Environments , 48: 537–550 .

Wei Hu , M.. , Shao, A., Quan, J., Wang, J. F., Klaus, R. (2008). Spatial variability of soil hydraulic properties on a steep slope in the Loess Plateau of China. Sci. agric. (Piracicaba, Braz.) .65 (3): 268-276.

Xu, M., Li, Q., and Wilson, G. (2016). Degradation of Soil Physicochemical Quality by Ephemeral Gully Erosion on Sloping Cropland of the Hilly Loess Plateau, China. Soil & Tillage Research 155 pp. 9–18 .

Yang, T., Adams J. M., Shi Y., He J., Jing X., Chen L., Leho,

T., and Haiyan, C. (2017). Soil fungal diversity in natural grasslands of the Tibetan Plateau: associations with plant diversity and productivity. New Phytol. 215 pp. 756–765.

Young, E. O. (2000). Hydraulic conductivity of saturated soil pp. 141 -181.In: R. A. Smith and Mullins (ed). Soil and Environmental Analysis: Physical Methods 2nd ed. Marcel Dekkar, Inc New York. NY.

Zhu, X. Zhu, B, . Chen, L., Zhu, B. Xing, B. (2017). Effects and mechanisms of biochar-microbe interactions in soil improvement and pollution remediation: a review . Environ. Pollut., 227 , pp. 98-115.

JJEES

JJEES (2020) 11 (3): 225-236
ISSN 1995-6681

Jordan Journal of Earth and Environmental Sciences

Rock Physics Analysis of Abnormal Pore Pressure Regime Offshore Niger Delta Basin

Chukwuemeka Abbey [1,2*], Adetola Oniku [1], Chukwudi Meludu [1], Abraham Sebastian[1]

[1]Modibbo Adama University of Technology, Department of Physics, Nigeria.
[2]American university of Nigeria, Department of Petroleum Chemistry and Physics, Nigeria.

Received 10 March 2020; Accepted 20 April 2020

Abstract

An accurate pore pressure prediction across a reservoir basin is an antidote to potential drilling hazards and proper positioning of infill wells. A formation is declared to be in a state of abnormal pore pressure when the pore pressure is lower or higher than the hydrostatic pressure (normal pore pressure). If the pore pressure exceeds the hydrostatic pressure, overpressure comes, and it is attributed to under compaction, fluid expansion, fluid migration, and tectonics. At this point the confined fluid in the pores of the rock formation finds it difficult to escape leading to a high-pressure regime in that formation. This research work was conducted in the offshore field of Niger Delta, using seismic and the only drilled well log. Cross-plot of the rock physics parameters was employed to predict the abnormal pressure region, and seismic velocity inversion was also conducted in addition to rock physics template. It was observed that the density of the predicted interval and P-wave velocity experiences a drastic decrease at the predicted interval while the porosity of this interval increases as against porosity decrease with depth. The VpVs ratio, acoustic impedance, lambda, and passion ratio cross-plots reveal that the interval in question is in the abnormal pressure range, which is far above the hydrostatic pressure of the region. This predicted result complemented the formation pore pressure of the formation.

Keywords: Pressure, rock physics, hydrostatic, prediction, cross-plot

1. Introduction

The study of pore pressure in sedimentary formations is of great importance in hydrocarbon exploration. In sedimentary basins around the world, the knowledge of pore pressure regime is necessary before, during, and even after exploration. This is because a good knowledge of formation pressure helps in well planning, well development, and its recovery plan (secondary production. Pore pressure ranges from normal hydrostatic pressure to abnormal pressure regime which is referred to as pressure above hydrostatic. Also, pressure can be said to be below the hydrostatic pressure and it is referred to as under pressure or subnormal pressure. This can be a result of burial or decrease in the formation temperature. In the case of burial, if the encapsulated unit is buried deeper, its original pressure is carried to a higher pressure environment. Failure for the rock to compact, means that the trapped pressure is abnormally low for the new depth. The same thing happens if there is a decrease in the heat associated with the formation, which is the cooling of pore fluids as they are uplifted and the overburden erodes.

Considering the Pressure above hydrostatic, Swarbrick and Osborne, 1998 attributed it to the under compaction of sediments, fluid expansion, and fluid migration. Under compaction, which is regarded as compaction disequilibrium, arises when the rate of deposition and burial are sufficiently great relative to the vertical permeability of sediments (Huffman, 2002). At this point, the confined fluid in the pores of the rock finds it difficult to escape so as to maintain a hydrostatic fluid pressure gradient as experienced in shale and clay deposits having high porosity with low permeability (Terzaghi, 1923). This effect is also associated with rocks with a young geological age. Other mechanisms of abnormal pressure include clay diagenesis, aqua thermal expansion, source-rock maturation, and fluid migration that can be traced to increase in temperature in the formation (Huffman, 2002). From the theory of anomalous expansion, can be realized that some fluids expand at certain temperatures, and fluids in the pore throat are not an exception to that. The same goes with the release of water due to mineral transformation. This will invariably lead to the change in the pressure of the fluids in the pores' space of the formation.

In order to optimize the output with more infill wells and recovery plans, there is a need to have a critical insight of what the pressure of the formation looks like, this is because the formation pressure has an important part role in predicting hydrocarbon reserves of a reservoir and its

* Corresponding author e-mail: emexabbey@gmail.com

recoverability. This is because the pressure differential is a major drive mechanism of hydrocarbon fluids during primary recovery and a good knowledge of the formation pressure helps the reservoir engineers during secondary recovery which is invariable in the pressurizing of the reservoir for optimal output. With the knowledge that the reservoir elastic properties might have an important role to play in pressure distribution across the formation, rock physics will definitely have a role to play in pore pressure determination.

The application of rock physics in abnormal pore pressure prediction will play a significant role in the delineation of formation areas with the likelihood of abnormal pressure regimes. Carcione and Helle (2002) reveal that Poisson's ratio is a good indicator of abnormal pressure regime; in gas-saturated rocks, Poisson's ratio decreases with a significant increase in formation pore pressure, while in formations saturated with liquids, Poisson's ratio increases with a decrease in formation pressure. Accordingly, this work intends to delineate abnormal/ overpressure regime within the formation of the study field that is penetrated by a well log, by looking at the relationship of rock physics parameters, porosity, and acoustic impedance in relation to pore pressure.

1.1. The Geology of the Study Area

The Niger Delta Province (Figure 1) is situated in the Gulf of Guinea as defined by Klett et al. (1997). The Delta contains only one identified petroleum system which is referred to as the Tertiary Niger Delta (Akata – Agbada) Petroleum System (Kulke, 1995; Ekweozor and Daukoru, 1994). Lehner and De Ruiter, (1977) stated that the delta is formed at the site of a rift triple junction which is related to the opening of the southern Atlantic starting in the Late Jurassic and continuing into the Cretaceous and stopped in the Late Cretaceous.

Gravity tectonism became the primary deformational process at the post rifting era. Shale mobility induced internal deformation, and occurred in response to two processes (Kulke, 1995). First, shale diapirs formed from the loading of poorly compacted, over-pressured, prodelta and delta-slope clays (Akata Formation) by the higher density delta-front sands (Agbada Formation). Second, slope instability occurred due to a lack of lateral, basinward support for the under-compacted delta-slope clays (Akata Formation).

The delta proper began developing in the Eocene, and has prograded southwestward, forming depobelts that represent the most active portion of the delta at each stage of its development (Doust and Omatsola, 1990). These depobelts form one of the largest regressive deltas in the world with an area of some 300,000 km^2 (Kulke, 1995), a sediment volume of 500,000 km^3 (Hospers, 1971), and a sediment thickness of over 10 km in the basin depocenter (Kaplan et al., 1994). For any given depobelt, gravity tectonics were completed before the deposition of the Benin Formation, and are expressed in complex structures, including shale diapirs, roll-over anticlines, collapsed growth fault crests, back-to-back features, and steeply dipping, closely- spaced flank faults (Evamy et al., 1978; Xiao and Suppe, 1992). These faults mostly offset different parts of the Agbada Formation and flatten into detachment planes near the top of the Akata Formation (Tuttle et al., 1999).

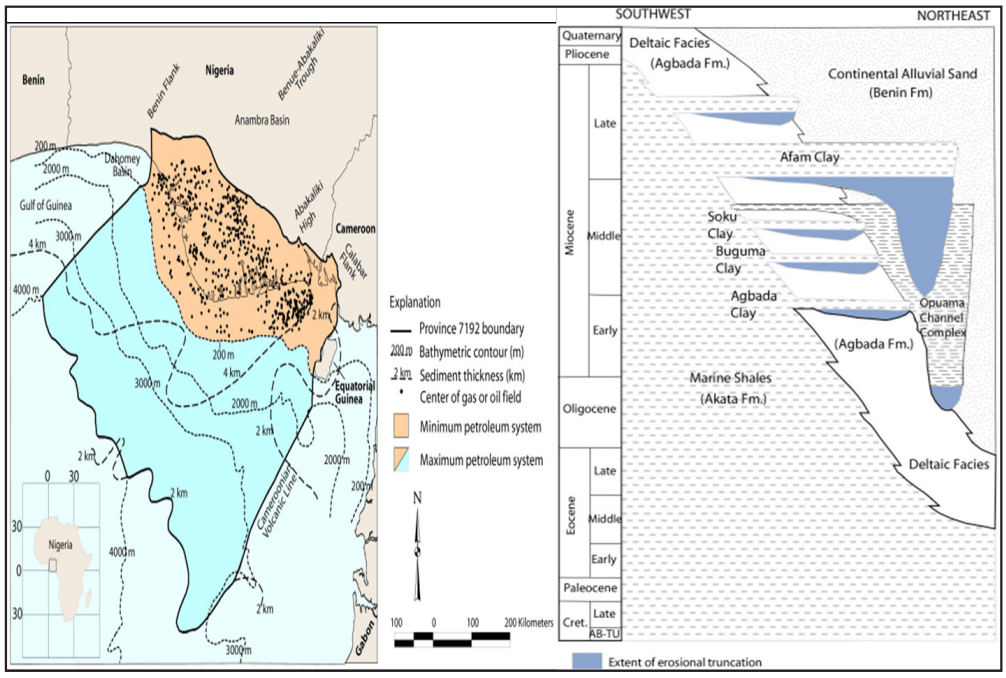

Figure 1. The Niger Delta Province Outline and Stratigraphic Column showing Formations of the Niger Delta modified after Tuttle et al., 1999 and Doust and Omatsola, 1990.

1.2. Stratigraphy and Structural Styles of the Area

The three main stratigraphic units, as shown in the stratigraphic column in Figure 1, are the Akata, Agbada and Benin Formations. It has been noted that the age of the formations becomes progressively younger in a down dip direction and ranges from Paleocene to Recent. The Akata Formation is a marine sedimentary sequence composed of shales, clay, and silts at the base of the known Delta sequence. Doust and Omatsola (1990) stated that the thickness of the sequence is not known for certain, but may reach 7,000 m in the central part of the Delta. The Akata shales are mobile, undercompacted and typically overpressured. They are considered to be the main source rock of the Niger Delta with the upper part considered a matured source rock (Weber and Daukoru, 1975; Ekweozor and Daukoru, 1984). According to Avbovbo (1978), the hydrocarbon, generated in the Akata Formation, probably migrated up dip through growth faults to accumulate in the shallow reservoirs of the Agbada Formation. The Agbada Formation occurs within a depth interval of about 1,700 m to about 2,900 m). It is characterized by the alternation of sandstone and sand bodies with shale layers. The thickest known section of the Agbada Formation is about 10,000 feet, but the maximum thickness may well be much greater. The Benin Formation consists of predominantly massive highly porous fresh water bearing sandstones with thin shale interbeds. Short and Stauble (1967) noted that genetically, the Benin sands and sandstones are mainly deposits of the continental upper deltaic plain environment. This formation is characterized by a high sand percentage (70-100%) and variable thickness, which may be more than 6,000 feet. The age spans from Oligocene in the north and becomes progressively younger southwards.

The structural architecture is characterized by the interplay of subsidence and supply rates which resulted in the deposition of discrete depobelts. When further crustal subsidence of the basin could no longer be accommodated, the focus of sediment deposition shifted seaward, forming a new depobelt (Doust and Omatsola, 1990). Each depobelt is a separate unit that corresponds to a break in regional dip of the delta and is bounded landward by growth faults and seaward by large counter-regional faults or the growth fault of the next seaward belt as shown in figure 2 (Evamy et al., 1978; Doust and Omatsola, 1990). The northern delta province, which overlies a relatively shallow basement, has the oldest growth faults that are generally rotational, evenly-spaced, with their steepness increasing seaward. The central delta province has depobelts with well-defined structures such as the successively deeper rollover crests that shift seaward for any given growth fault. Last, the distal delta province is the most structurally complex due to the internal gravity tectonics on the modern continental slope.

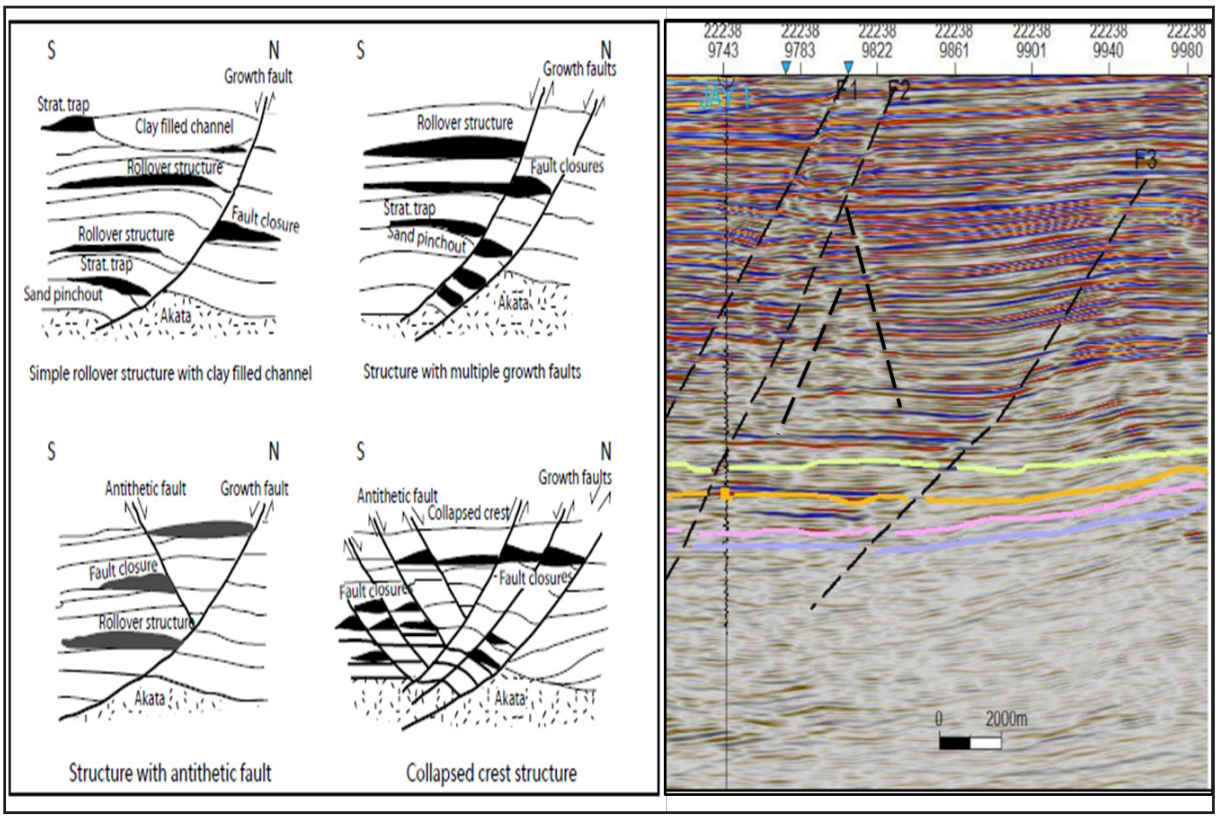

Figure 2. Structural styles of Niger Delta, Modified from Doust and Omatsola (1990) and Okpogo et al. (2018)

2. Materials and Method

Jay Field is situated in the Niger Delta Hydrocarbon Province. The field comprises 3D seismic data and a Well log, with suits of logs, density, resistivity, gamma, neutron, and sonic logs. The data were analyzed for quality control check, and were processed using Rok Doc and HRS software. The base map of the study area is displayed in Figure 3, while the seismic section with the inserted drilled well is presented in Figure 4. The quality of the section as transversed from the Benin down to Agbada formation is appreciably good, but becomes chaotic when moving down the Akata formation (marine shales) that is described in the literature to be diapiric in nature.

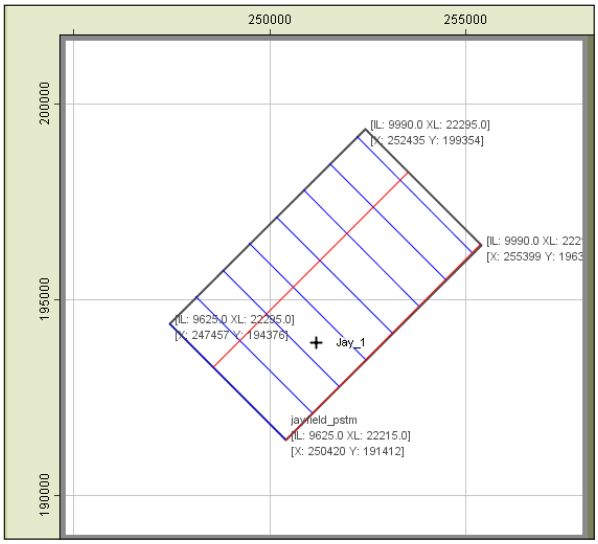

Figure 3. The base map of the study field.

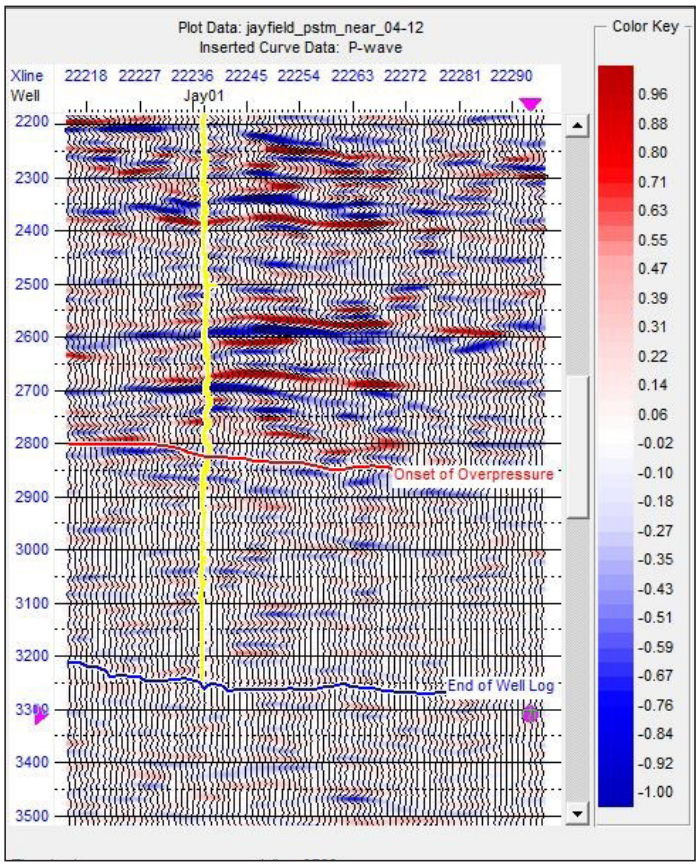

Figure 4. Display of seismic section with the Well, showing the quality of seismic section and the investigated region.

Goodway et al. (1997) calculated rock physics parameters such as velocity ratio, Lamé parameters and Poisson's ratio using P-wave and S-wave logs.

Velocity ratio, which is given as $v = \frac{Vp}{Vs}$ 2.4

Where Vp and Vs are the P-wave and S-wave velocities respectively

Incompressibility (lamba Rho) $\lambda = \rho(Vp^2) - 2(\rho Vs^2)$ 2.5

Rigidity modulus (mho Rho) $\mu = \rho(Vs^2)$ 2.6

Poisson's ratio $\varphi = \frac{\lambda}{2(\lambda+\mu)}$ 2.7

The cross-plot of P-wave (Vp) and density log is expected to reveal compaction/ disequilibrium trend, since the density and compressional wave velocity increase with depth. In a situation where the reverse becomes the case, disequilibrium compaction sets in. This implies that instead of decreasing with depth, the porosity of sediments appreciated significantly at some depth, causing the abnormal pressure regime in the formation.

Velocity ratio is independent of the rock density and acoustic impedance (Abbey et al. 2018) and can be employed to determine the over-pressured region in the formation. In a normally compacted formation, Vp/Vs ratio decreases with depth, while the acoustic impedance increases with respect to burial depth. Thus, the abnormal/ overpressure regime within the formation can be easily mapped out from the cross-plot template. Again from Hamada (2014), the Vp/Vs ratios for most consolidated rocks vary from 1.5 to 2 and Poisson's ratio for the same is between 0.1 to 0.3 3, so with the cross-plot template of Velocity ratio against Poisson's ratio, unconsolidated/un-compacted rocks' materials within a greater depth of burial will be identified.

3. Results and Discussion

Figure 5 displays the well view showing the logs of gamma-ray, resistivity, neutron porosity, density and P-wave. The gamma-ray log appears in yellow and grey colorations which represents the sand and shale stone formations respectively. The reservoirs in this well fall within 2350 ms - 2775 ms and 2900 -3700 in meters. The mapped interval with the inscription of overpressure region to the end of well is the area of interest. This is because density and p-wave velocity increases with depth in a normal compaction setting, but the area in consideration comes with a decrease in density and velocity when moving down the formation. Also, porosity decreases with depth due to compaction as a result of overburden, the reverse applies in this mapped out region due to experiencing an increase in porosity in the probed region against the former.

P-wave and density increase with depth due to the compaction of sediments in formations. According to the cross-plot in Figure 6, the en-circled clusters ought to appear at the arrow point, since from the color key it represents sediments with a greater depth of burial. This was not so because of the under-compaction of sediments which is also regarded as a disequilibrium compaction becoming a major source of overpressure regime in sedimentary formations around world. By the virtue of overburden on the overlying formation, the porosity of sediment decreases as the fluids escape the pores' space bringing about a reduction in pore space and compaction. Based on this principle, clusters which represent deposited sediments about 3700 to well end are predicted to be overpressure and are in the abnormal pressure regime.

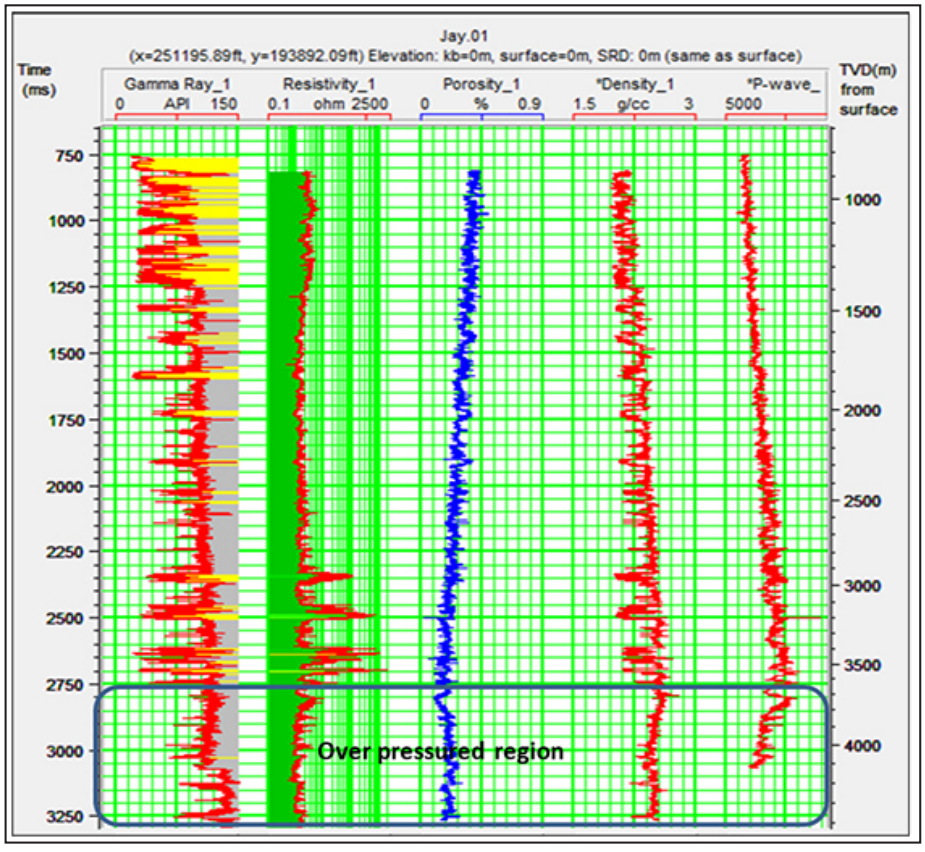

Figure 5. Well log display of in Jay field

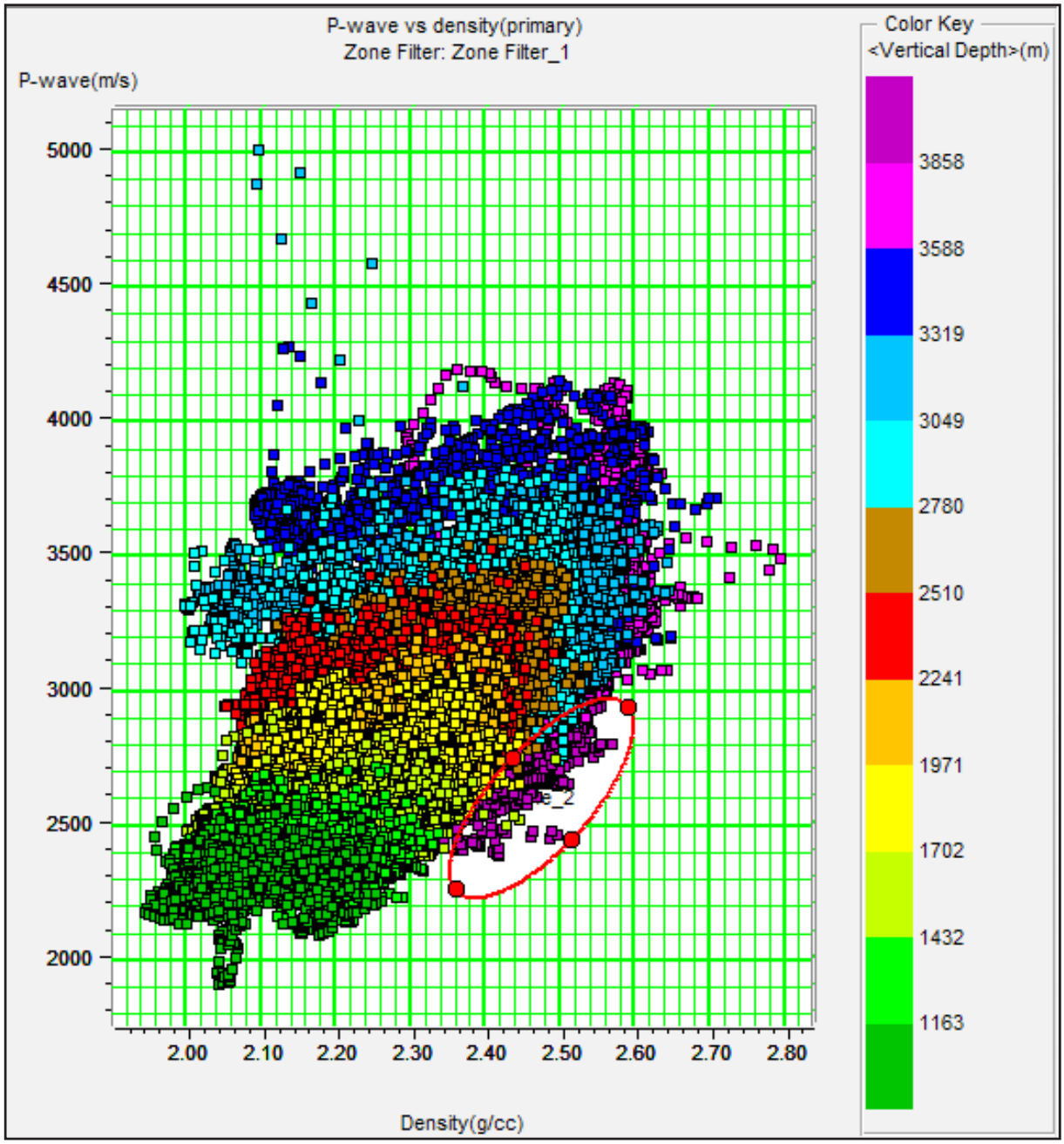

Figure 6. plot of P-wave against formation density, showing under-compacted sediment's

Consider the cross-plot of velocity ratio versus P-impedance in Figure 7a, this under compaction of sediments is made visible in the circled portions of the plots. In Figure 7a, the velocity ratio experienced an increase against what is expected when there is an increase in burial depth. The acoustic impedance, on the other hand, reveals a reduction which is against the principle when acoustic impedance increases as the depth of burial increases. The same is also applicable in Figure 7b, which is colored by porosity. Porosity decreases with the depth of burial, the porosity of the sediments in the investigated formation is observed to be greater than those above it, as observed in the circled part in Figure 7b. In Figures 7c and 7d, the same anomaly is also pictured out in the VpVs plot against porosity and the Plot of VpVs against Lambda-Rho.

The plot of p-impedance against Poisson's ratio in Figure 8 depicts the un-consolidation of sediments at the burial depth of about 3600m to the end of the log. P-impedance increases with he increase in the depth, while Poisson's ratio decreases with the increase in depth of burial. At about the abovementioned depth mention, there is an indication of an increase in Poisson's ratio with a decrease in impedance of the formation. This abnormal relationship with depth reveals an abnormal pressure regime within the probe formation. Also, in Figure 9c, the velocity ratio and Poisson's ratio increased with increases in the depth in the investigated area. This is against a decrease due to compaction and cementation of sediments, as depth increases. In Figure 10, the inverted

seismic velocity displays a decrease in seismic velocity at the overpressured zone region. Sound energy increases in consolidated material and decreases in unconsolidated material. So it is expected that as burial depth increases, the velocity will also increase. From Figure 10, an increase in seismic velocity can be observed until the marked horizon of the onset of overpressure as shown from the colour indicator. The inverted seismic velocity is far better off in determining the true velocity of the formation compared to the interval transit velocity.

Furthermore, the Lame's Constant Lambda, was considered, which is a measure of rocks brittleness, and also a function of both Young's Modulus and Poisson's Ratio in this rock physics analysis of overpressure. Lambda relates stresses and strains in perpendicular directions which is closely related to the incompressibility and it is capable of revealing the resistance to a change in volume that is caused by a change in pressure. So the cross-plot of pressure and Lambda as in Figure 11 shows that the shale/clay is ductile based on the porosity and its properties. With the increased formation pressure, which has been identified as over pressured zones, comes an exponential decrease in lambda. This is anticipated since Young Modulus, similar to Lambda, is a measure of the stiffness of a material, at this point of lambda, the reduction or decrease signifies that the formation is unconsolidated with the increased porosity, thereby making the sediments accumulation at this interval not stiff otherwise ductile in nature. Considering the relationship that exists between the cross-plot of pressure against the acoustic impedance, Figure 12 reveals a direct linear relationship between pore pressure and acoustic impedance at the region where the pore pressure is normal, and an inverse relationship where there is an abnormal or overpressure regime. At this point a drastic reduction occurs in the acoustic impedance since this is a function of density and velocity when burial depth increases.

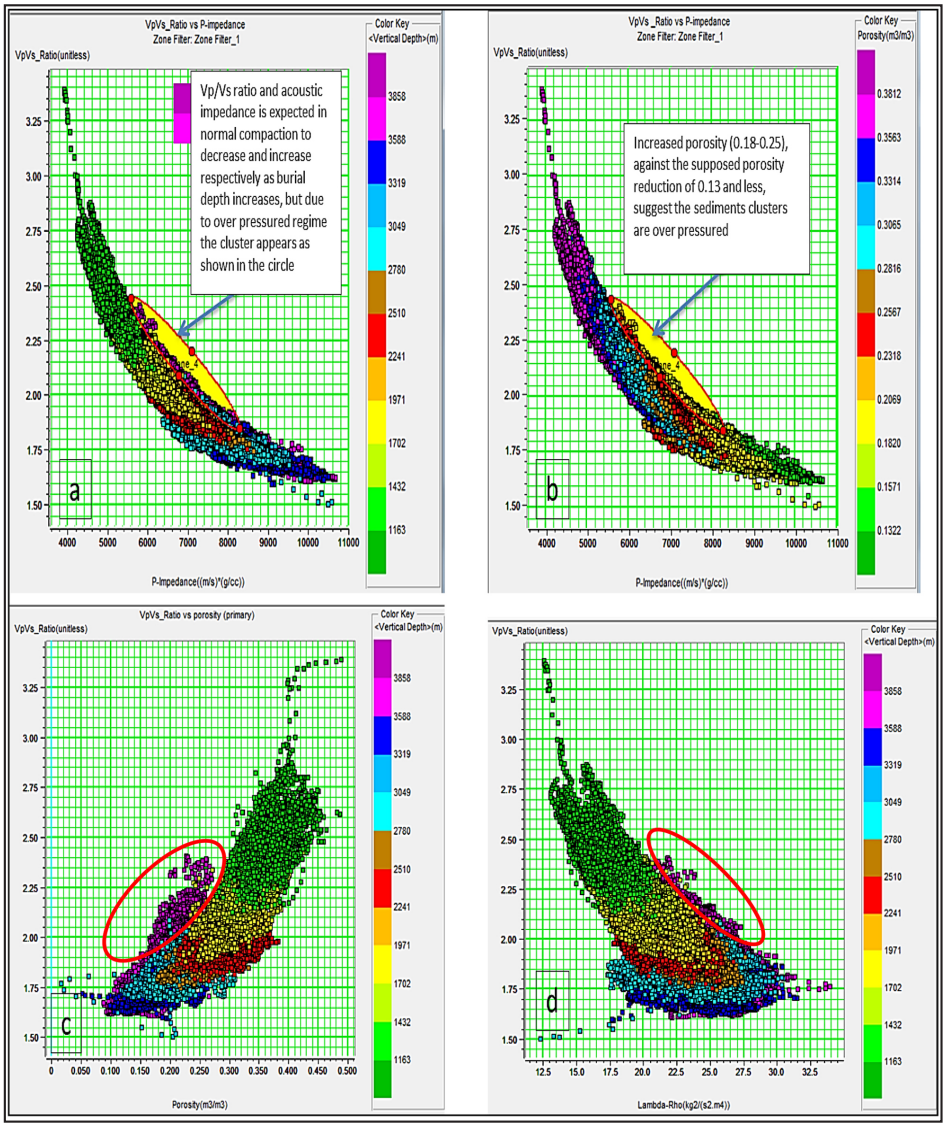

Figure 7. a and b: Plot of Velocity ratio against P-impedance revealing under-compaction, c: Plot of VpVs against porosity, d: Plot of VpVs against Lambda-Rho.

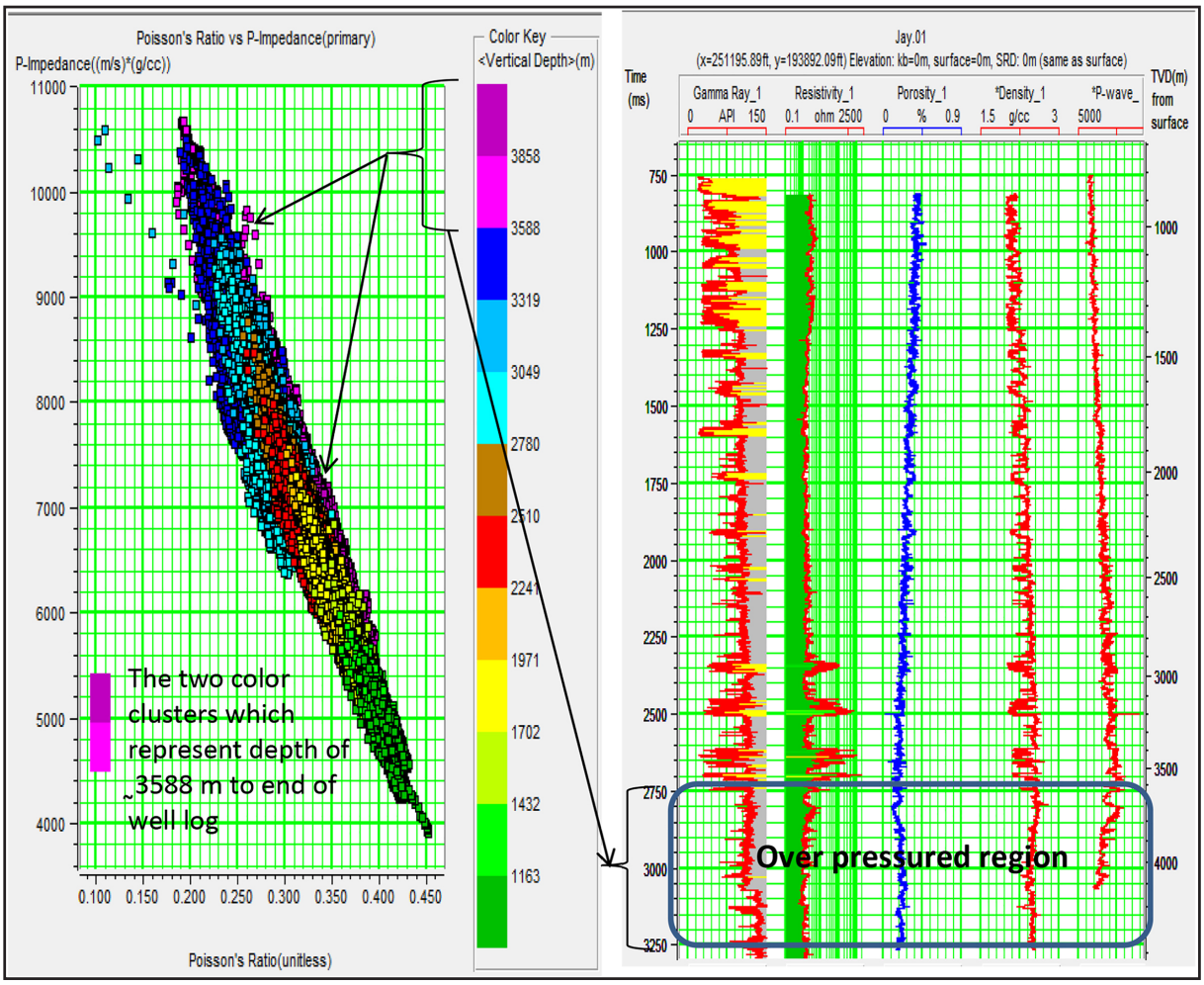

Figure 8. Plot of P-impedance vs Poisson's ratio showing the two clusters with abnormal pressure

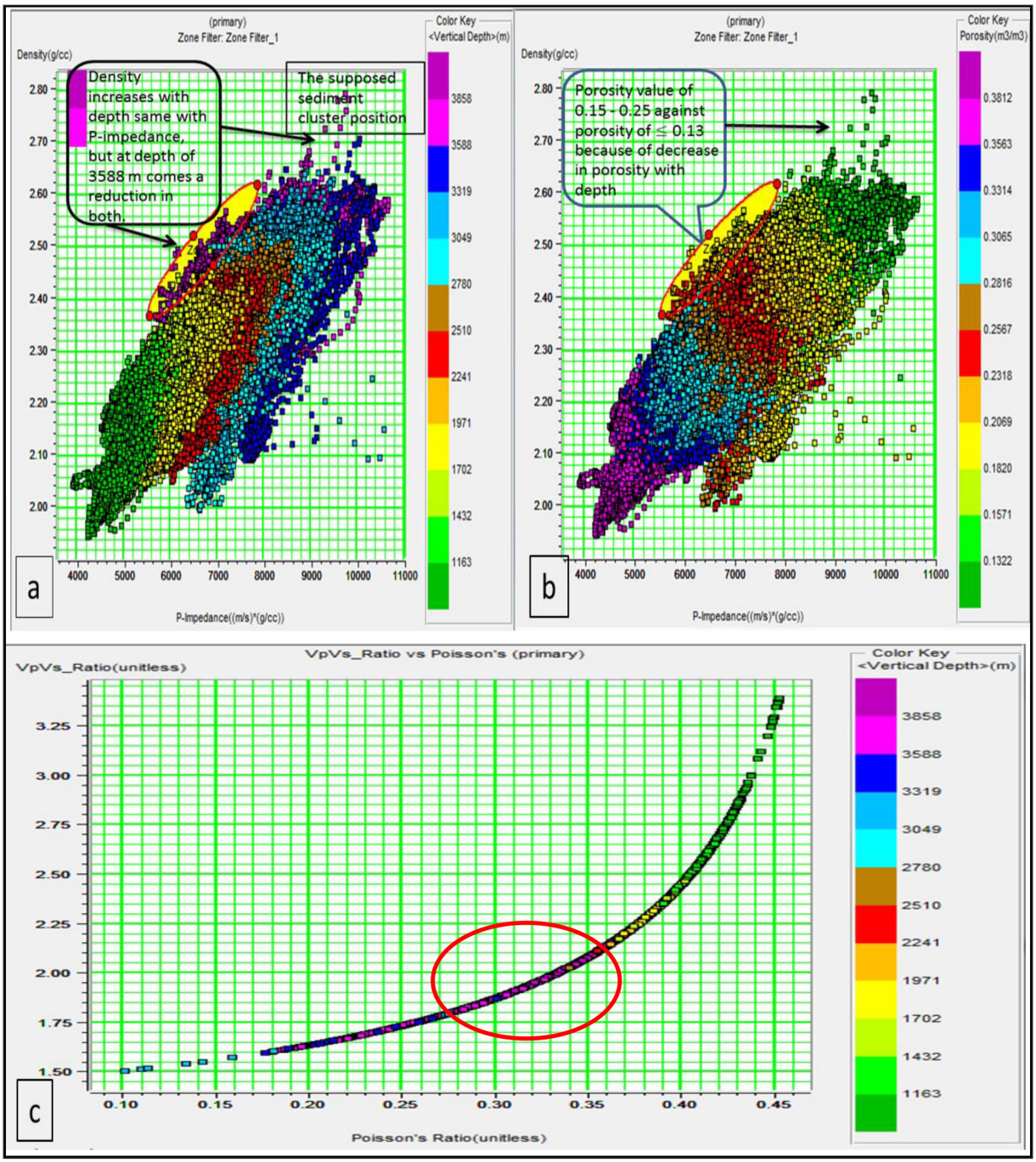

Figure 9. a and 9b: Plot of Density against P-impedance, 9c: Plot of VpVs against Poisson's ratio

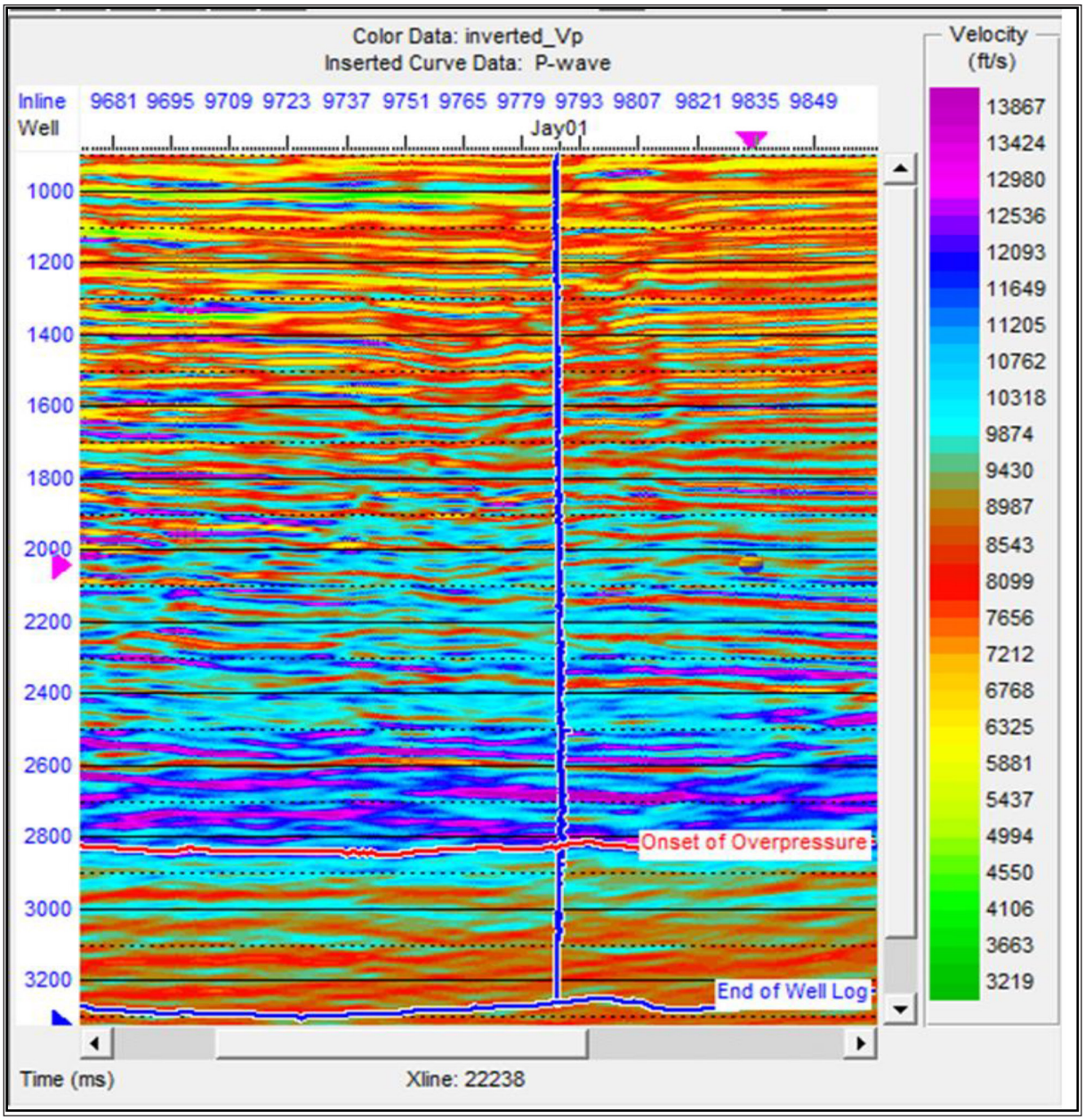

Figure 10. The seismic inverted velocity from Xline 2238

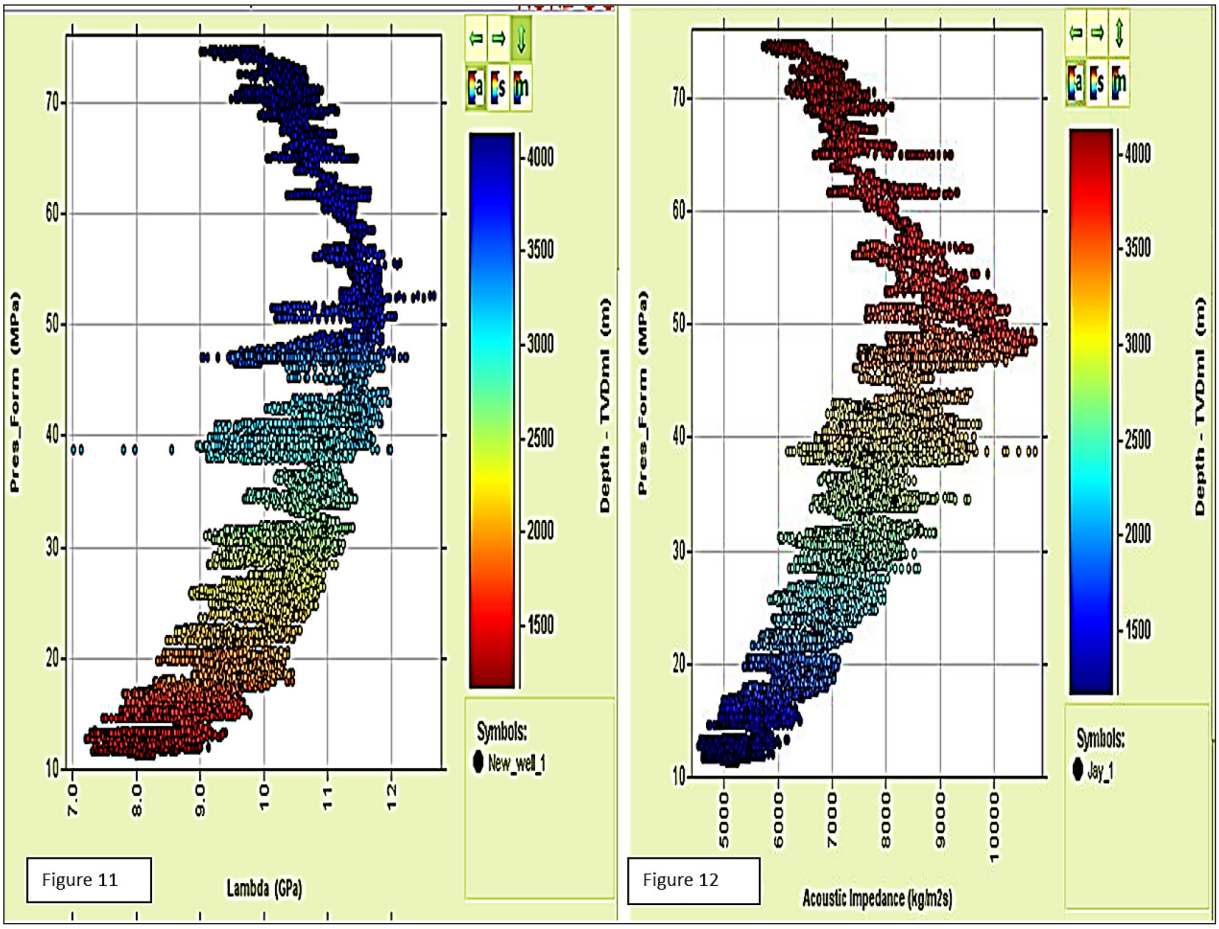

Figure 11. The Cros- plot of Pressure against Lambda and **Figure 12.** Cross-plot of pressure versus Acoustic impedance

4. Conclusions

This research was carried out with the purpose of predicting abnormal pore pressure regime in the basin through rock physics parameters and cross-plots. The field has one drilled well and a 3-D seismic volume. From the well plot, it was observed that P-wave and density logs were decreasing with depth due to the compaction of sediments. Nearly at the mapped interval, there was a reversal from the trend, with both the P-wave and density logs increasing down the hole. Porosity was also observed to be decreasing with depth till the point of the mapped interval where it began to increase, which shows that the interval is unconsolidated having a higher porosity against the depth interval. The relationship between lambda and acoustic impedance with formation pressure reveals an exponential decrease in lambda at the point of overpressured region and an inverse relationship at the over-pressured region. The acoustic impedance decreases with the increase of formation pressure which validates the un-consolidation or disequilibrium compaction within the predicted abnormal pressure interval.

References

Avbovbo, A.A. (1978). Tertiary Lithostratigraphy of Niger Delta. American Association of Association of Petroleum Geologists, 10(14): 96-200.

Hamada, G.M. (2014). Reservoir Fluids Identification Using Vp/Vs Ratio. Oil and Gas Science and Technology, 59(6): 649-654.

Swarbrick, R.E., and Osborne, M.J. (1998). Mechanisms that generate abnormal pressures: an overview. In: Law, B.E., Ulmishek, G.F., Slavin, V.I. (Eds.), Abnormal pressures in hydrocarbon environments: American Association of Petroleum Geologists Memoir 70: 13–34.

Short, K.C., and Stauble, A.J. (1986). Outline of the Geology of Niger Delta, American Association of Petroleum Geologists Bulletin 51: 761 – 779.

Abbey, C.P, Okpogo, E.U, Atueyi, I.O. (2018). Application of rock physics parameters for lithology and fluid prediction of 'TN' field of Niger Delta basin, Nigeria. Egyptian Journal of Petroleum, 27: 853–866, https://doi.org/10.1016/j.ejpe.2018.01.001

Goodway, W., Chen, T., Downton, J. (1997) Improved AVO fluid detection and lithology discrimination using Lamé petrophysical parameters; fluid stack," from P and S inversions: 67th Annual International Meeting, Society of Exploration Geophysicists, Expanded Abstracts, 183–186,

Doust, H., and Omatsola, E. (1990). Niger Delta. In: Divergent and Passive Margin Basins. Edwards. P. A. and Santogrossi, P.A. (Eds.). The American Association of Petroleum Geologist, 48: 239-238.

Ekweozor, C.M., and Daukoru, E.M. (1984). Petroleum Source Bed Evaluation of Tertiary Niger Delta—reply. American Association of Petroleum Geologists Bulletin, 68: 390-394.

Ekweozor, C.M., Daukoru, C.M. (1994). Northern Delta Depobelt Portion of the Akata-Agbada (!) Petroleum System, Niger Delta, Nigeria: Chapter 36: Part VI. Case Studies--Eastern Hemisphere, in The Petroleum system—from source to trap. American Association of Petroleum Geologists Memoir, 60: 599–613.

Evamy, B.D., Haremboure, J., kamerling, P., Knaap, W. A., Molloy, F.A., Rowlaands, P. H. (1978). Hydrocarbon Habit of Tertiary Niger Delta. America Association of Petroleum Geologists Bulletin, 62: 277-298.

Okpogo, E.U., Chukwuemeka P. A., Atueyi, I. O. (2018). Reservoir characterization and volumetric estimation of Orok Field, Niger Delta hydrocarbon province. Egyptian Journal of Petroleum, 27 (4): 1087–1094, https://doi.org/10.1016/j.ejpe.2018.03.014

Kaplan, A., Lusser, C.U., Norton, I.O. (1994). Tectonic Map of the World, panel 10: Tulsa, American Association of Petroleum Geologists, 1:10,000,000.

Klett, T. R., Ahlbrandt, T. S., Schmoker, J. W., Dolton, J. L. (1997). Ranking of the World's Oil and Gas Provinces by Known Petroleum Volumes: U.S Geological Survey Open-file Report, 97 – 463.

Kulke, H. (1995). Nigeria Regional Petroleum Geology of the World Part II. In: Kulke, H (Ed.), Africa, America, Australlia and Antarctica: Berlin, Gebruder Borntraeger, 11: 143-172.

Lehner, P., and De Ruiter, P.A.C. (1977). Structural History of Atlantic Margin of Africa. American Association of Petroleum Geologists Bulletin, 16: 961 – 981.

Carcione, J.M., and Helle, H.B. (2002) Rock Physics of Geopressure and Prediction of Abnormal Pore Fluid Pressures Using Seismic. Cseg Recorder, (27)7

Hospers, J. (1971). The Geology of Niger Delta area. In: Delany, F.M. (Ed.), the Geology of East Atlantic Continental Margin, Great Britain Institute of Geological Science Report, 70(16): 121.

Terzaghi, K. (1923) Calculation of the permeability of the tone from the course of the hydrodynamic stress phenomena, Mathematical-natural, class. Academy of Sciences, Vienna, 125-138.

Tuttle, M.L.W., Charpentier R.R., Brownfield, M.E. (1999). The Niger Delta Petroleum System: Niger Delta Province, Nigeria, Cameroun and Equatorial Guinea, Africa. United State Geological Survey Open-File Report 99 - 50H.

Xiao, H. and Suppe, J. (1992). Origin of Rollover. American Association of Petroleum Geologists Bulletin, 76: 509-529.

Huffman, A. R. (2002). The Future of Pressure Prediction Using Geophysical Methods. In: Huffman, A.R. and Bowers, G. L. (Eds.), Pressure Regimes in Sedimentary Basins and Their Prediction, American Association of Petroleum Geologists Memoir, 76: 217-233.

Weber, K. J. and Daukoru, E. M. (1975). Petroleum Geological Aspects of the Niger Delta. Proceedings of Ninth World Petroleum Congress, Tokyo, 5(2): 209-221

المملكة الأردنية الهاشمية

صندوق دعم البحث العلمي

الجامعة الهاشمية

المجلة الأردنية
لعلوم الأرض والبيئة

JJEES

مجلة علمية عالمية محكمة

المجلد (١١) العدد (٣)

http:// jjees.hu.edu.jo/

ISSN 1995-6681

المجلة الأردنية لعلوم الأرض والبيئة

مجلة علمية عالمية محكمة

المجلة الأردنية لعلوم الأرض والبيئة: مجلة علمية عالمية محكمة ومفهرسة ومصنفة، تصدر عن عمادة البحث العلمي في الجامعة الهاشمية وبدعم من صندوق البحث العلمي - وزارة التعليم العالي والبحث العلمي، الأردن.

ترسل البحوث إلكترونيا إلى البريد الإلكتروني التالي:

رئيس تحرير المجلة الأردنية لعلوم الأرض والبيئة

jjees@hu.edu.jo

لمزيد من المعلومات والأعداد السابقة يرجى زيارة موقع المجلة على شبكة الانترنت على الرابط التالي:

www.jjees.hu.edu.jo

المملكة الأردنية الهاشمية صندوق دعم البحث العلمي الجامعة الهاشمية
صندوق دعم البحث العلمي
Scientific Research Support Fund
THE HASHEMITE UNIVERSITY JORDAN

JJEES

المجلة الأردنية لعلوم الأرض والبيئة

المجلد (١١) العدد (٣)

مجلة علمية عالمية محكمة تصدر بدعم من صندوق دعم البحث العلمي

ISSN 1995-6681 jjees.hu.edu.jo أيلول ٢٠٢٠